A STUDY OF THE DISINTEGRATION OF ACTINIUM X BY THE NUCLEAR EMULSION METHOD

Thesis

submitted by

Benjamin F. Bayman

B.Ch.E. (The Cooper Union, New York)

for the Degree of

Doctor of Philosophy

University of Edinburgh

November, 1954.

C O N T E N T S

C O N T E N T S (Contd.)

CHAPTER III

CONVERSION ELECTRON SPECTROMETRY IN NUCLEAR EMULSIONS

CHAPTER IV

THE LEVEL SCHEME OF THE EXCITED STATES OF ACTINON

C O N T E N T S (Contd.)

PREFACE

The research described in this thesis was carried out in the Department of Natural Philosophy of the University of Edinburgh under the joint direction of Professor N. Feather, F.R.S. and Dr. M.A.S. Ross. A paper based on the results to be presented here, and prepared in collaboration with Dr. Ross, has been accepted for publication in Section A of The Proceedings of the Physical Society of London.

CHAPTER I.

INTRODUCTION AND HISTORICAL REVIEW

I.1 Introduction.

In 1900, Sir William Crookes separated from uranium another substance which possessed all its photographic activity (i.e. its β-activity) and which he named uranium X. Rutherford and Soddy (1902) applied a similar technique to thorium, obtaining a substance which was, weight for weight, over a thousand times more active than the original material. By analogy with the nomenclature of Crookes, this was called thorium X. It was largely from the results of his study of the relationship between thorium X and its parent and daughter products that Rutherford inferred the principles with which he was successfully to analyze the enormous complexity of the phenomena of natural radioactivity.

Proceeding in the same way, Giesel (1904) and Godlewski (1905), working independently, separated from actinium a very active substance which came to be called actinium X (AcX). Lise Meitner (1925), on the basis of the evidence she had obtained during her study of the homogeneous groups of electrons emitted by AcX, was able to conclude that when the process of internal conversion occurs in association with a disintegration,

it occurs after the disintegration. She compared the energy differences between lines in the AcX electron spectrum which she had attributed to conversion in the K, L and M shells with the energy differences between the K, L and M absorption edges of both AcX and actinon (An). The closer agreement obtained with the An absorption edges convinced her that conversion actually took place in this atom, which is the product of the AcX α-disintegration.

Present interest in AcX has two principal causes. The first refers to its anomalously low disintegration energy, as revealed by the study of the systematics of α-decay among the heavy radioactive nuclei. The second is due to the fact that An $\left(\frac{219}{86}\right)$ has seven neutrons outside a closed shell of 126 neutrons. This places it between the regions of validity of the single-particle model of Mayer (1949) and Haxel Jensen and Suess (1949) on the one hand, and the collective model of A. Bohr (1951, 1953) on the other. The former applies only to configurations of particles near to closed shells, while the latter applies only when the configuration contains a large number of particles outside closed shells. A better understanding of the relationship between these two models should result from a determination of the extent to which they can explain the properties of an intermediate nucleus such as An.

The experiments to be described attempt to provide information relating to these questions. They employ the newly-developed nuclear emulsion technique in a study of the internal conversion spectrum of the decay of AcX. The results of this study, combined with the available data on the AcX α- and γ-radiations, yield some of the properties of the level structure of An and illustrate some of the characteristics of α-disintegration in the heavy even-odd nuclei.

I.2. Summary of Studies of the Radiations of AcX.

I.2.1. The disintegrations of the actinium series.

The processes that constitute the lower part of the actinium series are represented diagrammatically in Figure 1. Each horizontal line represents an element of the series, the half-life of each element being shown adjacent to its line (the letters S, M, D, Y stand for seconds, minutes, days, years, respectively). A single vertical line represents decay by β-emission; a double vertical line represents decay by α-emission. In those cases in which branching occurs, the fraction of disintegrations following each mode is

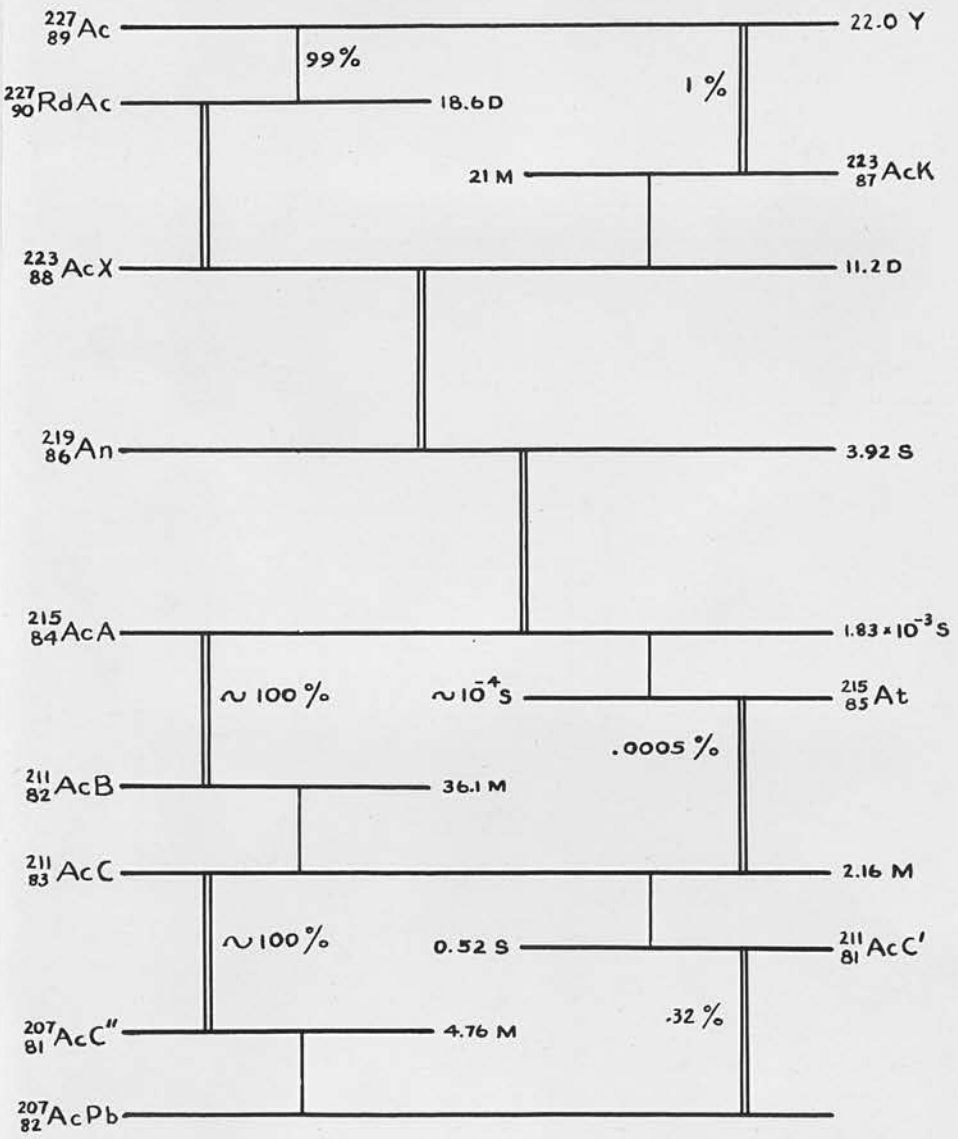

FIGURE 1.

SCHEMATIC REPRESENTATION OF THE LOWER PART OF THE ACTINIUM SERIES

FROM THE DATA TABULATED BY HOLLANDER, PERLMAN, AND SEABORG (1953)

indicated as a percentage.

The chemistry of these elements is such as to make it relatively simple to separate AcX from the others. However, because of the short half-lives of An and actinium A (AcA), all previous investigators of the radiations emitted by elements of the chain have been faced with considerable difficulties of attribution.

I.2.2. The α-radiation.

The first workers to observe the fine structure of the AcX α-radiation were Mme. P. Curie and S. Rosenblum (1932). Using the 180° magnetic focussing method which they had developed during the preceding few years, they observed, in a plate exposed for seven days to a radioactinium (RdAc) source, two lines (energies 5.589 and 5.524 MeV) which they attributed to AcX. These lines did not appear in the exposures made with fresh RdAc. They were very feeble, and no attempt was made to estimate their relative intensities. They continued this work (1933) by investigating the spectrum of a preparation of AcX which had been separated from RdAc by precipitation with $BaSO_4$.+ This time they observed the two lines found previously, but

+ AcX, a radium isotope, has very nearly the same chemical properties as barium; this can be inferred from their relative positions in the periodic table.

these were accompanied by a third line of greater energy and intensity which had been masked by a line of the RdAc spectrum. Its energy was reported as 5.776 MeV and the relative intensities of the three lines, in order of decreasing energy, were given as 6:4:1. The next advance was by Rosenblum, Guillot and Perey (1936) who replaced the photographic recording apparatus by a counter which could be moved along the spectrum. In this way they obtained the spectrum of a sample of RdAc which had just been separated from all other active material, and then of this same sample after it had aged for 11 days. This second spectrum showed lines due to disintegrations occurring throughout the chain. The authors assumed that the only lines overlapping the RdAc spectrum were those of AcX, and obtained the AcX spectrum by difference. In resolving the total observed spectrum into component lines, they took as the line shape that of the principal ray of An. In this way they found a fourth AcX line, and indicated that there were probably others of still lower energy and intensity. Further measurements made on the RdAc spectrum (Rosenblum, Guillot, Perey, 1937) using an improved technique (condensation of the emanation by a foil cooled with liquid nitrogen) showed that the energies reported previously were, on the average, 19 keV too high. This question need not be considered too deeply at this point, since only the

differences between the disintegration energies corresponding to the various α-groups are of importance in the determination of the level structure of the An nucleus. ~~These differences in disintegration energy depend almost entirely on the differences between the corresponding α particle energies, and only to a very slight extent on the absolute values of these energies (i.e. through the calculation of the energy of the recoil nucleus).~~ In a recent survey and re-evaluation of the results obtained by the Paris workers during the period 1931-1937, Briggs (1954) gives the values listed in Table 1.

A detailed study of the complex α-spectra of the heavy elements has been published by Asaro (1953). His α-particle spectrograph employed a 60° symmetrical magnetic analyzer, the normal trajectory having a radius of curvature of 75 cm. AcX was removed from a sample of actinium and thorium by means of a cold Dowex 50 ion exchange column, and vacuum sublimed onto a source whose final surface density was about 10 $\mu g/cm^2$. The α-particles were detected in Eastman NTA plates having emulsions 25 to 30 microns thick. After exposure these plates were scanned under a magnification of X450, a count being made of the number of tracks whose direction lay within a certain cone of acceptance. Nothing was done to eliminate the fogging effect of the emanating actinon, and hence his plates

TABLE I - α-Particle and α-Disintegration Energies for AcX.

Author	α-particle energy (MeV)	Disintegration energy (MeV) (corrected for An recoil)	Abundance (per 100 disintegrations)
Rosenblum, et al. (1931-1937); re-evaluated by Briggs (1954)	5.700 ± .006	5.804 ± .006	41
	5.538 ± .006	5.690 ± .006	35
	5.514 ± .006	5.615 ± .006	17
	5.425 ± .008	5.524 ± .008	7
Asaro (1953)	5.735	5.840	11
	5.704	5.808	53
	5.595	5.697	25
	5.528	5.629	9
	5.420	5.519	2
Rosenblum (1952)	5.860	5.967	weak
	5.730	5.835	9
	5.704	5.808	53
	5.596	5.698	24
	5.528	5.629	9
	5.487	5.587	2
	5.419	5.518	3

showed an enormous number of background tracks. Asaro measured the differences between the energies of the five groups he detected, but made no attempt to determine the absolute values of these energies.

In an unpublished communication to G.T. Seaborg, Rosenblum (1952) gave his latest results on the AcX α-particle fine structure. These are listed in Table 1, along with the results of Asaro. The energy of the 53% line in the Asaro spectrum is set equal to 5.704 MeV, the energy observed for this line by Rosenblum. No experimental details of this latest work of Rosenblum have been published.

I.2.3. The conversion electron spectrum.

A detailed study of the extensive results previously obtained from magnetic analysis of the conversion electrons of RdAc and its derivatives forms an important part of the present work. For this reason it will not be given in this historical summary, but will be deferred until Chapter IV. The experiments by which these results were obtained will now be described.

The earliest investigations used the absorption technique. However, the first study that achieved the resolution required for precise analysis was that of Hahn & Meitner (1925). AcX was precipitated with ammonia from a solution of RdAc in equilibrium with its products. After purification it was electrolyzed

onto a very thin platinum wire which was subsequently used as the source of the radiations. The spectrum was analyzed with a semi-circular focussing magnetic spectrograph with photographic recording, the energy range 12.5 - 465.7 keV being covered. 49 lines were attributed to RdAc, 21 to AcX and 9 to the active deposit (AcB + C). The energy of each line was measured relative to the F-line of ThB (taken as $B\rho$ = 1385 gauss-cm), and a visual estimate was made of the amount of photographic blackening it produced.

Hahn & Meitner were not aware that the disintegration of the actinium emanation is accompanied by the emission of internal conversion electrons. All rays emitted by the AcX source and not by the active deposit were therefore attributed to the AcX disintegration. This must be kept in mind when their results are considered. It weakens their proof that internal conversion takes place in the daughter atom, since as far as their work went, the transitions that were correctly shown to be converted in An might have arisen in An as well, and not in the parent AcX. Fortunately the An spectrum is in fact much feebler than that of AcX, and the attribution by Hahn & Meitner of the parentage of the strong conversion lines to AcX has proved to be correct.

A very extensive magnetic spectrographic investigation of the conversion spectra of radioactinium and

its products was performed by Surugue (1937). He made no attempt to work with AcX sources, but obtained the AcX spectrum from the difference between the spectra produced by new and old sources of RdAc. He avoided AcX sources because these emit An freely, and this results in the fogging of the photographic plates used for recording. RdAc sources, on the other hand, can be prepared in a form that is more effective in keeping entrained the An produced by the AcX disintegrations. This was noticed by Hahn & Meitner, but they still preferred to work with AcX sources.

The spectrum of the active deposit was studied separately by Surugue and presented no difficulties. An attempt was made to obtain the An spectrum by using as a source a glass ampoule containing an AcX preparation covered by a gold foil. It was intended that the An should diffuse around the foil into the space that was taken as the source. Another technique used was putting the AcX into a tube, a section of which was drawn out to very small diameter. The An diffused into this section and disintegrations taking place there were studied in the spectrometer. In either case the effective source dimensions were relatively large, resulting in poorer resolution than in the RdAc and active deposit investigations. Surugue attributed 76 conversion lines to RdAc, 30 to AcX,

9 to An, and 15 to the active deposit. He measured their energies relative to the F-line of ThB (taken as $B\rho$ = 1388) and obtained their relative blackening by microphotometering his plates.

In 1944 Surugue, in collaboration with Ouang, re-examined the part of the RdAc spectrum below 46 keV. They confirmed almost all of Surugue's previous attributions, and supplied better measurements of energy and relative blackening.

As will be shown in Chapter IV, the results of Hahn & Meitner differ in many important respects from those of Surugue. Another magnetic focussing β-spectrographic investigation of the AcX spectrum is urgently needed, but because of the speed of the actinium chain and the consequent difficulties of attribution of the observed conversion lines, this task is not an attractive one. Recently, however, the Paris group (Frilley, Rosenblum, Valadarès, Bouissières, 1954) have begun a study of the RdAc conversion spectrum. Using newly-developed extraction techniques they have produced solid-free, derivative-free sources of RdAc. The authors have published their results on the lines of energy less than 61.5 keV (F-line of ThB taken to be $B\rho$ = 1388.55). In the cases in which these results relate to a disagreement between Hahn & Meitner and Surugue, the work of Hahn &

Meitner appears to be confirmed.

A completely different approach to the investigation of the conversion spectrum of an element in the actinium series was made by Bennett (1938). He introduced An gas into a Wilson cloud chamber and made a study of the electron tracks associated with α-particles emitted by disintegrating An nuclei. He estimated the energies of electrons above about 15 keV from the curvature of the tracks (a magnetic field of 380 gauss parallel to the axis of the camera was produced by a pair of Helmholtz coils). The ranges of some of the lower energy electrons were also measured. On the basis of the 80 conversion electrons observed, Bennett concluded that his results confirmed those of Surugue, except that he found no evidence of the strong 105 keV line that Surugue had attributed to An. This point is of special significance for the present work, as will be made clear in Chapter IV.

I.2.4. The γ- and X-radiations.

These were studied by Frilley (1940), using a rotating-crystal spectrograph with photographic recording. As sources he used preparations of AcX which had just been separated from RdAc. However, because of the long exposures required, he was actually studying AcX in equilibrium with all its decay products.

Frilley also studied the spectrum of actinium in equilibrium with its decay products, and that of freshly separated RdAc. The exposures for the latter lasted for a few days, during which time the AcX radiations remained weak compared to those of RdAc. This permitted him to identify the RdAc γ-rays. Of course, Frilley could not supply the attribution of any of the γ-rays emitted by AcX or one of its products. The results of his work are summarized in Table 2.

TABLE 2.

γ-Spectrum of AcX and its derivatives. (Frilley, 1940).

Energy (keV)	Approx. Relative Intensity	Energy (keV)	Approx. Relative Intensity
44		155	12
52	0.1	180	1
62		270	20
90.5		340	15
123	4	415	
144	6	590	

Note: Frilley has published no quantitative intensity data for AcX and its derivatives. The values given here were kindly supplied by him in a private communication to Dr. M.A.S. Ross.

The most striking feature of Frilley's investigation of the characteristic K-X-radiation is the

predominance of the $K\alpha_1$- and $K\alpha_2$ - radiations of element 86. Their combined intensity is over ten times as great as that of any other element in the actinium series, whereas in both the uranium and thorium series it is the K-X-radiation of element 83 that predominates.

I.3. Outline of the Present Work.

At the time this investigation was begun+ the available information about the disintegrations of AcX led to a number of anomalies. The above-mentioned experiments on the conversion spectrum indicated that strong transitions of energies 122, 144, 154 and 268 keV take place during the de-excitation of the An nucleus. This is confirmed by the lines of the γ - spectrum and by the intensity of the characteristic X-rays of An. Yet none of these transitions could be fitted between the energy levels deduced from the energies of the α-particles that had, up to that time, been observed to accompany the AcX disintegration (see Table 1). This suggested that the ground state of An is not directly excited by α-disintegration of AcX, but is reached only by transitions from states of higher energy which are directly excited. A forbiddenness of this type is of considerable interest in the theory of α-systematics. However, on the basis of

+ January, 1952.

the existing information it was not possible to prove this conjecture, because only the relative intensities of the transitions were known, whereas the absolute intensities (transitions per disintegration) would have been required to demonstrate the inadequacy of the level scheme deduced from the α-spectrum. Furthermore, the rapidity with which the successive disintegrations of the actinium chain follow each other prevented all the previous workers from providing really convincing proof that the observed conversion and γ-transitions are to be associated with the de-excitation of the An nucleus. The object of the present work has been to check the attributions of these transitions, and to estimate their absolute intensities.

This has been done by impregnating Ilford G5 (electron sensitive) emulsions with AcX citrate. In this form, the AcX was probably bivalent, and thus able to form a structural bond with the gelatine of the emulsion until its disintegration. However its chemically inert daughter product, An, was unable to enter into such a bond, and hence was free to diffuse through the emulsion by Brownian motion. The other disintegration products could all exist in the charged form, and hence were trapped by the gelatine. While it is true that the disintegrations occurring farther down the series ruptured these gelatine-heavy atom

bonds, the distances moved by the recoiling atoms before other bonds were formed were too small to be observed. The result was that the α-particle track associated with the AcX disintegration was sometimes separated by several microns from the "star" produced by particles emitted during subsequent disintegrations. If it is assumed that the transitions between the excited and ground states of An all took place within, say, $\frac{1}{10}$th second of the time of formation of the An nucleus, then the internal conversion electrons associated with these transitions must have produced tracks which had a common origin with the separated α-particle track. A study of these electron tracks yielded information about the spectrum of conversion electrons emitted during these transitions only. And since the nuclear emulsion technique permits a study of the disintegrations one at a time, the absolute intensities of the lines of this spectrum could be obtained.

CHAPTER II

DESCRIPTION OF THE METHOD

II.1 Experimental Procedure.

II.1.1. Source preparation; Impregnation of the plates.

One of the standard methods of separating barium from fission product mixtures is precipitation of $Ba(NO_3)_2$ by fuming HNO_3 (Lieber, 1939; Glendenin, 1951). Since barium and AcX have almost identical chemical properties, this method could be used for the separation of AcX. To a drop of a solution of actinium in equilibrium with its decay products, and containing 20 mg. Ba^{+2} carrier, were added several ml. of fuming HNO_3. The precipitate of $Ba(NO_3)_2 + AcX(NO_3)_2$ was separated by centrifuging, dissolved in water, and then re-precipitated as the carbonate by the addition of aqueous sodium carbonate solution. This was washed with water four times, and then dissolved in about 3 ml. of 5% citric acid solution. The pH of the resulting solution was adjusted to 7.5 by the addition of dilute NH_4OH.

It has been found (Yagoda, 1949; Jarvis, 1950) that the impregnation of nuclear emulsions with heavy elements is complicated by the tendency of these elements to form chemical bonds with the outer layers of the emulsion. This is the reason for the use of the

citrate ion. It forms a complex with the heavy element which prevents the occurrence of this bonding, and so permits effective penetration of the impregnating material (Zajac and Miller, 1952). The citrate also prevents the barium from precipitating in the emulsion when carbonates are added during development.

Because the exact activity of the source was unknown, it was necessary to perform tests covering a wide range of source dilutions in order that a satisfactory density of events be obtained in the final plates. Ilford G5 and Kodak NT4 plates (emulsion thickness 200 microns) were cut into 1" x 1" sections, and these were soaked in the diluted active solution for 30 minutes at room temperature. They were then dried for an hour in a current of warm air (about 30°C), and stored for four days in the presence of a saturated solution of K_2CO_3 (relative humidity 44%).

The addition of wetting agent to the impregnating solution caused no significant increase in the speed of penetration. Best results were obtained when none was used. The quality of the Kodak emulsion seemed to be slightly better than the Ilford product, but this was more than offset by the tendency of the Kodak emulsions to separate from their glass backing during impregnation or drying. The presence of a few per cent of glycerine in the impregnating solution seemed to have little effect. For this reason an Ilford plate

was used for all the AcX measurements. It was impregnated on the 21st February, 1952, two days after its manufacture.

II.1.2. Exposure of the plates; Development and post-development treatment.

All the work on AcX to be described in this thesis depends upon the diffusion of An through the nuclear emulsion. The ability of the An to diffuse is a rapidly increasing function of the moisture content of the emulsion, which in turn is an increasing function of the relative humidity of the surrounding air. Because of the short half-life of An, ease of interpretation of the events requires the emulsion to be as porous, and hence as moist, as possible. However, high relative humidity during storage introduces other complications. It increases the grain spacing of the electron tracks, and this makes it more difficult to decide whether the beginning of a given electron track coincides with that of the separated α-track or with the vertex of the $3-\alpha$-track star. Also high relative humidity during storage introduces uncertainties regarding the stopping power and shrinkage factor of the emulsion. For these two reasons, especially the last, the relative humidity used, namely 44%, was no higher than that normally employed for nuclear

emulsion work in this laboratory.

Since the stopping power of the emulsion depends markedly on its moisture content and since the initial energies of the particles studied were inferred from their ranges, it was desirable that all the disintegrations should have taken place while the emulsion condition was constant. It was inevitable, however, that some of the disintegrations would occur in wet emulsion during impregnation and development. In order that these be relatively few, a weakly active impregnating solution should be used and the plates should be given as long an exposure at 44% relative humidity as possible. But the rate of disintegration of the AcX decreases exponentially with a half-life of 11.2 days, while the formation of cosmic ray background goes on at an approximately constant rate. Hence, an optimum must be found; after several trials, an exposure time of four days appeared to be a reasonable approximation to this optimum.

The plates were developed according to the temperature development method of Dilworth, Occhialini and Payne (1948). The solutions used are specified in Table III.

The developer was chilled to approximately $4^{\circ}C$ (temperature of water at its maximum density). The plates were immersed in distilled water at room temperature, the water + plates were gradually cooled to

$4^{o}C$, and then the plates were transferred to the developer. After 30 minutes, during which time the developer diffused into the plate but reacted chemically to only a very slight extent, the plates and developer were transferred to a bath at $22.2^{o}C$. The development was allowed to proceed for 20 minutes since it was found that this produced plates in which even minimum ionization tracks were fully developed, yet caused the formation of relatively few 'fog' grains. The plates were then put into the stop bath for 20 minutes. ~~By the end of this time a layer of silver had formed on the emulsion surface. This was~~ At the end of this time the layer of silver present on the emulsion surface was gently rubbed off with a moist finger. Next the plates were transferred to the fixing bath ($18.5^{o}C$), and left there in a horizontal position for one-and-a-half times the length of time required for complete clearing. The total fixing time varied from one batch of plates to another, but was usually about 15 hours.

At the end of this time, water at room temperature was dripped into the fixing bath at the rate of about 3 ml. per minute. After an hour, this rate was increased gradually until the initial hypo concentration had been reduced by a factor of about 10. Then the plates were washed in a current of tap water until a sample of the wash water was no more effective in decolourizing a dilute $KMnO_4$ solution than was water straight from the tap+. The plates were then set out

+ For details of this sensitive test for residual hypo, see Ilford Manual (Jan. 1953), p. 211.

to dry, still in a horizontal position.

After drying, the plates were soaked in the glycerine solution for an hour, and then set out to dry again. This was an attempt to replace the glycerine leached out of the emulsion during processing, in order that the emulsion be tougher and less likely to peel in the dry atmosphere of the laboratory.

Amidol (2,4 diaminophenol dihydrochloride) developers, with or without restrainers, produced poorer results than the Elon development described above. Even if the plates were removed from the developer during the 'warm stage', the uppermost five or ten microns of emulsion showed excessively heavy development. It was thought that this was an oxidation effect, and so it was hoped to avoid it by providing the emulsion with a close-fitting cover of tissue paper. This caused a slight improvement, but the Elon result was still much better.

II.1.3. Microscopic examination of the plates.

The plates were studied under a Watson Bactil binocular microscope (2 mm oil immersion objective, X10 holoscopic eyepieces), the rated overall magnification being 980 diameters. Photographs of representative events are shown on the following pages.

Before the events in a region of a plate were studied intensively, the entire region was mapped out

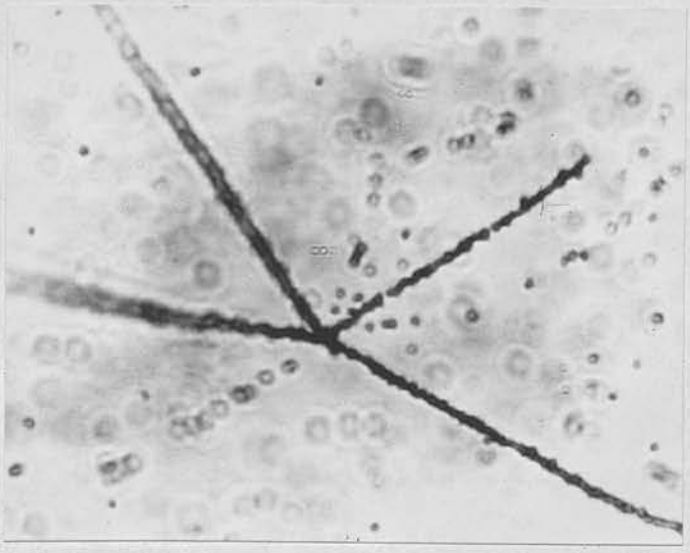

Figure 2a. A typical example of a star in which no α-track separation can be discerned. In addition to the four α-tracks, three electron tracks radiate from the origin of this event. Two of these are due to β-particles and the third to an internal conversion electron. However, it is possible neither to decide which is the internal conversion electron, nor to attribute it to a particular decay in the series.

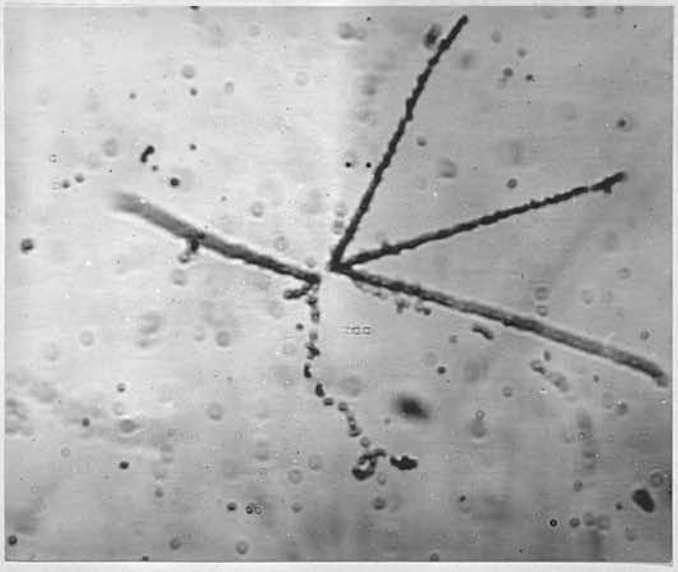

Figure 2b. A case of clear separation of the AcX α-track. Two internal conversion electrons have been emitted in cascade during the de-excitation of the An nucleus. The two β-particles of the series can be seen associated with the 3-α-track star.

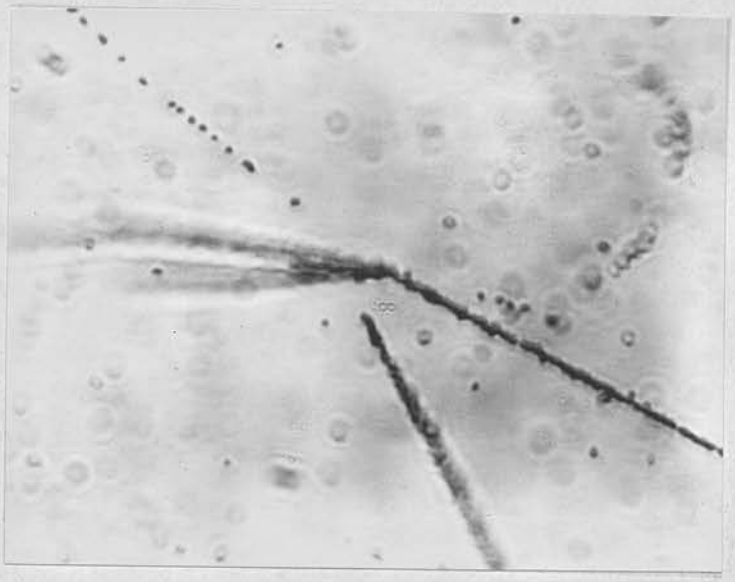

Figure 2c. An event in which no conversion electron tracks are associated with the separated α-track. The two β-tracks radiate from the 3-α-track star.

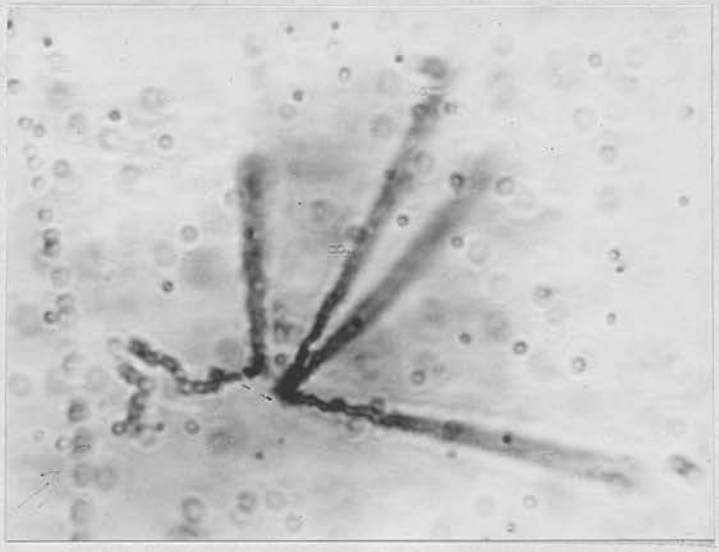

Figure 2d. Here a single conversion electron track has a common origin with the separated α-track. The β-particle tracks have too steep an inclination with the plane of the photograph to be visible. A background electron track passes the event on the left.

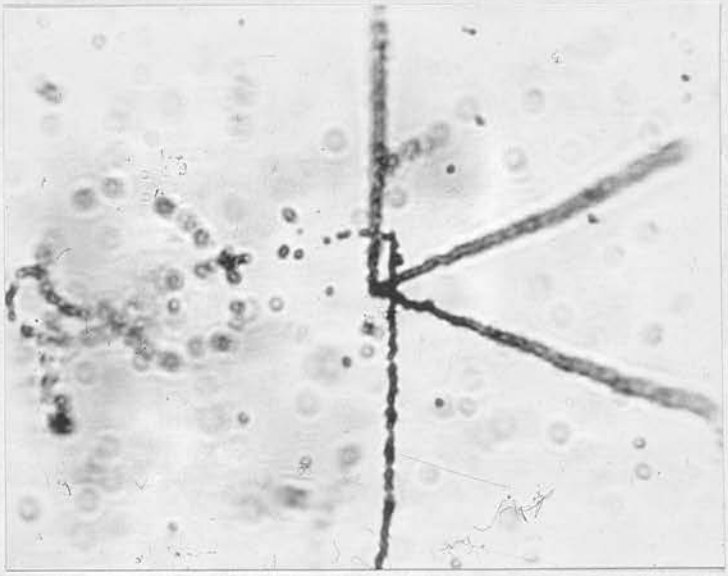

Figure 2e. One electron track is definitely associated with the separated α-track. The two or three grains at the right of this α-track near its beginning may or may not be a second electron track.

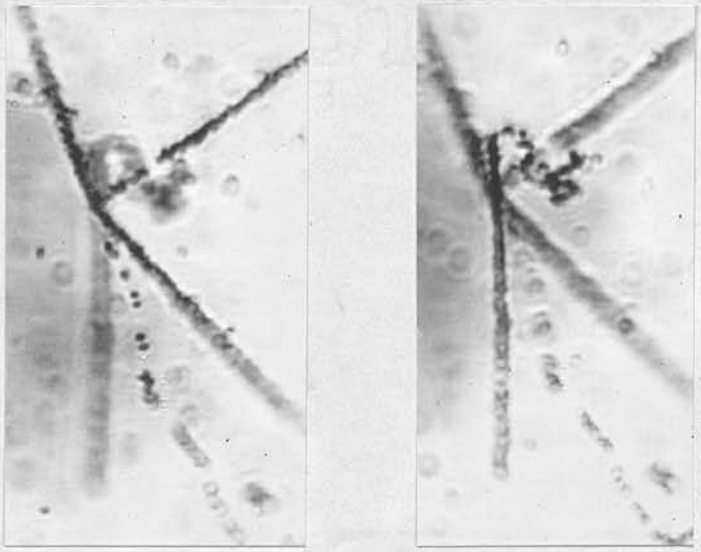

Figure 2f. These two photographs, taken at slightly different depths in the emulsion, show that the low energy electron track is associated with the separated α-track rather than the star, while the reverse is true of the high energy electron track.

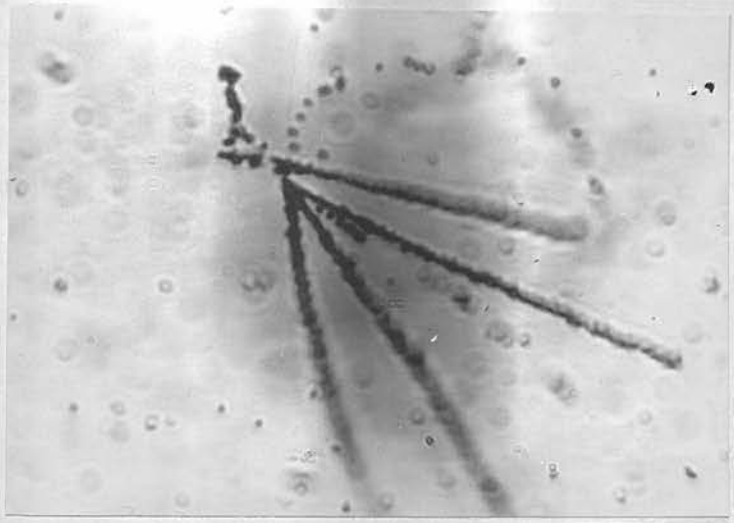

Figure 2g. Here an α-track is definitely separated, but it is impossible to decide whether the electron track on the left has as its origin the vertex of the 3-α-track star or the separated α-track. Hence this track may or may not have been produced by an AcX conversion electron.

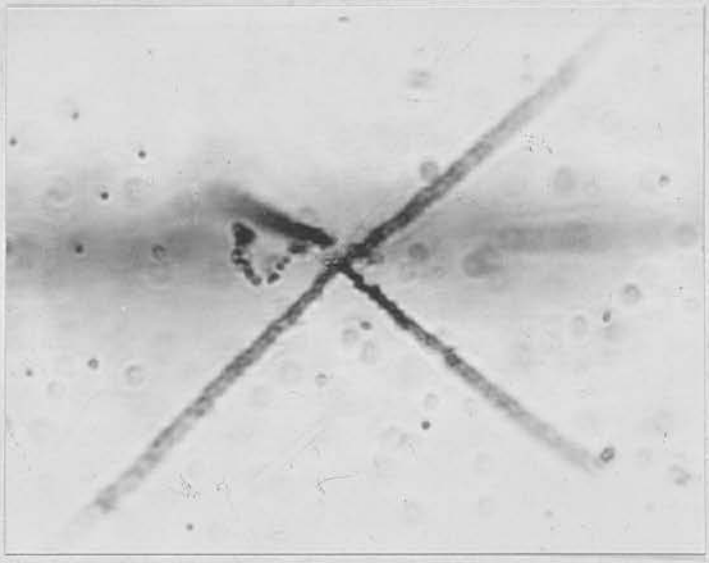

Figure 2h. The origin of the low energy electron track probably coincides with that of the separated α-track, but one cannot be certain of this. The dark band across the middle of the photograph is due to a heavily ionizing background particle passing immediately under the event.

onto squared paper, using a magnification of 450 diameters. Then the events were studied in turn under the higher magnification. Because of this, and because each α-particle star had a distinctive geometry, it was possible to locate at will any previously studied event.

As has been pointed out in §I.3, the experiments to be described depend upon the possibility of identifying the tracks produced by the conversion electrons accompanying the AcX disintegration as those having a common origin with the separated α-track. Since electrons were emitted during disintegrations that occurred farther down the series, electron tracks also radiated from the 3-α-particle stars. The principal difficulty of this work arose during the attempt to attribute each individual electron track to one of these two classes.

It was of the greatest importance that the criterion used in the selection of events for study should have no distorting effect on the various spectra that it was the purpose of this investigation to determine. Such distortion might have been introduced if the events were accepted or rejected on the basis of difficulty of interpretation. It is fairly certain that this would have resulted in a bias against those events in which two or more internal conversion electrons were associated with a single AcX

disintegration. The criterion finally accepted was the following: accept an event for study if and only if the An nucleus had diffused to a point outside a cylinder of unlimited length whose axis lay along the AcX α-particle, and whose radius was one micron. Since the phenomena governing this diffusion were independent of the mode of de-excitation of the An nucleus, it can be assumed that the sample of events studied was random with respect to the spectrum of internal conversion electrons resulting from this de-excitation.

The reason that account was taken not only of the magnitude of the resulting diffusion but also of its direction, is that occasionally gaps one or two microns long were seen in apparently well-developed α- tracks. If such a gap had occurred at the very beginning of an α-track which did in fact radiate from a 4-α-track star, the event would have been indistinguishable from one in which genuine diffusion had taken place. However this seemingly separated α-track would have pointed directly to the intersection of the other three α-tracks, and hence would have been unacceptable according to the criterion specified above.

There remains another possible source of statistical error. From the data of Rosenblum (1952), the most energetic AcX α-particles produced recoiling An

atoms of energy 107 keV, while the recoil energy due to the slowest AcX α-particles was 99 keV. Is it possible that the additional recoil energy in the first instance increased the probability that the diffusion criterion would be satisfied? If this were the case, a bias would have been introduced against events in which the higher energy levels of An were excited by α-disintegration. However, the recoil impulse given to the An atom lay along the direction of the AcX α-particle, whereas it was the amount of diffusion perpendicular to this direction that decided whether an event was to be accepted or not. Also, the increment of 8 keV out of approximately 100 keV is small. No data are available on the stopping power of nuclear emulsion for An atoms, but using Weyl's (1953) results for neon penetrating an atmosphere of hydrogen, this extra energy would have resulted in a range difference of about 0.05 microns. For these two reasons, the possible error arising from this effect has been considered to be negligible.

Approximately 10,000 4-α-track stars were examined; 809 of these were acceptable according to the above criterion. Even among this class of acceptable events, considerable difficulties of interpretation were encountered. A disproportionally great amount of time was spent on these difficult events, and rather little information was obtained from them. Other

methods of selecting events were considered, with the hope of increasing the speed or efficiency of data collection. In each case it was felt that any gains achieved were hardly worth the sacrifice in statistical validity that the faster method entailed.

After each of the 809 events was interpreted, measurement was made of the three-dimensional path lengths of all electron tracks that could be identified with definiteness as having been produced by AcX conversion electrons. The number of grains in each of these tracks was estimated. A grain count was also taken for those tracks which could possibly have been due to AcX conversion electrons, but for which a definite decision was impossible. The three-dimensional range of the separated α-track was measured for the first 556 events studied.

Measurements of horizontal projection were performed with a calibrated eyepiece graticule (approximately 1.0 microns per division); depth measurements involved the use of a graduated fine-focussing adjustment (approximately 0.8 microns per division). The scales used in both cases could be nominally read to the nearest 0.1 micron. This, however, does not reflect the true accuracy of the measurements. Further consideration of this point is given in the next section.

II.2. The Effects of Observational Errors.

In nuclear emulsion spectrometry, the initial energy of an ionizing particle is inferred from an estimate of its path length. This estimate must be made from a study of the configuration of the grains that compose the track of the particle. The track is first analyzed into straight line segments, the length of each segment is obtained from measurements of its horizontal and vertical projections, and then these lengths are summed to give the total track length. In the case of an α-particle track, the entire track usually consists of just one segment. The path of an electron is more tortuous, especially near the end of its range, and so an estimate of its path length requires the measurement of a large number of segments+.

In accordance with current practice the measurements were made between the centres of the grains that defined the ends of the segments. It is of importance to know how this population of grain centre to grain centre distances is related to the population of true path lengths, since only the former is accessible to measurement, while the latter is the one of theoretical interest. Unfortunately, the connection between these two populations is hopelessly complicated. It depends upon the exact spatial distribution of grains in the original emulsion and upon the exact positioning

+ For tracks produced by electrons of initial energy about 350 keV, the number of segments was sometimes greater than 90.

of the path of the particle with respect to these grains. There is no guarantee that the centre of the observed clump of silver (diameter 0.6 - 0.7 microns) coincides exactly with the centre of the undeveloped grain (mean diameter ~ 0.18 microns). ~~(diameter 0.3 - 0.4 microns).~~ Superposed on these uncertainties are the difficulties of measuring such small distances. This is especially true of the depth measurements, where the finite depth of focus of the microscope and the imperfections in the focussing mechanism severely limit the accuracy.

A complete mathematical treatment of the problem is out of the question. A mathematical model which can be handled, and which has some of the features of the actual situation, is the following:

Segments whose true lengths, ℓ , are distributed with mean $\bar{\ell}$ and standard deviation $s = \sqrt{\overline{(\ell - \bar{\ell})^2}}$, have directions which are distributed isotropically in space and independently of the segment lengths. Consider a large number of segments, all produced by particles whose true horizontal projections are equal to x. Then it is assumed that the measured horizontal projections, ξ , are distributed with mean $\bar{\xi} = x$. Similarly for segments whose true vertical projections are equal to y, the measured values, η , have as their mean $\bar{\eta} = y$. Moreover, $(\xi - x)$ and $(\eta - y)$ are distributed independently of each other and of ℓ. Then for ξ and η sufficiently close to x and y

respectively, the measured length, λ , is approximately given by the Taylor expansion,

$$\lambda = \sqrt{\xi^2 + \eta^2} \doteq \sqrt{x^2 + y^2} + \frac{x}{\sqrt{x^2 + y^2}}(\xi - x) + \frac{y}{\sqrt{x^2 + y^2}}(\eta - y) , \quad (1)$$

or $$\lambda = \ell + \cos\theta\,(\xi - x) + \sin\theta\,(\eta - y), \quad (2)$$

where θ is the angle between the segment and the horizontal plane. For tracks all having the same value of θ ,

$$\overline{\lambda} = \overline{\ell} + \cos\theta\,\overline{(\xi - x)} + \sin\theta\,\overline{(\eta - y)} = \overline{\ell}, \quad (3)$$

since $\overline{\xi} = x$ and $\overline{\eta} = y$. Also

$$\overline{\lambda^2} = \overline{\ell^2} + \cos^2\theta\,\overline{(\xi - x)^2} + \sin^2\theta\,\overline{(\eta - y)^2} + 2\cos\theta\,\overline{\ell\,(\xi - x)} + 2\sin\theta\,\overline{\ell\,(\eta - y)} + 2\sin\theta\cos\theta\,\overline{(\xi - x)(\eta - y)} . \quad (4)$$

Because of the independence of $(\xi - x)$, $(\eta - y)$, and ℓ ,

$$\begin{aligned} \overline{\ell\,(\xi - x)} &= \overline{\ell}\;\overline{(\xi - x)} \\ \overline{\ell\,(\eta - y)} &= \overline{\ell}\;\overline{(\eta - y)} \\ \overline{(\xi - x)(\eta - y)} &= \overline{(\xi - x)}\;\overline{(\eta - y)} , \end{aligned} \quad (5)$$

and since $\overline{\xi} = x$, $\overline{\eta} = y$, equation (4) reduces to

$$\overline{\lambda^2} = \overline{\ell^2} + \cos^2\theta\,\overline{(\xi - x)^2} + \sin^2\theta\,\overline{(\eta - y)^2} . \quad (6)$$

Hence

$$\sigma_\theta^2 \equiv \overline{(\lambda - \overline{\lambda})^2} = \overline{\lambda^2} - (\overline{\lambda})^2 = \overline{\ell^2} - (\overline{\ell})^2 + \cos^2\theta\,\overline{(\xi - x)^2} + \sin^2\theta\,\overline{(\eta - y)^2}$$

$$= s^2 + \cos^2\theta\,\overline{(\xi - x)^2} + \sin^2\theta\,\overline{(\eta - y)^2} . \quad (7)$$

This still refers to tracks inclined to the horizontal plane at an angle θ. Since, according to the assumptions, $\bar{\lambda} = \bar{\ell}$ is independent of θ, σ^2 for all angles may be obtained from σ_θ^2 by simple averaging:

$$\sigma^2 = \int_{\theta=0}^{\frac{\pi}{2}} \sigma_\theta \, P(\theta) \, d\theta \quad . \tag{8}$$

Here $P(\theta)d\theta$ is the probability distribution of angles θ. From Figure 3 it can be seen that the assumption of an isotropic spatial distribution implies that $P(\theta) = \cos\theta$. Then

$$\sigma^2 = s^2 \int_{\theta=0}^{\frac{\pi}{2}} \cos\theta \, d\theta + \overline{(\xi-x)^2} \int_{\theta=0}^{\frac{\pi}{2}} \cos^3\theta \, d\theta + \overline{(\eta-y)^2} \int_{\theta=0}^{\frac{\pi}{2}} \sin^2\theta \cos\theta \, d\theta$$

$$\sigma^2 = s^2 + \frac{2}{3}\overline{(\xi-x)^2} + \frac{1}{3}\overline{(\eta-y)^2} \quad . \tag{9}$$

This derivation makes no assumption about the natures of the various populations involved. However, the validity of the expansion (1) depends upon the uncertainty in the measurements of horizontal and vertical projection being small compared to the segment lengths. This invalidates formula (9) for use with low energy electron tracks. It should be applicable to the α-track measurements if suitable values are taken for $\overline{(\xi-x)^2}$ and $\overline{(\eta-y)^2}$. Upon consideration of the various factors involved, these are taken to be 0.04 microns^2 and 0.25 microns^2 respectively. For normal distributions of ξ and η about x and y,

$$\frac{\left(\begin{array}{c}\text{AREA SUBTENDING THE SOLID}\\ \text{ANGLE BETWEEN } \theta \text{ AND } \theta+d\theta\end{array}\right)}{\text{AREA OF OCTANT}} = \frac{\frac{1}{4} \times 2\pi R\cos\theta \times R\,d\theta}{\frac{1}{8} \times 4\pi R^2}$$

$$= \cos\theta\, d\theta$$

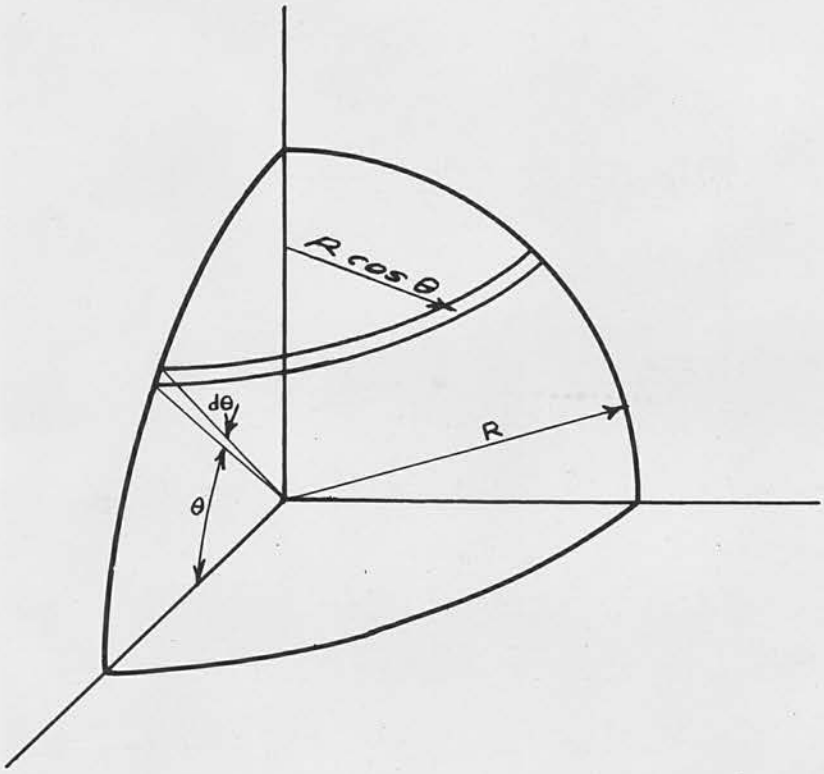

FIGURE 3.

these would correspond to curves whose widths at the points of inflection were 0.4 microns and 1.0 microns respectively. Using these values, equation (9) shows that the observational errors increase the square of the true population standard deviation by 0.11 microns^2.

The above derivation obtains only the measured standard deviation in terms of the true one. If it is desired to determine the complete measured distribution, more involved considerations are necessary. These are given in Appendix I.

II.3. The Depth Correction.

To compute the distance in the original emulsion between two nearby points, it is necessary to measure both the horizontal and vertical projections of the straight line segment joining them. As stated on page 26, the former was measured with a calibrated eye-piece graticule and the latter with the fine-focussing adjustment of the microscope. The problem to be discussed now is that of determining the relationship between the true vertical projection of the segment in the original emulsion and the angle through which the fine adjustment must be turned, when examining the processed plates, in order to change the plane of focus from one end of the segment to the other+. This

+ In order to minimize lag in the fine adjustment mechanism, the microscope tube was always racked upwards during measurement.

relationship may be conveniently expressed as,

vertical projection in unprocessed emulsion = K x reading of fine adjustment scale.

It is then necessary to determine K and to study its variation with position in the emulsion and with steepness of track. There are essentially two ways of doing this:

(i) One may create in the original emulsion a population of tracks having a known angular distribution, and choose K such that the observed angular distribution is identical with it.

(ii) One may create in the original emulsion a population of tracks whose range distribution is a known function of steepness, and choose K such that the observed range distribution is the same function of steepness.

Using a modification of method (i) in which a spatially isotropic distribution of α-tracks was obtained by bombarding lithium loaded plates with thermal neutrons, Rotblat and Tai, (1949), found that K is independent of depth in the emulsion. Using method (ii), they found that the value of K obtained from the ratio of the thicknesses of the unprocessed and processed emulsions caused their ranges to increase with track steepness, whereas they could expect that the true ranges were independent of steepness. They concluded that this value of K is applicable to tracks

whose angle with the horizontal is less than about 30°, but that a smaller value must be used for steeper tracks. Jenny and Hürlimann (1951) have pointed out that if Rotblat and Tai had decreased their value of K by 23% they would have observed no dependence of length on angle. Their own work indicated that K is indeed independent of both depth in the emulsion and steepness of track. Again, Horan (1953) has exposed plates to Po^{210} α- particles and, in agreement with Rotblat and Tai, observed an increase of length with angle, whereas Greenberg and Haslam (1953) have remarked that if Horan had used a lower shrinkage factor he would have observed none. These latter authors have applied both methods (i) and (ii) of page 32, and like Jenny and Hürlimann, have reached the conclusion that K is independent of steepness and depth.

Rotblat and Tai (1949) suggest as explanation of their observed dependence of K on steepness that during shrinkage, grains on a steep track come into contact with each other, and so are prevented from following the further displacement of the emulsion. The important range measurements of the present work are of the tracks of electrons which, except at the very ends of their paths, have a much lower grain density than those of the heavily ionizing α- particles studied by Rotblat and Tai. For this reason, and also because the method of depth correction used in this

work is modelled on those of Jenny and Hürlimann (1951) and Greenberg and Haslam (1953), K is considered to be independent of track angle.

Under ordinary conditions of observation, K may not be constant in time. Its variation with the relative humidity of the surrounding air has been investigated by Martin (1949). In the present investigation a day to day change of 7% was not uncommon. However, this variation was not so rapid as to cause a change in the ratio of the vertical projection of a segment to the overall thickness of the processed emulsion at a fixed reference point. Therefore, this overall thickness was measured at the beginning and end of each session of observations, and the vertical projection of each segment was expressed as such a ratio. It then remained only to find the thickness of unprocessed emulsion to which the overall thickness at the reference point corresponded. This was done by method (ii) of page 32.

The tracks used for this purpose were those of the AcX α-particles.+ Let M be an assumed thickness of unprocessed emulsion corresponding to the overall thickness at the reference point and $M(1 + \epsilon)$ be the true thickness. The problem now is the determination of ϵ. For a track for which the horizontal projection is ξ microns, the depth scale reading y divisions, and at a time when the depth scale reading for the

+ For confirmation of the identification of these tracks see § II.4 below.

overall thickness of the processed emulsion at the reference point is d,

$$\text{computed length} = z' = \sqrt{\xi^2 + \left(\frac{M}{d} y\right)^2} \,,$$

$$\text{true length} = z = \sqrt{\xi^2 + \left(\frac{M(1+\epsilon)}{d} y\right)^2} \,. \tag{10}$$

Then $$z'^2 - z^2 = -\left(\frac{M}{d} y\right)^2 \epsilon(2+\epsilon)$$

$$1 - \frac{z^2}{z'^2} = -\frac{\left(\frac{M}{d} y\right)^2}{z'^2} \epsilon(2+\epsilon) = -\epsilon(2+\epsilon)\sin^2\theta'$$

where θ' is the track angle computed on the basis of the assumed M. Then

$$z' = \frac{z}{\sqrt{1 + \epsilon(2+\epsilon)\sin^2\theta'}} \,. \tag{11}$$

The AcX α-tracks did not all have the same true range. However the mean true range, $\overline{z}$, should have been independent of angle. Then from (11) the mean measured range, $\overline{z'}$, should have had the following angular dependence+

$$\overline{z'}(\sin\theta') = \frac{\overline{z}}{\sqrt{1 + \epsilon(2+\epsilon)\sin^2\theta'}} \,. \tag{12}$$

For purposes of comparison with experiment it is useful to have the average value of $\overline{z'}(\sin\theta')$ over a finite range of $\sin\theta'$. To get this from (12) one must have the probability distribution of $\sin\theta'$. If it is assumed, as in §II.2, that the true angle, θ, is distributed isotropically, the distribution of $\sin\theta$, $P(\sin\theta)$, is given by (see Figure 3, page 30).

$$P(\sin\theta)\, d(\sin\theta) = d(\sin\theta).$$

+ $\overline{z'}(\sin\theta')$ indicates that $\overline{z'}$ is to be regarded as a function of $\sin\theta'$.

Then the distribution of $\sin\theta'$ is simply

$$P'(\sin\theta')\, d(\sin\theta') = \frac{d(\sin\theta)}{d(\sin\theta')}\, d(\sin\theta') \qquad (13)$$

From the equation $\tan\theta = (1+\epsilon)\tan\theta'$, it follows immediately that $\sin\theta = \frac{(1+\epsilon)(\sin\theta')}{\sqrt{1+\epsilon(2+\epsilon)\sin^2\theta'}}$ and hence

$$P'(\sin\theta')\, d(\sin\theta') = \frac{(1+\epsilon)\, d(\sin\theta')}{\left[1+\epsilon(2+\epsilon)\sin^2\theta'\right]^{3/2}} \qquad (14)$$

Then the mean value of $\overline{z'}(\sin\theta')$ over that range of θ' for which $h_1 < \sin\theta' < h_2$, which is designated as $\overline{z'}_{h_1 h_2}$, is

$$\overline{z}_{h_1 h_2} = \int_{\sin\theta'=h_1}^{h_2} \overline{z'}(\sin\theta')\; P(\sin\theta')\, d(\sin\theta') = (1+\epsilon)\overline{z}\int_{\sin\theta'=h_1}^{h_2} \frac{d(\sin\theta')}{\left[1+\epsilon(2+\epsilon)\sin^2\theta'\right]^2}$$

$$\overline{z'}_{h_1 h_2} = \frac{1}{2}\frac{(1+\epsilon)\overline{z}}{\sqrt{\epsilon(2+\epsilon)}}\left[\arctan\left(\sin\theta'\sqrt{\epsilon(2+\epsilon)}\right) + \frac{\sqrt{\epsilon(2+\epsilon)}\sin\theta'}{1+\epsilon(2+\epsilon)\sin^2\theta'}\right]_{\sin\theta'=h_1}^{h_2} \qquad (15)$$

Making use of the expansions

$$\arctan\phi = \phi - \tfrac{1}{3}\phi^3 + \tfrac{1}{5}\phi^5 - \tfrac{1}{7}\phi^7 + \cdots \qquad \phi^2 < 1$$

$$\frac{1}{1+\phi^2} = 1 - \phi^2 + \phi^4 - \phi^6 + \cdots$$

equation (15) can be written

$$\overline{z'}_{h_1 h_2} = \overline{z}(1+\epsilon)\left[\sin\theta' - \tfrac{2}{3}\epsilon(2+\epsilon)\sin^3\theta' + \tfrac{3}{5}\epsilon^2(2+\epsilon)^2\sin^5\theta' - \cdots\right]_{\sin\theta'=h_1}^{h_2}$$

$$= \overline{z}(1+\epsilon)\left[(h_2-h_1) - \tfrac{2}{3}\epsilon(2+\epsilon)\left(h_2^3-h_1^3\right) + \tfrac{3}{5}\epsilon^2(2+\epsilon)^2\left(h_2^5-h_1^5\right) - \cdots\right] \qquad (16)$$

$$\doteq \overline{z}(1+\epsilon)(h_2-h_1)\left[1 - \tfrac{2}{3}\epsilon(2+\epsilon)\left(h_2^2 + h_2h_1 + h_1^2\right)\right]$$

where the terms of higher orders of ϵ have been neglected since ϵ is small.

Now if the range of $\sin\theta'$ (i.e. 0 to 1) is divided up into equal intervals, and if the lower and upper limits of a typical interval are h_1 and h_2 respectively, a plot of $\overline{z'}_{h_1 h_2}$ versus $(h_2^2 + h_2h_1 + h_1^2)$ should, according to (16), yield a straight line of slope $-\frac{2}{3}\epsilon\overline{z}(1+\epsilon)(2+\epsilon)(h_2 - h_1)$ and intercept $\overline{z}(1+\epsilon)(h_2 - h_1)$. From the ratio of these quantities, ϵ is directly obtainable.

Figure 4 shows such a plot for the best 400 tracks measured. Here $(h_2 - h_1)$ is taken to be 0.1, and the track lengths were computed on the basis of an assumed M of 182μ,+ since work on a previous plate indicated that this was a reasonable value. The vertical line at each point represents plus and minus the standard deviation of $\overline{z'}_{h_1 h_2}$, as computed from the lengths of the tracks in the particular interval of $\sin\theta'$. The trend line shown is that obtained by the method of least squares, weighting each point with the square of the reciprocal of its estimated standard deviation. The point for the interval $0.9 < \sin\theta' < 1$ ($64^0 9' < \theta < 90^0$) has been omitted in this calculation since it was felt that the shrinkage behaviour of such

+ The reason that this is considerably less than the nominal thickness of 200μ is that the emulsion surface was rubbed during processing to remove surface stain (see page 21).

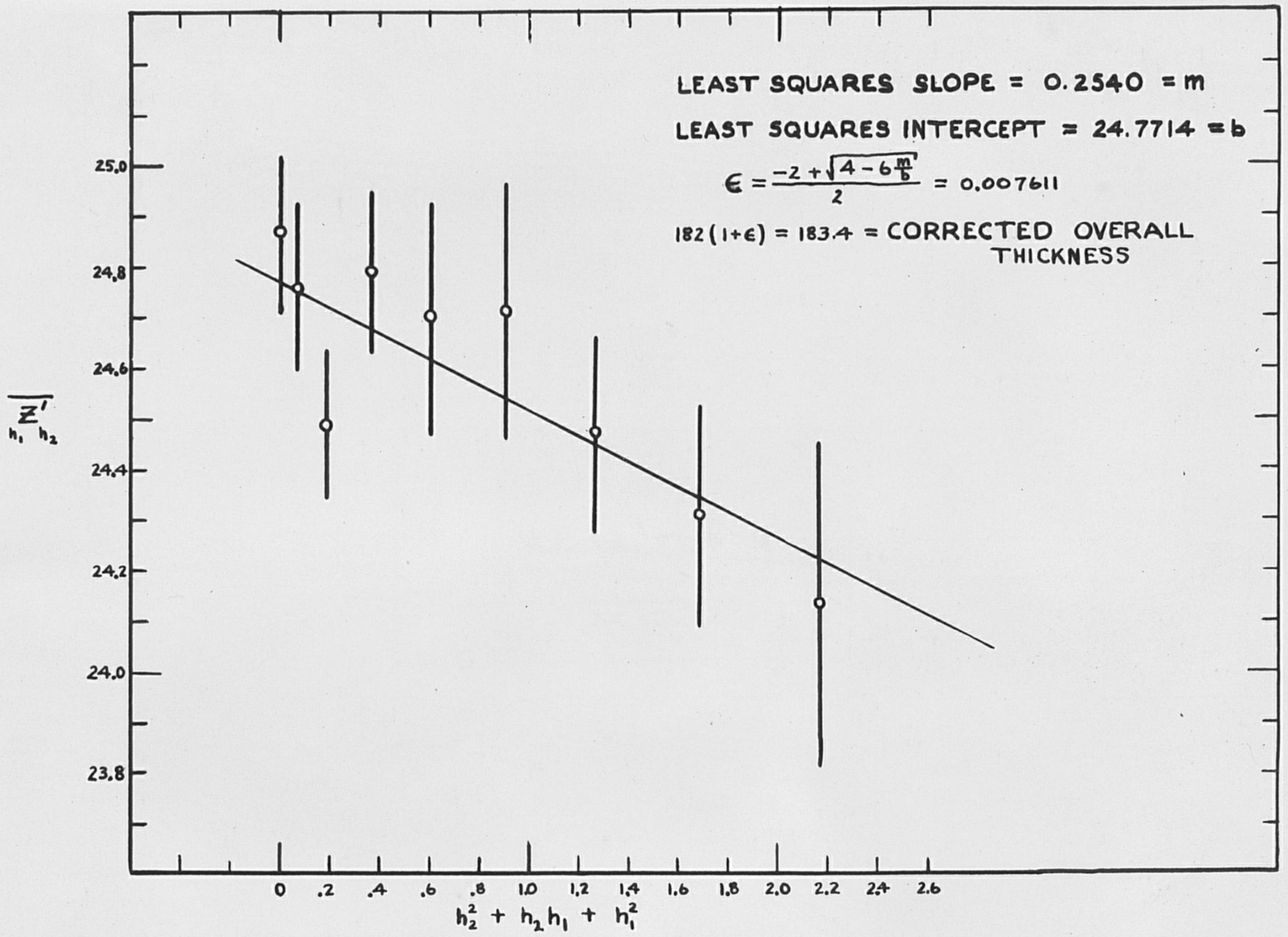

FIGURE 4. DETERMINATION OF DEPTH CORRECTION

steep α-tracks would be totally different from that of electron tracks. From the ratio of the least squares slope and intercept it has been calculated that the true overall thickness at the reference point should have been $183.4 \pm 0.4\ \mu$. (The figure given here for the uncertainty is the standard deviation of $182(1 + \epsilon)$ computed on the basis of the observed standard deviation of each value of $\overline{Z'}_{h.h_2}$ and on the functional dependence of ϵ on these values of $\overline{Z'}_{h.h_2}$ as expressed by the method of least squares).

II.4 The α-ranges.

The 3-1 disjunction of the AcX stars illustrated in Figures 2a to 2h could conceivably have been caused by the diffusion of either An or AcB or C, that is, the separated α-track may have been that of either the first or fourth α-particle in the series $^{223}Ra \rightarrow {}^{207}Pb$ (see Figure 1, page 3). If the mechanism of star formation proposed by Eichholz and Flack (1951) is correct, only the electrically neutral An should have been capable of diffusion, and hence the population of separated α-tracks should have been identical with the population of AcX α-tracks. However, Demers (1947) has detected diffusion in a nuclear emulsion of ThA, ThB, ThC and ThC' as well as Tn. Hence it is of importance to investigate this question

further in the case of the actinium series.

To this end, measurements were performed of the ranges of all four of the α-tracks radiating from each of 100 stars in which no diffusion had taken place. A histogram of these measurements is shown in Figure 5. Also shown there are a histogram of the measured ranges of those separated AcX α-tracks in which no discernible bends occurred, and a histogram computed on the following assumptions:

(i) The energies of the mono-energetic groups of α-particles emitted by AcX, An, AcA and AcC are those given in the Table of Isotopes (Hollander, Perlman, Seaborg, 1953).

(ii) The ranges of the tracks of a mono-energetic group of α-particles are distributed normally with mean equal to the value given by the mean range-energy calibration of Rotblat (1950) and with standard deviation equal to one micron.

This histogram is normalized to 400 tracks since it is to be compared to the histogram of the α-tracks from the 100 stars. It is clear that the computed and observed histograms agree fairly well, which serves to confirm assumptions (i) and (ii). The few anomalously long and short tracks are probably caused by the line shape for the tracks of a mono-energetic group not going to zero as strongly as the normal curve for large

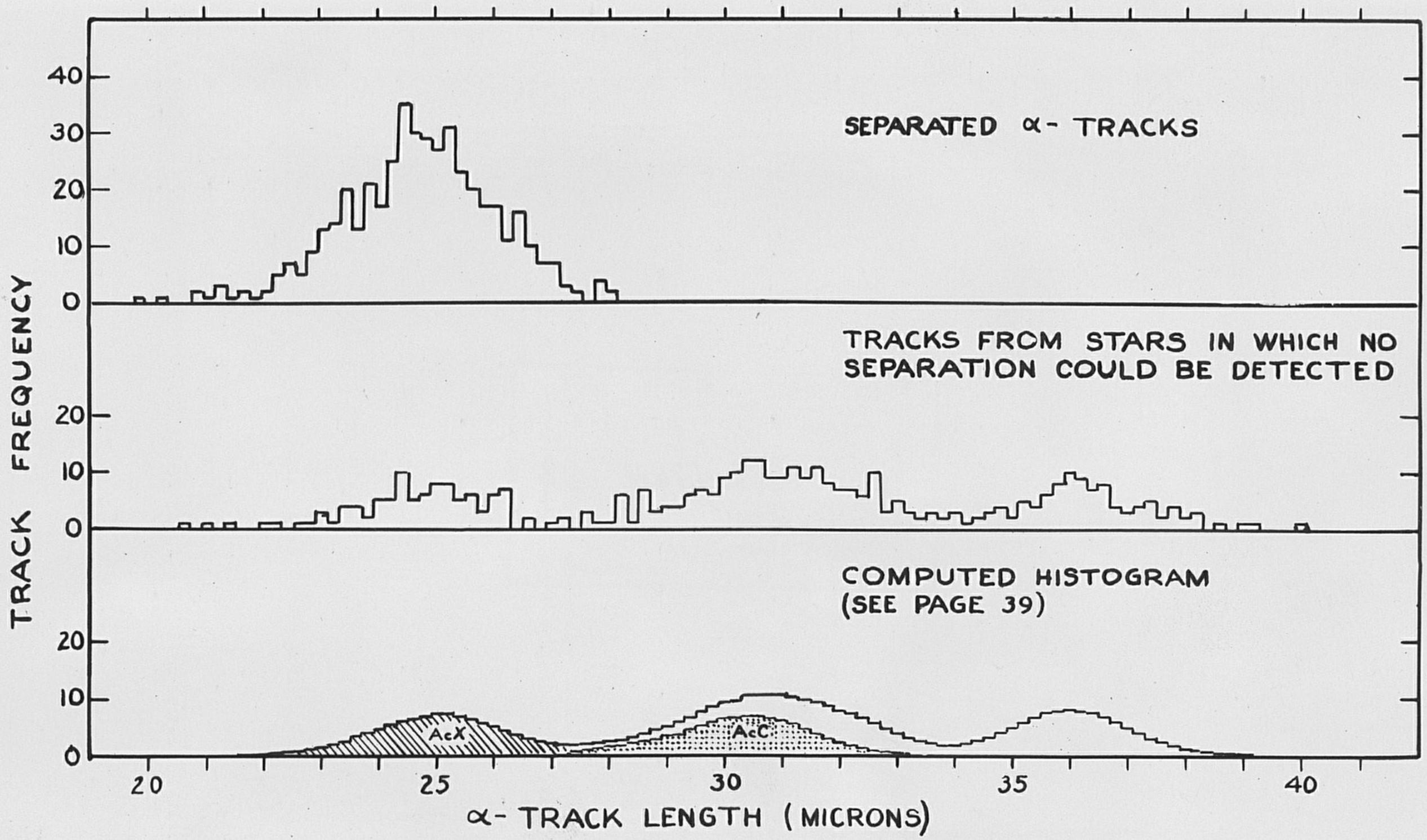

FIGURE 5. α-PARTICLE HISTOGRAMS FOR THE SERIES AcX → AcPb.

deviations from the mean.

It is also clear from Figure 5 that the histogram of separated α-tracks coincides with the computed AcX histogram rather than with the computed AcC histogram. Of the 457 ranges of separated tracks, only the longest ten or fifteen could have been due to AcC α-particles. However, in each of these cases the other three α-tracks, the ones radiating from the 3-track star, were too long to be attributable to AcX α-particles, and indeed had ranges compatible with the assumption that they were due to the α-particles of An, AcA and AcC. It is therefore concluded that the population of separated α-tracks is identical with the population of AcX α-particle tracks.

Figure 6 shows the contributions of the component groups of the AcX α-spectrum, computed on assumptions (i) and (ii) of this section. The histogram of ranges of the separated α-tracks is shown here as well. From this figure it is evident that the energy differences between the groups are too small compared with the resolution of the nuclear emulsion to enable the α-track measurements of this work to be of any value in the analysis of the AcX α-spectrum.

FIGURE 6

OBSERVED AND COMPUTED HISTOGRAMS OF THE RANGES OF AcX α-PARTICLES IN G5 EMULSION

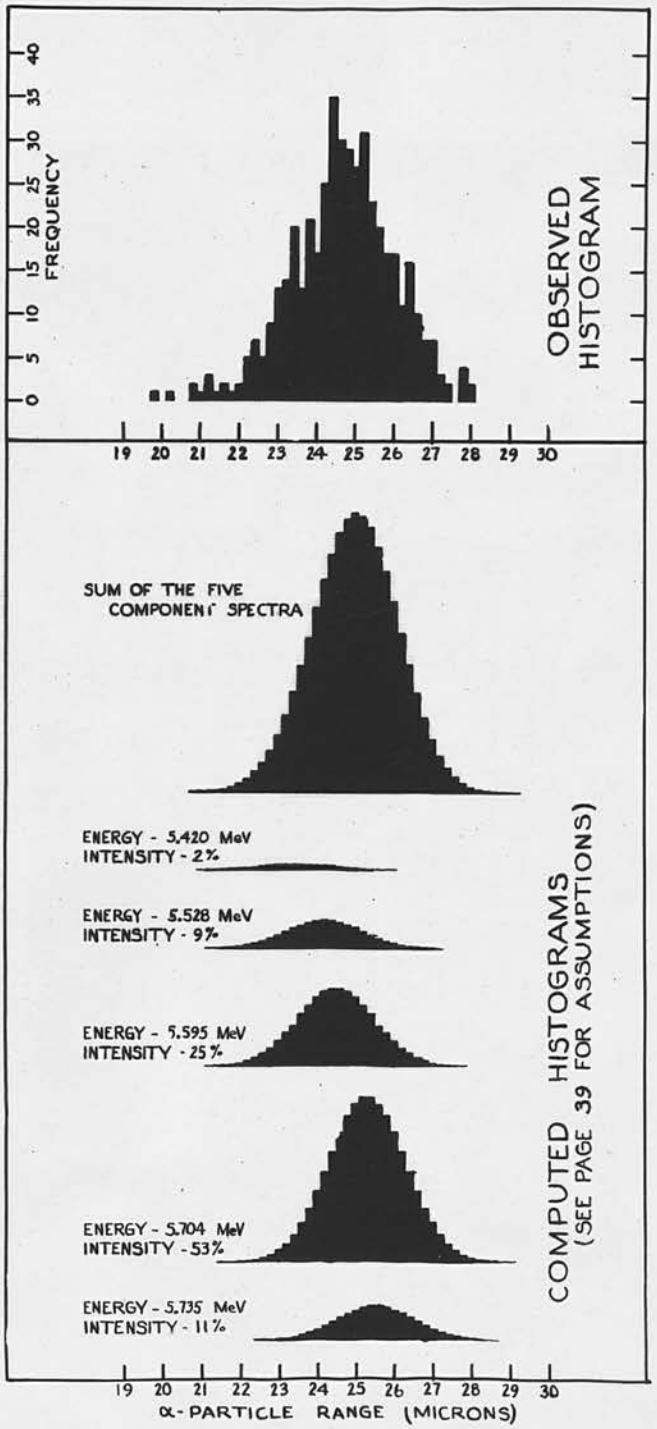

CHAPTER III.

CONVERSION ELECTRON SPECTROMETRY IN NUCLEAR EMULSIONS.

III.1. Introduction.

From the point of view of nuclear emulsion spectrometry the most important attribute of the conversion electron spectrum is its discreteness. Each homogeneous group of electrons produces its characteristic population of tracks; the total track population of the plate is the superposition, with appropriate intensities, of these characteristic populations. In spectrometry, the total population is inferred from a random sample of tracks and then an attempt is made to analyze this into its component characteristic groups. Clearly, the population of tracks produced by a monoenergetic group of electrons is of fundamental importance in this work. Therefore, this chapter will begin with a discussion of the nature of this population. Then the problem of analyzing an observed histogram will be considered. Some of the points raised will be illustrated in the last part of the chapter when the experimental results on the AcX internal conversion spectrum are presented.

III.2. The Track Distributions.

When a rapidly moving electron interacts with the atoms of a surrounding material, its energy is decreased by three different processes: excitation,

ionization, and Bremsstrahlung (radiation). To compare the importance of the radiation losses to the other two processes, an approximate formula given by Bethe and Heitler (1934) can be used:

$$\frac{\left(\frac{\overline{dE}}{dR}\right)_{rad.}}{\left(\frac{\overline{dE}}{dR}\right)_{ion.\ excit.}} \approx \frac{E Z}{816{,}000} \quad . \qquad (17)$$

This refers to electrons of energy E keV moving in a material of atomic number Z. $\overline{dE}$ is the average energy lost by these particles in moving the distance dR; $\frac{\overline{dE}}{dR}$ is frequently referred to as the stopping power. For 350 keV electrons, the most energetic ones encountered in this investigation, and for silver, the heaviest atom in the nuclear emulsion, this ratio is about $\frac{1}{50}$. Hence the ionization and excitation processes are principally responsible for the degradation of the energy of the electron.

The average energy transferred in a single collision is of the order of 20 eV. Thus an electron of initial energy 200 keV will experience about 10,000 of them. For a process of this sort - one consisting of an enormous number of very small additive contributions - the central limit theorem of statistics shows that most characteristics of the overall process are distributed normally. However these conditions are not rigorously met in the stopping of electrons since although the average energy loss per collision is small,

large single-energy transfers do occur. The result is that instead of the characteristics being distributed normally, and hence symmetrically, the distribution is skew. This effect is due principally to Bremsstrahlung. The reason is that for ionization and excitation collisions a large energy transfer is much less probable than a small one. But in the case of Bremsstrahlung the probability is roughly the same for emission of photons of all energies up to very nearly that of the incident electron. Hence, although the total energy transferred is governed principally by ionization and excitation, phenomena which depend upon the rare large collisions are governed by Bremsstrahlung.

The tracks produced by electrons whose initial energies are between about 20 and 350 keV are conveniently described by either their path lengths (ranges) or grain numbers. The concept of path length is more ambiguous than it at first appears. For, during the occasional large ionizing collision the incident electron may transfer enough energy to the atomic electron to enable the latter to produce a track of its own. Because of the indistinguishability of electrons, and because the incident electron can transfer any fraction of its energy to the atomic electron, it is absolutely impossible to say which of the resultant tracks is due to the deflected incident electron.

All that can be concluded is that the collision has resulted in two electrons having energies great enough to produce tracks. Thus the configuration of grains is not linear and the expression "length of an electron track" requires further definition. In cases such as this the convention is usually adopted that the longer of the two branches is taken as the track of the deflected incident electron. The principal advantage of this is the ease with which it can be formulated analytically, e.g. if the probability that an electron of energy E transfers an amount of energy between ϵ and $\epsilon + d\epsilon$ in a single collision is $P_E(\epsilon)d\epsilon$, then the probability of an observed (according to the above convention) energy transfer between ϵ and $\epsilon + d\epsilon$ is+ $\left[P_E(\epsilon) + P_E(E-\epsilon)\right] d\epsilon$ and the maximum single energy transfer is equal to $\frac{E}{2}$.

The best method of incorporating the length of the shorter of the two branches is the one that results in the smallest width for the track measurement population produced by a mono-energetic group of electrons. As has been pointed out, the amount of straggling depends principally on the radiation losses. For this reason it is usually considered that the contribution to the line width due to those collisions that produce branch tracks is so small that it is not worth taking

+ This is not strictly true since the longer of the two branches is not necessarily produced by the more energetic of the two electrons.

account of the ranges of the shorter of the two branch tracks. However, the usual practice is to count all the grains in both the branches. The idea here is that the grain number should depend on the total ionization, i.e. primary and secondary, in analogy with proportional counter methods.

The first experimental investigations of the populations of tracks in nuclear emulsion produced by mono-energetic groups of electrons were those performed by Zajac and Ross (1949). They exposed NT2A and NT4 plates to the β-rays of Pb^{212}, Bi^{210} and Ir^{192} in a low resolution β-spectrometer. By examining the tracks entering the surface of their emulsion within a 2 mm x 0.5 mm rectangle they obtained energy distributions whose half-widths were 1.2 keV at 30 keV and 2.3 keV at 250 keV. They measured both the ranges and grain numbers of tracks produced by electrons of energies 30, 40, 50, 60, 80, 100, 147, 200 and 250 keV. The number of tracks measured at each energy (25 to 50) was too small to justify an exact analysis of the line shape. The present author has tested these distributions for departure from normality using their third and fourth moments (Fisher, 1950). No significant departure was revealed. However, when dealing with small samples such tests are rather insensitive.

The standard deviation of each of these grain count and range distributions is about 20% of its

mean, a result very similar to that obtained by Williams (1930) from his measurements of the ranges of 20 keV electron tracks in a cloud chamber. Since there is approximate proportionality between group width and mean, it is convenient to plot histograms with log range or log grain count as abscissae. In the case of low grain numbers this procedure breaks down since a logarithmic interval may have zero population simply because there is no integer whose logarithm falls between limits of the interval. But the advantage of having the group width independent of energy fully compensates for this slight difficulty.

The mean range for each energy was found by Zajac and Ross to be in close agreement with the value predicted by collision theory. $\overline{\frac{dE}{dR}}$ for the emulsion was computed using Marton's and Schiff's (1941) ionization potentials in the Bethe (1933) stopping power expression, and the mean range for a homogeneous group of electrons of initial energy E was taken as,

$$\overline{R}(E) = \int_0^E \frac{1}{\overline{\frac{dE}{dR}}}\, dE. \qquad (18)$$

It has been pointed out by Williams (1928) that this procedure is not correct. The quantity that should have been integrated is $\overline{\frac{dR}{dE}}$ rather than $1/\overline{\frac{dE}{dR}}$. The first of these quantities refers to the mean

FIGURE 7.

MEAN RANGE vs. ENERGY FOR MONO-ENERGETIC GROUPS OF ELECTRONS

CALIBRATION OF ZAJAC AND ROSS (1949)

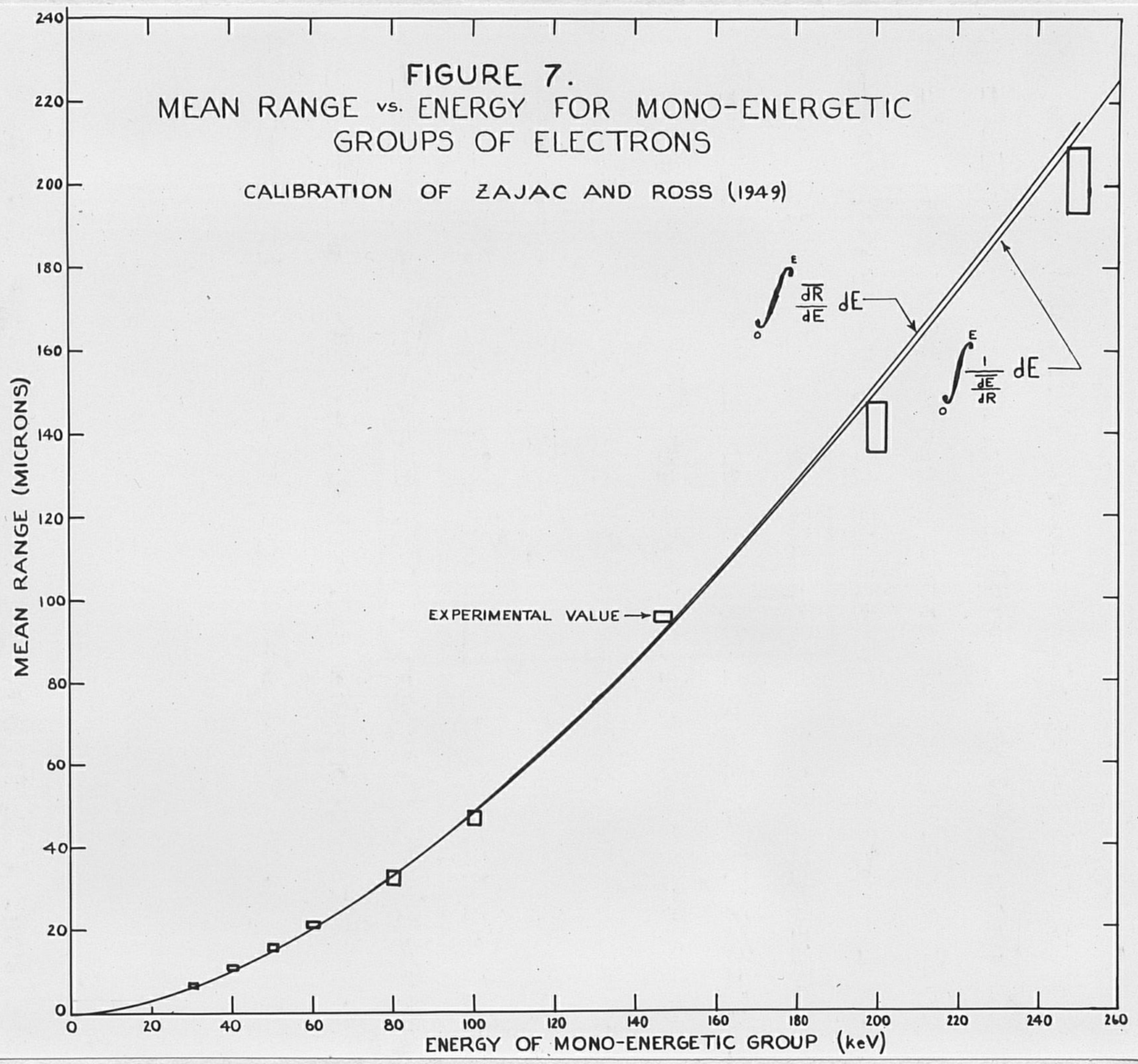

distance $\overline{dR}$ gone by particles all of which lose energy dE, whereas the second refers to the mean energy $\overline{dE}$ lost by particles all of which move a distance dR. The numerical difference between these two quantities arises because of the straggling of the energy loss and the non-linearity of $\overline{R}(E)$. Although this difference is small, the fact that it is so universally ignored makes it worth while to give a calculation of it (see Appendix II).

Figure 7 shows the observed mean ranges of Zajac and Ross and the curves obtained by integrating $1/\frac{\overline{dE}}{dR}$ and $\frac{\overline{dR}}{dE}$. It is seen there that the correctly calculated mean-range vs. energy curve gives a slightly poorer fit with the observations than does the incorrectly calculated one.

III.3. The Use of Smoothing in Nuclear Emulsion Spectrometry.

The results of a series of track measurements are usually displayed as a frequency histogram. The next step is the analysis of the observed histogram into its component mono-energetic groups. In the course of this work one frequently encounters the following problem: given a certain amount of structure in one portion of the observed histogram, does this represent a genuine feature of the population which has been

sampled or is it merely due to statistical fluctuations? If the sample is sufficiently large the effect of the statistical fluctuations will be negligible, but since it is uneconomical to measure enormous numbers of tracks it is important to develop techniques for dealing with smaller samples.

Whereas the true population distribution will be described by a smooth curve, the contribution of the statistical fluctuations to the observed histogram will usually be a series of irregular "peaks" and "valleys". Hence if this discontinuous histogram is replaced by the smooth curve which retains its principal features but not its irregular fluctuations, one is at least moving in the right direction. In statistical practice this is usually done by fitting the best (in the least-squares sense) polynomial of degree n to each adjacent set of m points ($m > n$) and taking the value of this polynomial at the centre of its range as the ordinate of one point of the smoothed curve. By varying m and n one can obtain different degrees of smoothing.

But this procedure is rather arbitrary since by choosing a suitable degree of smoothing one can suppress whatever detail one desires. More confidence could be placed in any particular method if it could be tested under controlled conditions, that is if one

could see what it does to a random sample from a known population. If such a population were available, and if its distribution were similar to the ones that can be expected to be encountered, it would be possible to determine experimentally whether or not smoothing is of any use, and if so, which smoothing method is best. A simple way of constructing such a population will now be illustrated.

Figure 9a is a curve which the author has drawn to resemble a distribution that will be encountered in §III.4. By dividing the abscissa into equal intervals and by integrating over each interval, the histogram of Figure 8a is obtained. To obtain a population whose relative frequencies are given by this histogram one need only write a different number at the boundary between each adjacent pair of intervals such that these numbers form an ascending series, and such that the number of integers between the two numbers bordering any interval is proportional to the histogram frequency for that interval. For example, if one of two adjacent frequencies is double the other, the series of numbers written at the boundaries of these two intervals might be 100½ , 200½ , 250½ . If, now, one had a random sequence of integers in which the occurrence of any integer was equally probable, the probability that an integer from that sequence would fall between the numbers bordering any interval would be proportional

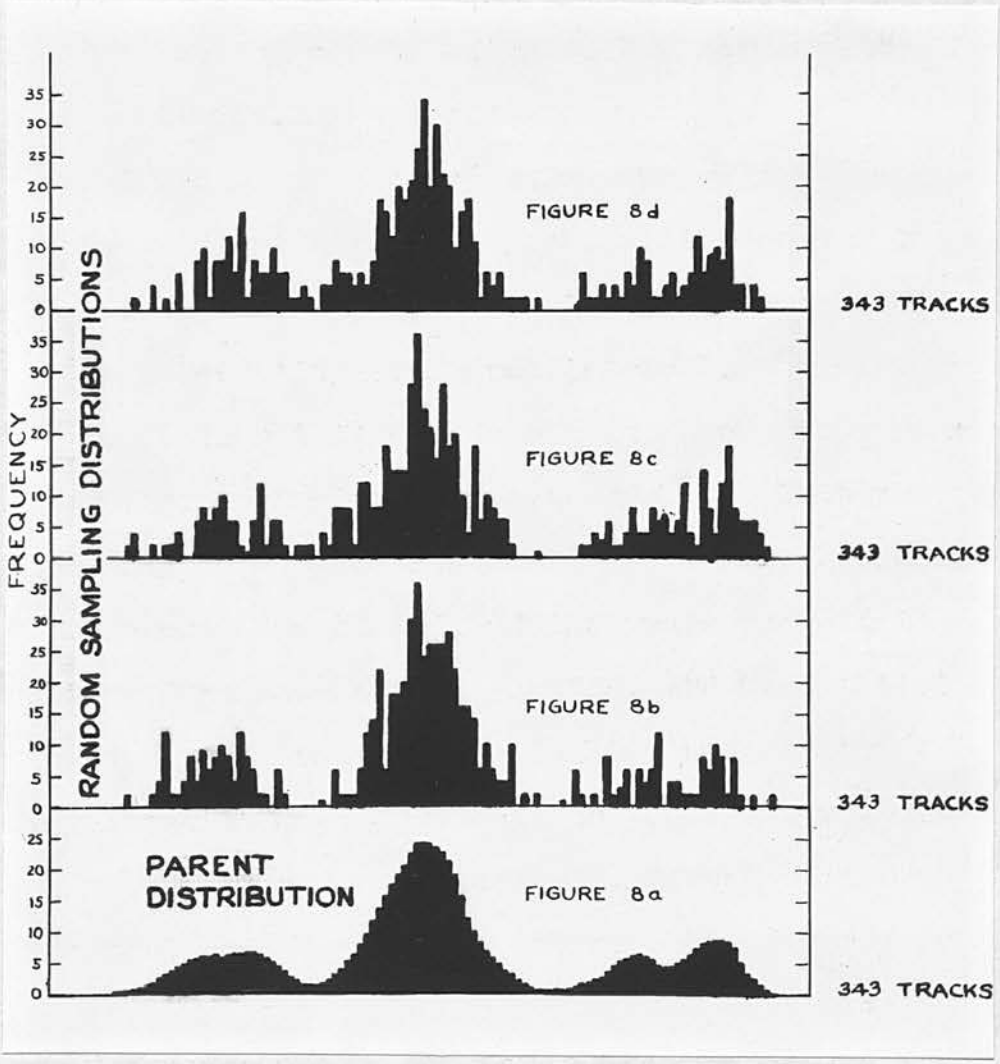

FIGURE 8

PARENT AND SAMPLING HISTOGRAMS FOR THE DISTRIBUTION SHOWN IN FIGURE 9a

FIGURE 9 PARENT DISTRIBUTIONS AND SMOOTHED CURVES FOR THE HISTOGRAMS OF FIG.8

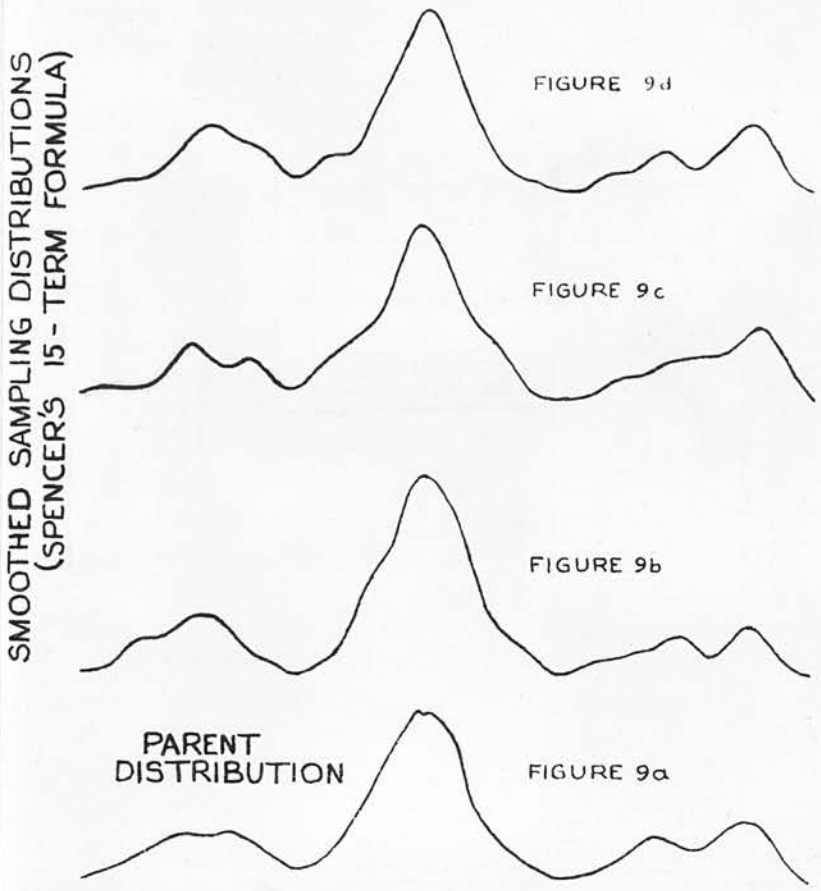

FIGURE 10. PARENT DISTRIBUTION AND SMOOTHED CURVES FOR THE HISTOGRAMS OF FIG. 8

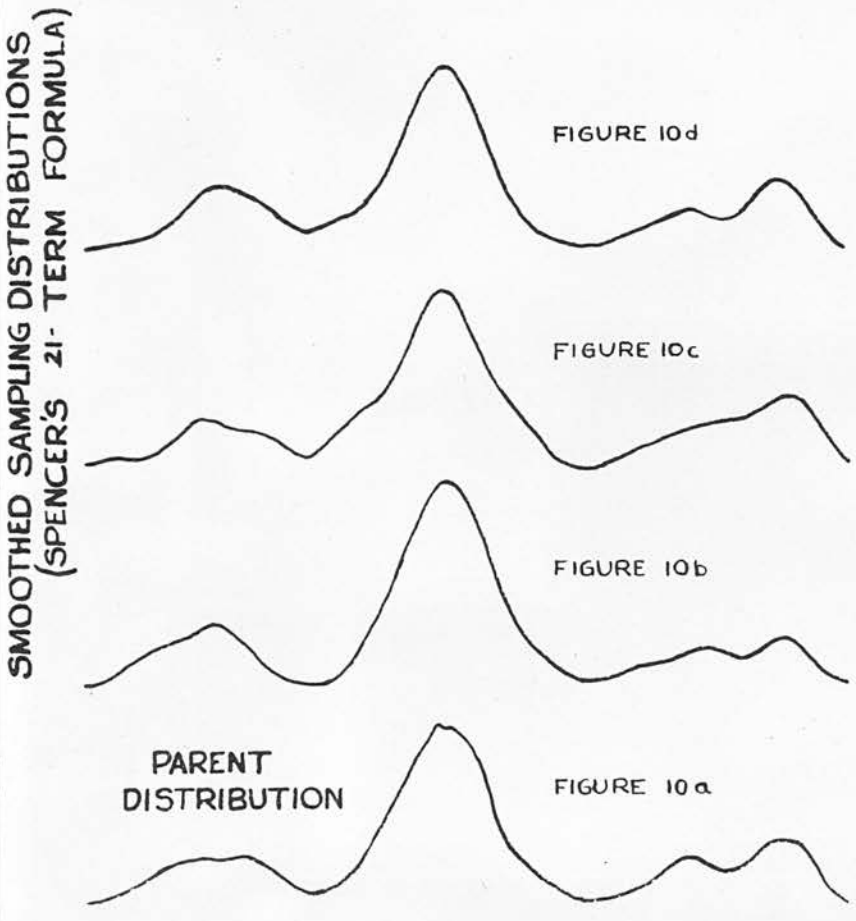

to the histogram frequency for that interval. Random sequences of integers are available in published tables and so, in effect, a population has been constructed whose relative frequencies are described by the given histogram.

This has been done for the histogram of Figure 8a. Three samples of 343+ integers chosen in succession from the random sequence given by Fisher and Yates (1949) yield the histograms of Figures 8b, c and d. Applying Spencer's 15-term formula (Kendall, 1952) to these histograms one obtains the smoothed curves shown in Figures 9b, c and d, respectively. It can be seen immediately that although each smoothed curve has the same principal features as the true distribution (Figure 9a), there remains a residual lumpiness which one might erroneously interpret as a genuine property of that distribution. By applying a more powerful smoothing method, Spencer's 21-term formula (Kendall, 1952), to the sampling histograms of Figures 8b, c and d, one obtains the curves of Figures 10b, c and d. The residual lumpiness has been decreased, and for the present application the 21-term formula is the better of the two. Reference to the sampling histograms, the smoothed curves, and finally to the true distribution makes it clear that smoothing <u>is</u> of value when one attempts to infer a parent distribution from

+ The number 343 was chosen because this happened to be the size of the sample in the set of observations for which the best smoothing method was wanted.

observed data. But even so one is not justified in associating every ripple in the smoothed curve with a ripple in the parent. Figures 9 and 10 show that with a parent distribution of this type and for a sample of this size, such ripples can be introduced into the smoothed curve by statistical fluctuations in the sampling histogram.

III.4. The AcX Internal Conversion Spectrum: Experimental Results.

As stated on page 23, difficulty was frequently encountered in the attempt to decide whether the origin of an electron track was coincident with the separated α-track or with the 3-α-track star. If an electron track[+] was definitely associated with the separated α-track (that is, if it was definitely attributable to an AcX conversion electron) it was recorded as a 'certain' electron. If the association was possible but not definite the electron was recorded as 'doubtful'. For the 809 events satisfying the criterion of acceptance there were 390 'certain' electrons distributed among 367 events. There were 260 'doubtful' electrons. Some of these were associated with events that had 'certain' electrons as well,

+ A configuration of grains was not recorded as a track unless it consisted of three or more grains. One- or two-grain tracks were indistinguishable from irregularities at the beginning of the AcX α-particles.

but there were 172 events with which 'doubtful' electrons alone were associated. The remaining 270 events were unaccompanied by AcX conversion electrons.

Of the 390 'certain' electrons it was possible to estimate the grain numbers of 354, and to measure the ranges of 343. In the other cases the tracks passed out of the emulsion or were not sufficiently well-defined to yield definite grain counts or range measurements. Histograms of frequency vs. log grain number and log range (see page 46) are shown in Figures 11 and 12. The smoothed curves were obtained with Spencer's 21-term formula. It is evident that these spectra are substantially the same.

Figure 14 shows an attempt to make simultaneous use of the ranges and grain numbers. Each of the 343 tracks for which both measurements could be obtained was represented by a point in a range-grain number plane. These points were grouped into intervals by a series of equally spaced lines drawn perpendicular to the regression line. The frequency histogram drawn along the diagonal shows the number of points in each interval. Whether this histogram will exhibit better resolution than the range or grain number histograms taken separately depends upon the nature of the correlation between the ranges and grain numbers of tracks produced by a mono-energetic group of electrons. If this correlation has a coefficient near to +1, nothing is gained

FIGURE II.

INTERNAL CONVERSION SPECTRUM OF AcX DECAY

HISTOGRAM OF LOG_{10} GRAIN NUMBER OF 'CERTAIN' ELECTRONS

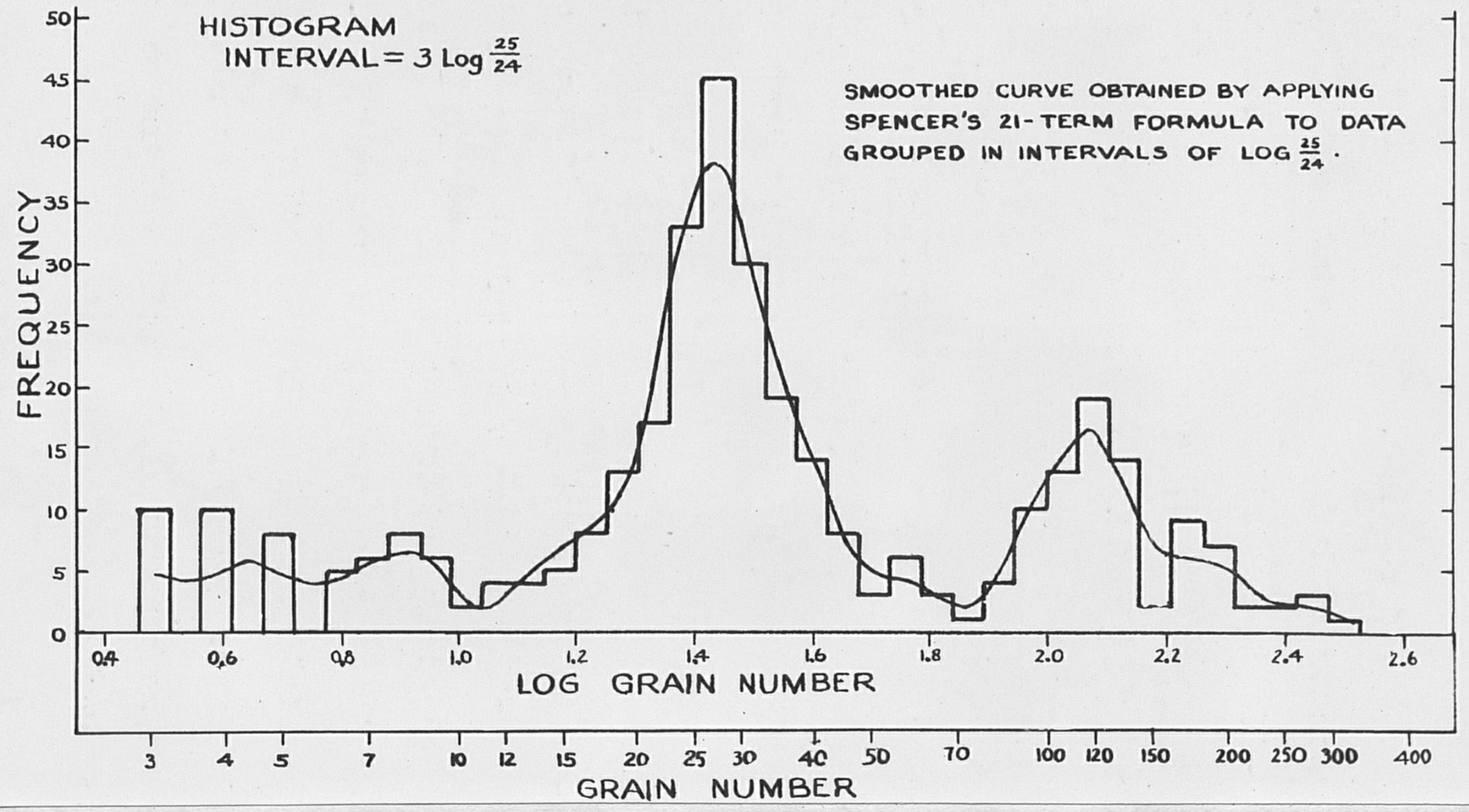

FIGURE 12

INTERNAL CONVERSION SPECTRUM OF AcX DECAY

HISTOGRAM OF LOG_{10} RANGE OF 'CERTAIN' ELECTRONS

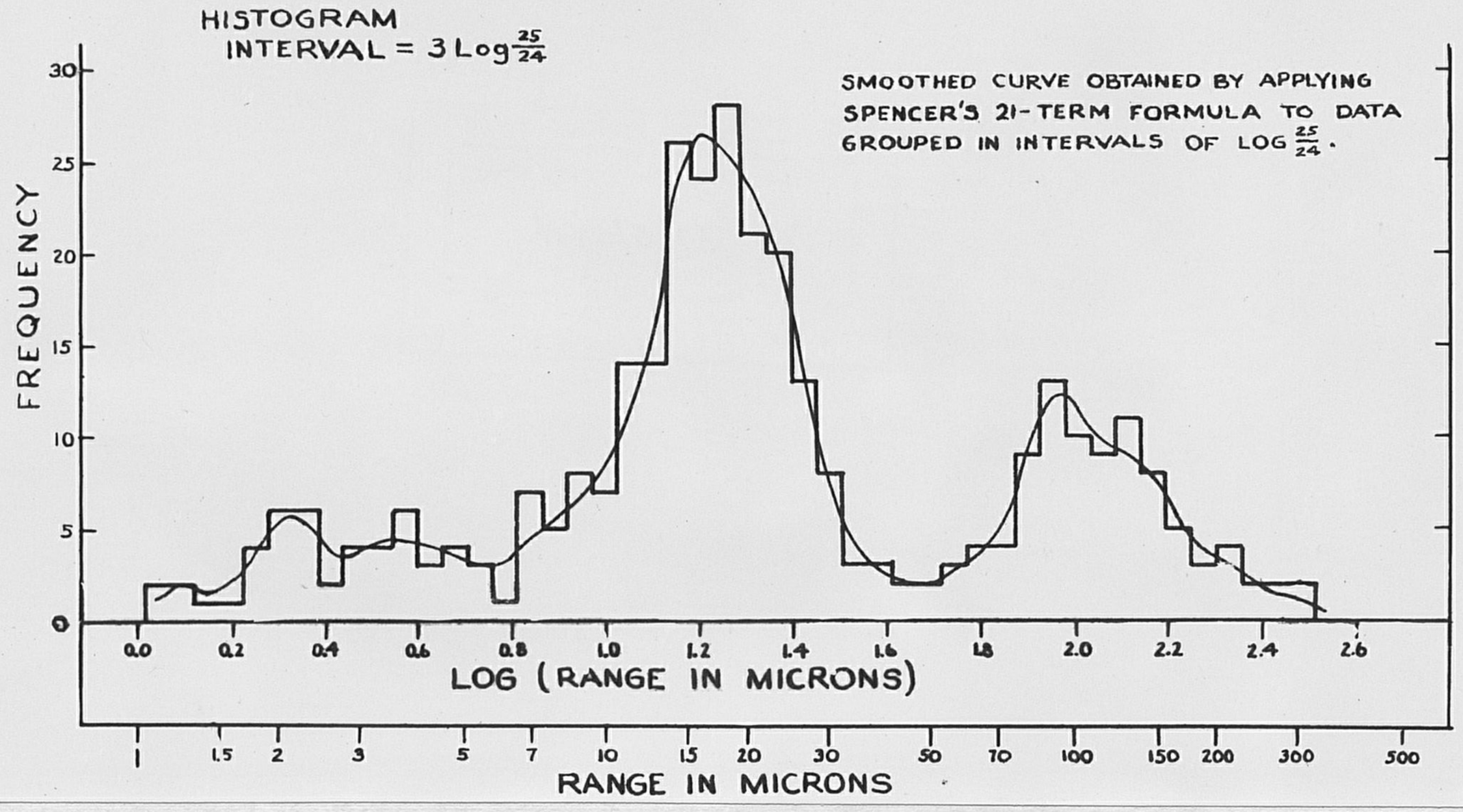

FIGURE 13.

INTERNAL CONVERSION SPECTRUM OF AcX DECAY

HISTOGRAM OF LOG_{10} GRAIN NUMBER OF 'DOUBTFUL' ELECTRONS

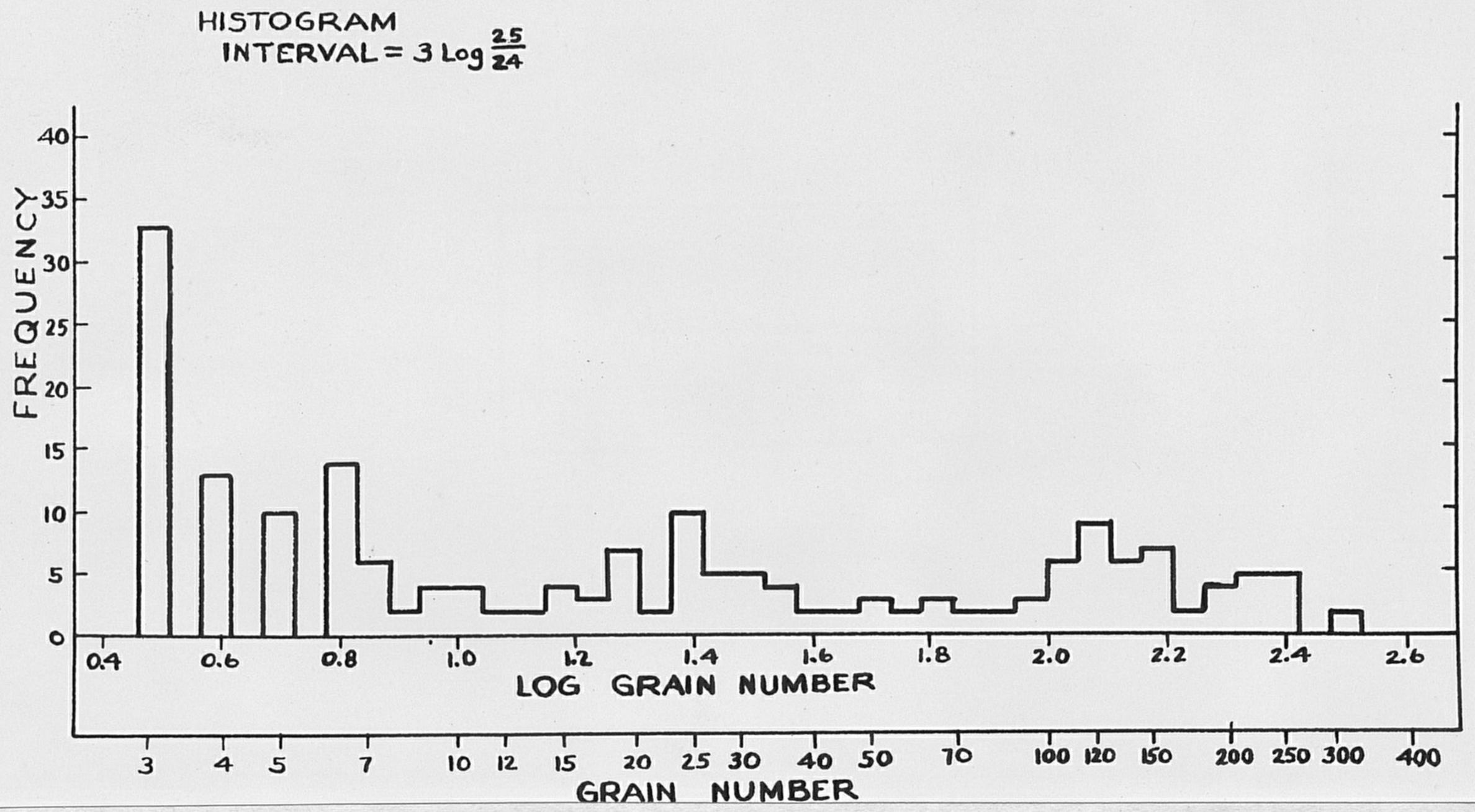

FIGURE 14.

INTERNAL CONVERSION SPECTRUM OF AcX

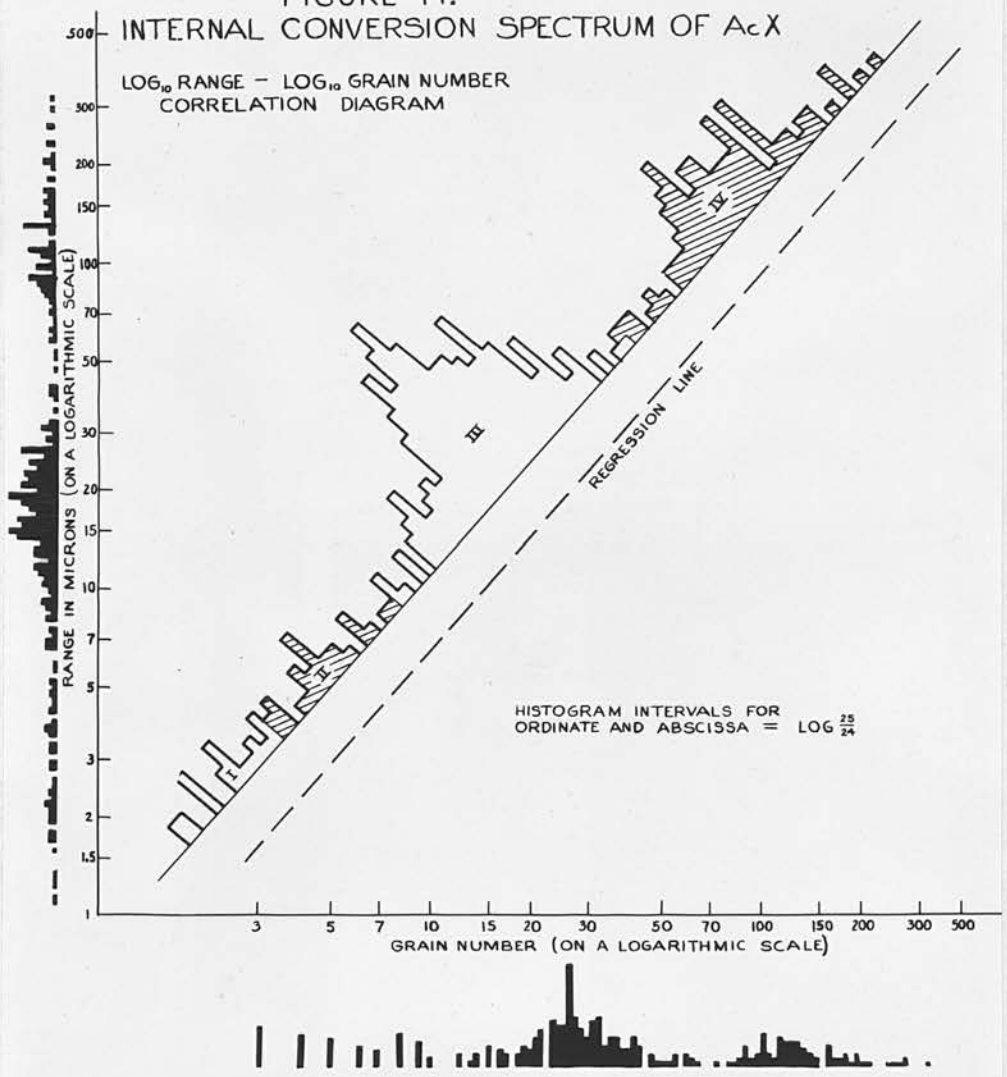

by combining the data since either measurement determines the other. However if the correlation coefficient were less than +1, and especially if it were negative, one would expect to get the greatest resolution from the histogram obtained from the 'scatter-point diagram'. A thorough study of this range-grain number correlation for a mono-energetic group of electrons has not been performed. From the fact that the histogram using the combined data shows little improvement over the others, it can be concluded that this correlation is not far from unity.

That this should be so is not obvious. According to the calculations of Zajac (1949) the stopping power of the silver halide grains of the nuclear emulsion is about four times that of the gelatine. From this one might expect that of two electrons of the same initial energy, the one that loses more of its energy in the gelatine would have the longer range, whereas the other would produce a track with a higher grain number. The observed correlation confirms the statement made on page 43 that it is the large single transfers that govern the straggling, since these would affect both the ranges and grain numbers in the same way.

These histograms, being confined to the 'certain' electrons, may not give a true picture of the AcX internal conversion spectrum. A histogram for the 195

'doubtful' electrons whose grain number could be ascertained is shown in Figure 13. It clearly has a relatively lower intensity of tracks having grain numbers between about 12 and 58 than the histogram for the 'certain' electrons. This is not inconsistent with the assumption that the 'doubtful' and 'certain' electrons have the same energy spectrum, since electron tracks with such grain numbers are less subject to difficulties of interpretation than those with either larger or smaller grain numbers.

The existence of so many 'doubtful' tracks makes a detailed analysis of the line shapes shown in Figures 11, 12, and 14 unjustified. Also, the discreteness of the grain numbers introduces irrelevant features at low energies into the first and third of these. However the spectra can safely be resolved into four main regions, and upper and lower limits for the populations of these regions can be given. The regions are shown by shading in Figure 14, and the populations are given in Table IV. The approximate energy limits were obtained by applying the mean-range vs. energy calibration of Zajac and Ross (1949). The absolute intensities listed in this table will provide the basis of the discussion of the next chapter.

The electron tracks of Group I include those produced by L-Auger electrons. Therefore, in seeking evidence of cascade de-excitation from electron-electron

TABLE IV.

The Number of Electrons in 309 Events

Group No.	I	II	III	IV	Unallocated
Approx. energy limits (keV)	<20	20-27	27-92	>92	
Range limits (μ)	<3	3- 6	6-42	>42	
Grain number limits	<5	5-11	12-58	>58	
No. of 'certain' electrons	21	38	212	109	10
No. of 'doubtful' electrons	56	47	66	79	12

coincidences, all cases are excluded in which one electron track belongs to Group I. This leaves 12 events having two 'certain' electron tracks, 18 events having one 'certain' and one 'doubtful' track, and 30 events in which two tracks were 'doubtful'. A discussion of the details of these cascade events will be given in § IV.7 , page 86.

CHAPTER IV

THE LEVEL SCHEME OF THE EXCITED STATES OF ACTINON

IV.1. Introduction.

The purpose of this chapter is the determination of those characteristics of the level scheme of An that are implied by the data presented in §III.4. This will be done according to the following general procedure:

1. A set of assumptions will be made about the level structure of An and the intensities and multipolarities of the transitions connecting the levels.

2. On the basis of this set of assumptions the expected track frequencies of the regions of Table IV will be computed.

3. These expected frequencies will be compared with the observed frequencies, and the significance of any deviations will be estimated with the χ^2-test.

4. If the expected and observed frequencies are consistent within some previously chosen level of significance+ no conclusion will be drawn from the calculation. However if there is a significant discrepancy, the assumptions made in Step 1 will be rejected.

+ A 1% level of significance will be used throughout this chapter.

5. In the latter event an alternative set of assumptions will be made and Steps 1 to 4 repeated. This will be continued until all assumptions inconsistent with the observations have been eliminated. If more than one possible set of assumptions remains, the observations of this experiment cannot decide between them.

In trying to extract the maximum amount of information from rather crude data of the sort presented in Table IV, considerations of statistical validity must be uppermost in one's mind. This is the reason for the use of the indirect approach outlined above. If a more direct calculation of the transition intensities is attempted, the effects of the statistical fluctuations in the observations cannot be estimated with the precision that the χ^2-test affords in Step 3.

In Step 2 it is necessary to relate the assumed transition intensities to the frequency of emission of the internal conversion electrons. This requires a knowledge of the internal conversion coefficients of these transitions. These coefficients are taken from the most recent calculations of Rose et al. (1954). The Zajac-Ross range-energy calibration is used to attribute, according to its energy, each conversion line to one of the regions of Table IV. Finally, one must have the fractional contributions to each region made by the individual conversion lines, i.e. the

relative intensities of these lines. These are given by the estimates made by Hahn and Meitner (1925) and Surugue (1937) of the photographic blackening of each line, as recorded in their magnetic spectrographs, normalized with Arnoult's (1939) curve of photographic sensitivity vs. electron energy. This step is necessary because the observations of the present work are unable to resolve the individual conversion lines.

IV.2. The χ^2-Test of 'Goodness of Fit.'

In this section an outline is given of those properties of the χ^2-distribution that are necessary for the calculations to follow.

Consider a set of measurements performed on N individuals drawn at random from some infinite population. It is assumed that these measurements can be grouped into k distinguishable classes. Let π_i be the number of measurements observed to fall into the i^{th} class $\left(\sum_{i=1}^{k} \pi_i = N\right)$. Furthermore, associated with the i^{th} class there is assumed to be a probability p_i, which is the probability that a single measurement falls into the i^{th} class $\left(\sum_{i=1}^{k} p_i = 1\right)$. Form the quantity

$$\chi^2 \equiv \sum_{i=1}^{k} \frac{(\pi_i - N p_i)^2}{N p_i} .$$

If another sample of the same size is drawn a new set

π_i are determined, and, in general, these will yield a different value of χ^2. If this process is repeated a large number of times, the population of values of χ^2 generated in this way will have approximately the following distribution+ (Kendall, 1952):

$$f(\chi^2)\, d(\chi^2) = \frac{1}{\Gamma(\frac{K-1}{2})\, 2^{\frac{K-1}{2}}} (\chi^2)^{\frac{K-3}{2}} e^{-\frac{1}{2}\chi^2} d(\chi^2).$$

Here k - 1 is called the number of degrees of freedom. It is equal to the number of classes whose populations can be varied independently. The Np_i are referred to as expectation values.

The probability of an observed value of χ^2 exceeding χ_o^2 is therefore

$$F(\chi_o^2) = \int_{\chi_o^2}^{\infty} f(\chi^2)\, d(\chi^2) .$$

χ_o^2 is tabulated as a function of F and k - 1 in the Tables of Fisher and Yates (1949).

Now suppose that the p_i are unknown, but that a possible set can be computed on the basis of some hypothesis made about the population. It is desired to test this hypothesis by comparing the values of Np_i so computed with an observed set, π_i. At the outset a 'level of significance', F, is chosen and the corresponding $\chi_o^2(F)$ is obtained from the published tables. Then it is stated that the hypothesis will be rejected

+ This involves the further assumption that Np_i is greater than about 5 for each i.

TABLE · V

Internal Conversion Coefficients for Z = 86

(from the results of Rose at al. (1954))

Transition energy (keV)	Transition polarity	Internal Conversion Coefficients Shell of Conversion			
		K	L_I	L_{II}	L_{III}
122	E_1	0.24	0.0254	0.0101	0.00928
	E_2	0.485	0.0986	1.30	0.901
	E_3	0.57	1.58	30.4	9.80
	M_1	7.3	1.25	0.114	-
	M_2	31	11	1.20	2.29
144	E_1	0.216	0.018	0.0056	0.0059
	E_2	0.336	0.073	0.702	0.475
	E_3	0.56	0.82	13	3.95
	M_1	5.39	0.932	0.0788	0.0015
	M_2	20	5.8	0.67	1.04
154	E_1	0.163	0.0153	0.00528	0.0048
	E_2	0.285	0.060	0.515	0.346
	E_3	0.54	0.54	9.4	2.83
	M_1	4.39	0.772	0.072	0.0015
	M_2	16.5	4.51	0.54	0.779
268	E_1	0.0336	0.00445	0.00108	0.0008
	E_2	0.088	0.0156	0.0455	0.0226
	M_1	0.945	0.158	0.0152	0.0004
	M_2	2.72	0.561	0.0739	0.0511

if the observed χ^2 exceeds $\chi_o^2(F)$. From the definition of $\chi_o^2(F)$ it follows that even if the hypothesis were true, there would be a probability F that it would be rejected according to this criterion.

It must be emphasized that this method does not ascribe a probability to the hypothesis. It merely states that the hypothesis is to be rejected if its validity requires that the observed measurements are in the extreme F x 100% of the distribution. Nor does a χ^2 less than $\chi_o^2(F)$ constitute a proof of the hypothesis. It indicates that the hypothesis fits the available data; it does not eliminate the possibility that there are other hypotheses that fit the data equally well.

IV.3. The Internal Conversion Coefficients.

Table V lists the internal conversion coefficients of the principal transitions occurring during the reorganization of excited An nuclei. They were taken from the results of recent calculations of Rose et al. (1954), in which the effect of screening is taken into account using a Thomas-Fermi-Dirac central potential in the Dirac equation. These calculations were performed for z = 15 to 85 inclusive, (intervals of 10) and for energies between 25.54 keV and 1021.58 keV (intervals of 25.54 and 102.16 keV). The values in

Table V were obtained by logarithmic extrapolation to Z = 86, and logarithmic interpolation to the listed transition energies.

These coefficients, taken individually, do not provide all the information about conversion probabilities that is required in the ensuing calculations. The reason is that according to the selection rules for nuclear transitions, magnetic dipole and electric quadrupole transitions between the same two nuclear states may occur with comparable intensity. The same is true for magnetic quadrupole and electric octupole transitions, etc. For these mixed transitions, the observed conversion probabilities are given simply by linear combinations of the probabilities appropriate to the pure transitions, namely those obtained from Table V. It is noteworthy that no interference occurs between the two competing processes. This is connected with the fact that the two radiation fields transform according to different irreducible representations of the group of three-dimensional rotations (Casimir, 1936). It is of interest to note that such interference effects are encountered in the study of the angular correlations of successive nuclear radiations. In this case, the fact that the intermediate nucleus is polarized, and hence no longer invariant under the group of spatial rotations, precludes the use of the type of proof applicable to the internal conversion process.

It is a simple matter to work out the correct linear combination of "pure" coefficients. Let g be the fraction of the <u>transitions</u> that are electric 2^{n+1}-pole, and (1 - g) the fraction that are magnetic 2^n-pole. Furthermore, let α_K , α_{L_1} , etc. be the internal conversion coefficients appropriate to the former, and β_K , β_{L_1} , etc. be those appropriate to the latter. Then it follows that,

$$\text{Probability per transition of K-conversion} = g\frac{\alpha_K}{1+\alpha_K+\alpha_{L_1}+\dots} + (1-g)\frac{\beta_K}{1+\beta_K+\beta_{L_1}+\dots}$$

$$\text{Probability per transition of } L_1\text{-conversion} = g\frac{\alpha_{L_1}}{1+\alpha_K+\alpha_{L_1}+\dots} + (1-g)\frac{\beta_{L_1}}{1+\beta_K+\beta_{L_1}+\dots}$$

and analogous expressions apply to L_2- and L_3-conversion. Conversion in the M and higher shells is sufficiently rare compared to K- and L-conversion to justify its omission in all the following calculations.

IV.4. The Magnetic Spectrum of the AcX Internal Conversion Electrons.

Table VI summarizes the results pertaining to AcX obtained in the magnetic spectrographic investigations of Hahn and Meitner (1925) and Surugue (1937). It will be noted that this table is not symmetrical with respect to these two sets of results. The reason is that in those cases in which a conversion line was contributed to by several elements of the actinium series, Hahn

TABLE VI - Magnetic Spectrum of Internal Conversion Electrons of the AcX Decay.

(1)	(2)	(3)	(4)	(5)	(6)	(7)	(8)	(9)	(10)
1	-	-	-	8.02	.3	.3	3.5	RdAc,AcX	L Auger
2	-	-	-	9.10	.07	.07	.76	AcX	L Auger
3	-	-	-	17.75	12	12	76	AcX	-
4	-	-	-	21.70	.05	.05	.25	AcX	-
5	23.7	20	92	23.71	1.5	1.5	6.9	RdAc	122 K
6	45.5	80	121	45.64	60	49	74	RdAc,AcX	144 K
7	48.2	10	13	-	-	-	-	-	?
8	55.9	100	100	55.70	100	100	100	RdAc,AcX	154 K
9	-	-	-	59.20	.07	.07	.06	RdAc,AcX	-
10	59.6	40	35	60.33	4.5	4.0	3.5	RdAc	?
11	-	-	-	62.89	.3	.3	.24	AcX	K Auger
12	-	-	-	64.07	.08	.08	.06	RdAc,AcX	K Auger
13	67.2	15	11	65.92	.2	.2	.15	RdAc,AcX	K Auger
14	-	-	-	76.30	.05	.05	.03	AcX	K Auger
15	-	-	-	78.49	.05	.05	.03	-	K Auger
16	79.3	10	6	81.04	.4	.4	.22	RdAc,AcX	179 K
17	81.8	10	6	84.54	.2	.2	.11	RdAc,AcX	182 K
18	-	-	-	98.32	1.5	1.5	.78	AcX	?
19	104.2	10	5	103.8	2	2	1.05	An	122 L_I
20	-	-	-	104.3	.05	.05	.03	An	122 L_{II}
21	112.9	10	6	-	-	-	-	-	211 K
22	125.9	50	31	129.9	6	6	3.8	RdAc	144 L_I
23	-	-	-	130.9	.7	.7	.45	RdAc	144 L_{II}
24	-	-	-	133.7	.1	.1	.06	AcX	144 L_{III}
25	136.1	50	33	134.3	8	8	5.4	AcX	154 $L_{I,II}$
26	-	-	-	136.0	1	1	.7	AcX	154 L_{III}
27	138.7	25	17	139.1	.07	.07	.05	AcX	-
28	-	-	-	146.5	.05	.05	.04	AcX	?
29	147.2	15	11	149.2	.7	.7	.5	RdAc,AcX	154 M
30	151.3	15	11	151.3	.6	.6	.44	-	154 N
31	-	-	-	161.8	.05	.05	.04	AcX	179 L
32	170.9	100	77	169.8	20	20	15.5	RdAc,AcX	268 K
33	175.9	25	20	-	-	-	-	-	?
34	179.9	15	12	181.5	.8	-	-	AcX,An	An
35	-	-	-	213.4	.05	.05	.05	AcX	?
36	223.0	30	25	223.6	2	2	1.7	AcX	322 K
37	236.9	30	26	238.2	.05	.05	.05	-	335 K
38	250.9	30	26	249.0	2.5	2.0	1.8	RdAc,AcX,An	268 L
39	-	-	-	261.4	.4	-	-	RdAc,AcX	?
40	-	-	-	304.1	.1	.1	.1	AcX	322 L
41	-	-	-	329.6	.05	.05	.05	AcX	?
42	-	-	-	346	.05	.05	.05	AcX,	444 K
43	-	-	-	426	.05	.05	.05	active dep. AcX	444 L

Column headings: (1), Line number. (2), (3) and (4), energy (keV), relative blackening and relative intensity in the AcX spectrum of Hahn and Meitner. (5) and (6), energy (keV) and relative blackening in Surugue spectrum. (7), blackening attributable to AcX (see page 63 and discussion below). (8), relative intensities for AcX. (9), Surugue's attribution. (10), present interpretation (AcX lines).

Note: The factor given by Arnoult (1939) was used to convert the relative blackenings of columns (3) and (7) into the relative intensities of columns (4) and (8), respectively.

Lines 3,5,6,8,19,20,22,23,24. See discussion below.
Line 10. From Frilley et al. (1954) it can be estimated that 4.0 of the blackening 4.5 (Surugue) comes from AcX.
Line 38. From Hahn and Meitner it can be estimated that 2.0 of the blackening 2.5 (Surugue) comes from AcX.

and Meitner gave the fractional contribution of each to the total blackening of the line. Surugue gave only the total blackening. For the more important of these lines it is now possible, principally because of the work of Frilley et al. (1954), to make reasonable estimates of the AcX contributions to the blackening observed by Surugue. These estimates, together with Surugue's values for the total blackening are given in Table VI. Listed there are all the lines attributed in whole or in part to the AcX disintegration, and also a few lines to which Surugue has given a different attribution. The energies given in Table VI were computed from the experimental values of $B\rho$, using the physical constants listed by DuMond and Cohen (1951) and taking for the F line of ThB (the line used in both investigations for calibration purposes) a $B\rho$ value of 1388.55 gauss-cm (Lindström, 1951). The lines are divided into four energy groups, each corresponding to one of the regions of Table IV.

Table VII shows the total relative intensity of each of the four groups according to the results of Hahn and Meitner, Surugue, and the present work. The agreement is seen to be very poor. The relative intensities of the present work appear to fall somewhere between the other two sets. For example, whereas the Hahn and Meitner intensities for groups III and IV are roughly equal, Surugue's make the former about 5.5

times as great as the latter. The present observations indicate that the ratio is between 1.5:1 and 2:1. Table VII illustrates the two most serious limitations of the nuclear emulsion method as applied to AcX. On the one hand, the measured absolute intensities can be specified only within rather broad ranges due to the large number of "doubtful" events. But even more serious is the disparity that exists between the relative intensities observed in the two magnetic spectrographic investigations that have been performed. Compared with these two uncertainties, the effects of the statistical fluctuations of the figures in column 3 of Table VII are of secondary importance. Hence little would have been gained by increasing the size of the sample studied.

TABLE VII

Total Relative Intensities of the Four Energy Groups ~~(normalized to 100)~~

Group No.	Hahn and Meitner (1925)	Surugue (1937)	Present Investigation
I	0	26.9	2.6 - 9.5
II	13.4	2.3	4.7 - 10.5
III	42.7	60.1	26.2 - 34.4
IV	43.9	10.7	13.5 - 23.2

Table VII makes it evident that the data of Hahn and Meitner and Surugue cannot be used to obtain the relative intensities of two lines of very different energies. The method of the present investigation requires, however, only the relative intensities within each of the four energy regions. The disparities then are less serious than those shown in Table VII. At each stage of the calculations to follow, the effect of the remaining disagreement between the available relative intensity data will be explicitly stated.

IV.5. Discussion of the Transitions.

IV.5.1. The 144 keV transition.

Hahn and Meitner and Surugue agree that the conversion line at 45.6 keV arises partly from the RdAc decay and partly from the AcX decay. The RdAc contribution to Surugue's observed total blackening of 60 may be estimated as follows: The work of Frilley et al. (1954) shows, in agreement with Hahn and Meitner, that in the conversion spectrum of pure RdAc there exists a line at 43 keV whose intensity is $\frac{9}{10}$ths that of the RdAc contribution to the 45.6 keV line. This 43 keV line produces a blackening of 10 on Surugue's scale. Hence it can be concluded that $\frac{10}{9} \times 10 \doteq 11$ of the 60 of the blackening of the 45.6 keV line can be attributed to RdAc. If the

remaining 49 is due to the AcX disintegration, this 45.6 keV line must be one of the strongest in the AcX spectrum. This is the finding of Meitner (1925), who attributes it to the K-conversion of a strong 144 keV transition+. However, Surugue estimates that any AcX contribution to the total observed intensity is about 5% of the RdAc contribution. This implies that a strong 45.6 keV conversion line is associated with a disintegration further down the series, a possibility that cannot be ruled out by the results of the magnetic spectrograph work. If this were true a large number of the 3-α-track stars studied in the present investigation would have been associated with 45.6 keV electron tracks. More precisely, if f is the probability of a track occurring in Group III of the AcX spectrum, the probability of a 45.6 keV electron track radiating from a 3-α-track star, computed on the basis of Surugue's data (see column 8, Table VI) must be $\frac{74}{100}$ f. Then for a random sample of 809 events,

expectation number of electron tracks in Group III = 809 f,

expectation number of electron tracks radiating from the 3-α-track stars = $809 \times \frac{74}{100} f = 599$ f.

+ The absorption edges (in keV) of element 86 are (Cauchois and Hulubei, 1947): K, 98.4; L_I, 18.04; L_{II}, 17.35; L_{III}, 14.69; M_I, 4.46; M_{II}, 4.15; M_{III}, 3.53; M_{IV}, 3.00; M_V, 2.89.

At least 212 tracks were found to be in group III. A study of the 809 3-α-track stars showed that, at most, 79 had tracks whose grain number was between 10 and 30. These should have included all the 45.6 keV electron tracks, and tracks due to several other conversion lines of An and the active deposit as well. Hence 79 must certainly be an upper limit to the number of 45.6 keV electron tracks associated with the 809 3-α-track stars. To test the significance of the disagreement between the observed and expectation numbers, one forms

$$\chi^2 = \sum \frac{\left(\begin{matrix}\text{observed}\\ \text{number}\end{matrix} - \begin{matrix}\text{expectation}\\ \text{number}\end{matrix}\right)^2}{\text{expectation number}} = \frac{(809f - 212)^2}{809f} + \frac{(599f - 79)^2}{599f}.$$

If f is taken to be 0.22, $\chi^2 \doteq 27$, its minimum value with respect to f. In this case (2 degrees of freedom) this indicates that the disparity between observed and expectation numbers is of enormous significance (Fisher and Yates, 1949). If the relative intensities of Hahn and Meitner had been used the disparity would have been still greater. Hence the hypothesis that $\frac{42}{60}$ths of the observed blackening of the 45.6 keV conversion line is due to the disintegration of An or an element further down the series must be rejected, and its attribution to AcX by Meitner (1925) is confirmed. Meitner's assignment of this line to K-conversion of a

144 keV transition is supported by the observation of an intense γ-ray of this energy (Frilley, 1940; see Table II, page 13), and by Hahn's and Meitner's observation of relatively strong lines at energies appropriate for L_I and M_I conversion of this transition. The energy tabulated by Surugue for this L_I line appears to be about 4 keV too high.

IV.5.2. The 154 keV transition.

Surugue attributes a strong line at 55.7 keV to the disintegrations of RdAc and AcX. Hahn and Meitner find the AcX component, but not the RdAc one. Frilley et al. (1954) find no 55.7 keV line in the RdAc spectrum. Hence the full intensity of the 55.7 keV line can be attributed to AcX. The presence of strong conversion lines at the correct energies for L_I, L_{II}, and M-conversion of a 154 keV transition confirms the 154 K attribution of the 55.7 keV line made by both Meitner (1925) and Surugue. Finally, Frilley (1940) observes a strong 155 keV γ-ray.

IV.5.3. The 268 keV transition.

Surugue attributes a line at 169.8 keV to RdAc (274 K) and to AcX (268 K). As in the case of the 154 keV transition, Hahn and Meitner observe only the AcX component. The RdAc investigations of Frilley et al. (1954) that have been published to date do not extend above 61.5 keV, and so give no information pertaining

to this line. The feebleness of the 274 keV L-conversion line (intensity <.05) suggests that, in analogy with the 154 keV transition, all the blackening at 169.8 keV should be attributed to AcX. A strong line is observed by both Hahn and Meitner and Surugue at the energy appropriate for 268 keV L-conversion, and Frilley (1940) observes a strong γ-ray at 270 keV and its second order line at 134 keV (not listed in Table II). There can be little doubt that intense transitions of 154 and 268 keV occur during the re-organization of the excited states of An.

IV.5.4. The 122 keV transition.

Both Hahn and Meitner and Surugue find a moderately strong line at 23.7 keV. Hahn and Meitner attribute it to the AcX decay, while Surugue attributes it to RdAc. Frilley et al. (1954) say it is not a RdAc line. The spectrum of Figure 14, page 52, shows an appreciable intensity in the band 20-27 keV and supports the attribution of the 23.7 keV line to AcX. In Figure 2b the shorter electron track associated with the separated α-track belongs to this line. It is proposed that this line be assigned to K-conversion of a transition of 122 keV. In support of this assignment Frilley (1940) finds a γ-ray of 123 keV from AcX and its derivatives. Further, there is a line in the AcX spectrum of Hahn and Meitner at 104.2 keV and two lines in Surugue's spectrum at 103.8 and 104.3 keV.

Surugue's attribution of these lines to An is not confirmed by Bennett (1938) (see page 12). It is probable that these 104 keV lines are due to L-conversion of the 122 keV transition. However, further work is required to make this assignment as definite as those of the conversion lines of the 154 and 268 keV transitions.

There is a further difficulty in the low energy region. A very strong line (17.75 keV) occurs in the spectrum of Surugue which he attributes to AcX. There is no visible counterpart in the apparently amply sensitive recordings of Hahn and Meitner. This line is disregarded in the following discussion.

IV.6. The Modified Asaro Level Scheme.

IV.6.1. General considerations.

The full lines of Figure 15 represent the levels of the An nucleus as revealed by the α-particle fine structure investigation of Asaro (1953) (see Table I, page 7). It can be seen that of the four transitions discussed in §IV.5, only the one of 144 keV can be reconciled with this scheme. Yet the data of Tables II and VI provide strong evidence that transitions of 122, 154 and 268 keV also take place during the de-excitation of the excited states of An.

Furthermore, it can easily be shown that there must almost certainly exist a level below that excited

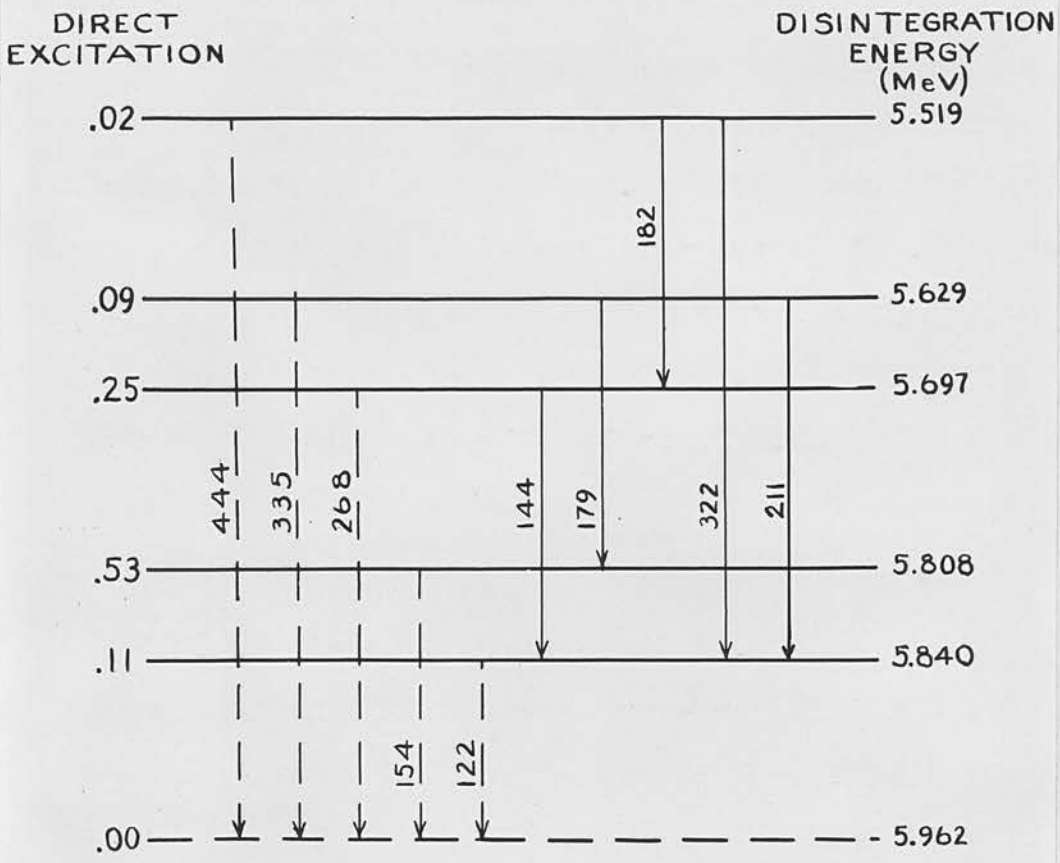

FIGURE 15.
THE MODIFIED ASARO LEVEL SCHEME
FOR THE EXCITED STATES OF $^{219}_{86}An$

by the swiftest α-particles. To see this, assume that the Asaro scheme is complete and consider the 268 keV transition. It must arise above the 9% level since the latter is only 211 keV above the Asaro ground level. But in this case its maximum intensity (per disintegration) is 2%. Hence, for 809 disintegrations the expectation value for the number of 268 keV transitions is less than about .02 x 809 $\doteq$ 16. Hence the total expectation number of 268 keV K- and L-conversions is less than about 16. Now Hahn's and Meitner's total relative intensity for group IV is 300, while their combined 268 keV K- and L-conversion intensities amount to 103 (see Table VI). Then the hypothesis of a 2% transition intensity for the 268 keV transition requires, on the data of Hahn and Meitner, an expectation value for group IV of less than $\frac{300}{103}$ x 16 $\doteq$ 47 tracks. The number computed on the basis of Surugue's data is even smaller. But at least 109 tracks were observed in group IV. If the expectation value were really 47 tracks, the actual numbers observed would have an approximately normal distribution+ with mean equal to 47 and standard deviation equal to $\sqrt{47} \doteq 7$. Hence the observed 109 tracks would be a deviation from the mean of approximately 9 standard deviations. Since the probability of so great a deviation is

+ This method of estimating the significance of the observed discrepancy is equivalent to the use of a χ^2-test with one degree of freedom.

infinitesimally small, it can be concluded that the hypothesis of a 2% intensity for the 268 keV transition is disproved. Hence, there must exist a level below the lowest level found by Asaro.

The difficulties raised in the preceding two paragraphs can be avoided in a very simple fashion by postulating that the true ground level of An lies 122 keV below the level indicated by the swiftest α-particles observed by Asaro (dashed lines in Figure 15). It then becomes immediately possible to accommodate the 122, 154 and 268 keV transitions, as well as transitions of 335 and 444 keV for which there is also definite evidence (see Table VI). As far as numerical energy values are concerned, therefore, this modified Asaro scheme can be reconciled with the principal features of the internal conversion and γ-spectra. It must now be decided whether this remains true when the absolute intensities of the transitions are taken into account.

It may be noted that Rosenblum (1952) found evidence of a weak AcX α-line which leads to a level lying within 10 keV of the energy proposed here for the ground state (see Table I). However, since Rosenblum has not published any experimental details it is impossible to estimate the reliability of this finding. In its principal features his scheme is identical with the Asaro scheme, except that the Asaro level spacings

provide a better fit with the observed transition energies. For this reason the discussion will be confined to the Asaro scheme, although all the conclusions to be drawn apply to the Rosenblum scheme as well.

IV.6.2. The multipole orders of the 144 and 154 keV transitions.

Before the intensities of these transitions can be computed from the observed conversion intensities, consideration must be given to their multipole orders. This is necessitated by the strong dependence of the internal conversion coefficients on these multipole orders (see Table V).

It will first be shown that the 144 keV transition, placed as in Figure 15, cannot be electric dipole. For if it were, its K-conversion coefficient would be 0.216, and its $L_I + L_{II} + L_{III}$ - coefficient would be 0.0295. Then if ω is the fraction of disintegrations accompanied by the 144 keV transition, and if conversion in the M and higher shells is ignored,

fraction of disintegrations accompanied by 144 K-conversion $= \frac{0.216}{1 + 0.216 + 0.0295}\,\omega$,

fraction of disintegrations accompanied by 144 L-conversion $= \frac{0.0295}{1 + 0.216 + 0.0295}\,\omega$.

According to the relative intensities of Hahn and

Meitner, group III has an intensity $\frac{292}{121}$ times that of the 144 K-conversion line, and group IV has an intensity $\frac{300}{31}$ times the sum of the intensities of the 144 L-conversion lines. Hence, for 809 disintegrations,

expectation number of tracks in group III $= 809 \times \frac{292}{121} \times \frac{0.216}{1.246}\omega = 338\,\omega$,

expectation number of tracks in group IV $= 809 \times \frac{300}{31} \times \frac{0.0295}{1.246}\omega = 185\,\omega$,

expectation number of tracks in neither group III nor group IV $= 809 - (338 + 185)\omega$.

An upper limit of $\omega = 0.36$ is set by the position of the 144 keV transition in the modified Asaro level scheme. The numbers of tracks observed in groups III and IV were at least 212 and 109, respectively. Therefore the minimum value of χ^2 is

$$\chi^2 = \frac{(212-122)^2}{122} + \frac{(109-67)^2}{67} + \frac{(212+109-122-67)^2}{809-122-67} = 120.$$

(2 degrees of freedom)

A value of χ^2 as large as this represents an irreconcilable contradiction between observed values and those predicted on the hypothesis that the 144 keV transition is electric dipole. This contradiction would have been still greater if the relative intensities given by Surugue had been used. Therefore, this hypothesis must be rejected.

Now consider the possibility that the 144 keV transition is mixed electric quadrupole - magnetic dipole. Let g be the fraction of the transitions that are electric quadrupole. Then, using the results of §IV.3, the fraction of 144 keV transitions that are accompanied by K-conversion is

$$\frac{g\alpha_K}{1+\alpha_K+\alpha_{L_1}+\cdots} + \frac{(1-g)\beta_K}{1+\beta_K+\beta_{L_1}+\cdots} .$$

Using the data of Table V and ignoring M-, N-, etc. conversion, this becomes 0.728 - 0.598g. In a similar way, the fraction of 144 keV transitions accompanied by L-conversion is calculated to equal 0.137 + 0.347g. Let ω be the fraction of disintegrations in which the 144 keV transition occurs. From Table VI it is seen that Surugue's data imply that group III has $\frac{179.18}{74}$ times the intensity of the 144 K-conversion line, and group IV has $\frac{31.91}{4.31}$ times the sum of the intensities of the 144 L-conversion lines. From this it follows that

probability of a track occurring in group III $= \omega \frac{179.18}{74} (0.728 - 0.598g)$,

probability of a track occurring in group IV $= \omega \frac{31.91}{4.31} (0.137 + 0.347g)$.

Multiplying by the number of events studied, i.e. 809,

expectation number of tracks
in group III $= \omega (1427 - 1172g)$,

expectation number of tracks
in group IV $= \omega (819 + 2076g)$,

expectation number of tracks in
neither group III nor group IV $= 809 - \omega [2246 + 904g]$.

These can now be compared with the observed group populations (Table IV), and the ranges of g and ω determined for which χ^2 is less than any specified value. According to the tables of Fisher and Yates (1949), the value of χ^2 for two degrees of freedom which is exceeded with a probability of 1% is 9.21. Numerical calculation shows that $\chi^2 = 9.21$ need not be exceeded if g in the above expectation values lies between zero and 0.3, but is exceeded otherwise. In fact in order to obtain a χ^2 as low as 9.21 with $\omega = 0.3$, it is necessary to assume that group IV contains all the unallocated electrons and all the group IV 'doubtful' electrons, whereas group III contains only its 'certain' electrons. This results in populations for groups III and IV of 212 and 210, respectively. Such an allocation is indeed unrealistic, yet it cannot be rigorously discounted on the basis of Table IV. In any case it may be said that, with the relative intensities of Surugue, and at the 1% level of significance, the fractional contribution of electric

quadrupole transitions is between zero and 0.3. If the data of Hahn and Meitner are used the upper limit comes down to 0.2.

Proceeding in the same way, one can investigate the implications of the assumption that the 144 keV transition is mixed electric octupole and magnetic quadrupole. Using Surugue's data an upper limit of 0.05 can be set to the octupole contribution, still at the 1% level of significance. As before, the lower limit is zero. If the data of Hahn and Meitner are used, there is no mixture of these two multipolarities that can be reconciled with the observed intensities.

Higher multipolarities for the 144 keV transition are ruled out on both sets of intensity data.

Summarizing, one can say that if the modified Asaro scheme is correct, the data of Hahn and Meitner, together with the observations of the present work, require the 144 keV transition to be pure magnetic dipole, or magnetic dipole with an electric quadrupole contribution of less than 20%. Surugue's data admit electric quadrupole contributions up to 30%, and also leave open the possibility that this transition is magnetic quadrupole plus a small amount of electric octupole (less than 5%).

It is now possible to deduce some of the properties of the 154 keV transition. If μ_K^{144} and μ_K^{154} are the K-conversion coefficients of the 144 and 154 keV

transitions, respectively, then by definition

$$\frac{\text{probability of 154 keV } \gamma\text{-emission}}{\text{probability of 144 keV } \gamma\text{-emission}} = \frac{\text{probability of 154 keV K-conversion}}{\text{probability of 144 keV K-conversion}} \times \frac{\mu_K^{144}}{\mu_K^{154}}.$$

The first ratio on the right-hand side is given by the magnetic spectrograph work; the second depends upon the polarities of the transitions. If the 154 keV transition is assumed to be electric dipole, $\mu_K^{154} = 0.163$. From the previous work, the minimum acceptable value of μ_K^{144} is obtained if the transition is regarded as 30% electric quadrupole plus 70% magnetic dipole. This yields $\mu_K^{144} = 2.61$, and requires the use of Surugue's relative intensities. Then,

$$\frac{\text{probability of 154 keV } \gamma\text{-emission}}{\text{probability of 144 keV } \gamma\text{-emission}} \geq \frac{100}{74} \times \frac{2.61}{0.163} = 21.6$$

If the relative intensities of Hahn and Meitner are used, the minimum value of μ_K^{144} at the 1% level of significance is 3.28 (20% electric quadrupole plus 80% magnetic dipole). On their data,

$$\frac{\text{probability of 154 keV } \gamma\text{-emission}}{\text{probability of 144 keV } \gamma\text{-emission}} \geq \frac{100}{121} \times \frac{3.28}{0.163} = 16.6$$

Reference to Table II, page 13, shows that Frilley (1940) observed a ratio of 2:1 for the intensities of these two γ-rays. Although his intensities are only approximate, the disparity between this ratio and those computed on the assumption that the 154 keV transition

is electric dipole is definitely significant. Hence, this assumption has been disproved.

Now consider the possibility that the 154 keV transition is a mixture of h parts electric quadrupole and $(1 - h)$ parts magnetic dipole. Then if,

$$K = \frac{\text{144 keV K-conversion intensity}}{\text{154 keV K-conversion intensity}}$$

$$\lambda = \frac{\text{144 keV L-conversion intensity}}{\text{154 keV L-conversion intensity}} ,$$

a straightforward calculation yields,

$$h = \frac{g(\nu x\lambda - \eta m K) + (\nu y\lambda - \eta n K)}{g(\xi m K - \mu x\lambda) + (\xi n K - \mu y\lambda)} ,$$

where g is, as before, the electric quadrupole fractional contribution to the 144 keV transition, and

$$x = \frac{\alpha_K^{144}}{1+\alpha_K^{144}+\alpha_L^{144}} - \frac{\beta_K^{144}}{1+\beta_K^{144}+\beta_L^{144}} \; ; \; \xi = \frac{\alpha_K^{154}}{1+\alpha_K^{154}+\alpha_L^{154}} - \frac{\beta_K^{154}}{1+\beta_K^{154}+\beta_L^{154}}$$

$$y = \frac{\beta_K^{144}}{1+\beta_K^{144}+\beta_L^{144}} \; ; \; \eta = \frac{\beta_K^{154}}{1+\beta_K^{154}+\beta_L^{154}}$$

$$m = \frac{\alpha_L^{144}}{1+\alpha_K^{144}+\alpha_L^{144}} - \frac{\beta_L^{144}}{1+\beta_K^{144}+\beta_L^{144}} \; ; \; \mu = \frac{\alpha_L^{154}}{1+\alpha_K^{154}+\alpha_L^{154}} - \frac{\beta_L^{154}}{1+\beta_K^{154}+\beta_L^{154}}$$

$$n = \frac{\beta_L^{144}}{1+\beta_K^{144}+\beta_L^{144}} \; ; \; \nu = \frac{\beta_L^{154}}{1+\beta_K^{154}+\beta_L^{154}} ,$$

the α's and β's having the same meaning as in §IV.3. Substituting values for these coefficients given in Table V one obtains

$$h = \frac{g[0.244K + 0.0812\lambda] + [0.0963K - 0.0988\lambda]}{g[0.199K - 0.169\lambda] + [0.0786K - 0.205\lambda]} .$$

According to Surugue's relative intensities (see Table VI), $K = \frac{74}{100}$ and $\lambda = \frac{4.31}{6.1}$. Also the permissible range of g is zero to 0.3. From this it follows that h, the electric quadrupole fractional contribution to the 154 keV transition, is between zero and 0.34. The Hahn and Meitner data give $K = \frac{121}{100}$, $\lambda = \frac{31}{33}$, $0 \leqslant g \leqslant 0.2$, and this results in a range for h of 0.08 to 0.32. This transition can also be regarded as magnetic quadrupole plus a few per cent of electric quadrupole without contradicting the observed absolute intensities at the 1% level of significance.

IV.6.3. The transition probabilities: test of the modified Asaro scheme.

The same calculation that determined the ranges of multipole mixtures for the 144 and 154 keV transitions yields the conclusions about their absolute intensities that are summarized in Table VIII.

TABLE VIII

Absolute Intensity Ranges at 1% Level of Significance

Relative Intensities of	144 keV	154 keV
Surugue (1937)	12.5% to 24%	18% to 34%
Hahn and Meitner (1925)	12.5% to 22%	12% to 20%

The higher intensities are associated with almost pure magnetic dipole transitions. This may appear strange since, for these energies, magnetic dipole K-conversion coefficients are more than ten times as large as those for electric quadrupole transitions. Hence, for the observed number of K-conversion electrons it might be expected that the assumption of predominant electric quadrupole polarity would imply the larger number of transitions. However, whereas the magnetic dipole $^{K}/_{L}$ intensity ratio is about 5, the electric quadrupole intensity ratio is less than 0.25. Therefore if one assumes a large electric quadrupole contribution, one must have a lower transition intensity to prevent the expectation number of tracks in group IV (which contains the tracks of the L-electrons) from becoming excessive. It turns out that this factor is more important than the difference in K-conversion coefficients when it comes to determining the multipole mixtures consistent with the largest number of transitions.

These results are sufficient to demonstrate the inadequacy of the modified Asaro scheme (Figure 15). For, consider the level 154 keV above the ground state. Its primary excitation is 53%, and therefore the sum of the intensities of the transitions de-exciting this level must be 53% or greater. According to the modified Asaro scheme this de-excitation can follow two

alternative modes: (1), a cascade between transitions of 32 keV and 122 keV, or (2), a transition of 154 keV direct to the ground state. Now there is no evidence, whether in conversion or emission, for the existence of a 32 keV transition. And Table VIII shows that the intensity of the 154 keV transition is almost certainly less than 34%. Hence the modified Asaro scheme fails to provide sufficient de-excitation of this level.

Moreover, consider the balance between the intensities of excitation and de-excitation of the level 122 keV above the ground state. Adding to its primary excitation intensity of 11% the minimum feed by the 144 keV transition (see Table VIII), one concludes that the intensity of the 122 keV transition must be at least 23.5%. An upper limit to the observed 122 keV K-conversion intensity can easily be estimated, since the range-energy relation of Zajac and Ross (1949) makes it almost certain that group II contains all the tracks produced by 122 keV K-conversion electrons. The total of 85 'certain' and 'doubtful' electrons in this group represents 10.5% of the events studied. However, the true probability of 122 keV K-conversion could be as high as 13.6%[+] without implying a difference between observed and expectation values that is significant at the 1% level. If the unlikely assumption is made that all the unallocated electrons belong to group II,

+ $p = 0.136$ is a solution of $\frac{809p - 85}{\sqrt{809p(1-p)}} = 2.576$.
See Fisher and Yates (1949), page 6.

this maximum K-conversion intensity is raised to 16.6%. Frilley's work on the γ-radiation (see Table II) shows that the 122 keV transition is weaker in emission than the 144 keV transition; the results of the magnetic spectrographic investigations (see Table VI) show that this is also true of their L-conversion intensities. These considerations lead to the conclusion that the 122 keV transition intensity is definitely not greater than 20%, and is probably a good deal lower than this figure. This provides another instance in which the modified Asaro scheme cannot be reconciled with the observed absolute intensities.

A method of avoiding both the foregoing contradictions and yet preserving the agreement between α-particle level spacings and transition energies is suggested by the presence, in the Hahn and Meitner conversion spectrum, of a 48.2 keV line. If this is regarded as the K-conversion of a weak 147 keV transition connecting the 268 and 122 keV levels, an even better agreement of energies is obtained, viz. 48.2 + 23.7 + 98.4 = 170.3 rather than 45.6 + 23.7 + 98.4 = 167.7.+ The strong 144 keV transition can then be used to de-excite the 154 keV level according to one of the modes shown in Figure 16. Either scheme is consistent with the absolute intensity measurements of this work, provided that almost all the 'doubtful' electrons of medium and high energy do belong to the

+ These should be compared with the observed energy of 170.9 KeV (Hahn and Meitner) or 169.8 KeV (Surugue).

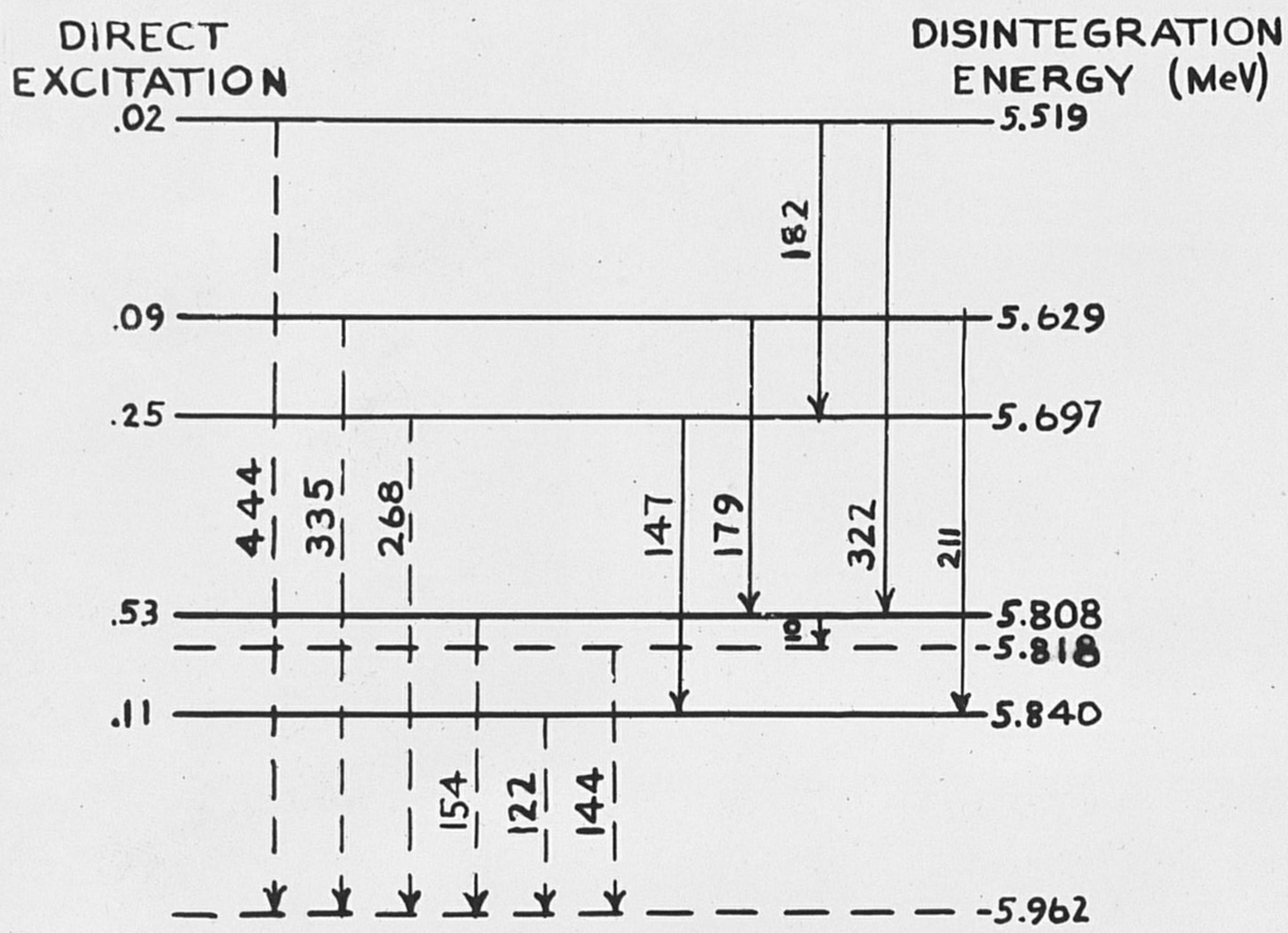

FIGURE 16. PROPOSED LEVEL SCHEMES

FOR THE EXCITED STATES OF ACTINON

AcX internal conversion spectrum, that the relative intensities given by Surugue are correct, and that both the 144 and 154 keV transitions are predominantly magnetic dipole. These conditions must be satisfied if the 144 and 154 keV transitions are to suffice for the de-excitation of the 154 keV level. The 268 keV transition is now the only strong transition de-exciting the 268 keV level, and its intensity is sufficient for this provided that this level is not fed from higher levels to any great extent.

The maximum intensities of the 335 and 322 keV transitions in K-conversion are each about 2%, and there are also K-conversion intensities of not greater than 1% in each of the transitions of 179, 182 and 211 keV. There is also a small intensity of 444 keV conversion. These intensities appear adequate for the de-excitation of the 335 and 444 keV levels and should not disturb the balance already discussed for the lower levels.

The level schemes of Figure 16 are thus capable of explaining the α-, γ-, and conversion electron spectra of AcX. There appears to be but one other simple way of fitting these data into a single scheme, and that is to assume that the 144, 154 and 268 keV transitions are all electric dipole. In fact if any one of these transitions is electric dipole, a proof similar to that given on page 78 and based on the

near-equality of their γ-ray intensities shows that they must all be electric dipole. Moreover the absolute conversion intensities observed in the present work would then require their transition intensities to be so large that they must occur in a cascade not originating higher than the level of 53% primary excitation. This would lead one to expect a large number of events with which the conversion electrons of at least two of these transitions were associated. On the other hand, coincidences between the conversion electrons of these transitions are irreconcilable with the level schemes of Figure 16. It will be seen in the next section that the 'double' events observed in the present work definitely indicate that these transitions do not occur in cascade, and hence the transitions cannot be electric dipole.

Of course, the above discussion of the various level schemes does not exhaust all possibilities. It is suggested, however, that the schemes of Figure 16 account for all the available information pertaining to the AcX decay in the simplest possible fashion. If one tries to fit any other scheme to this data, one is forced to postulate a large number of levels for which there is as yet no direct evidence.

IV.7. The Cascade Evidence.

The low resolution of the nuclear emulsion as a tool of electron spectrometry imposes especially severe limitations on an attempt to extract information from those events in which two electron tracks are associated with a single AcX α-track. Here it is necessary to attribute an energy to each of the tracks studied, whereas the previous work dealt only with the spectrum of a large number of tracks. Moreover the possibilities for confusion are increased by the presence of the second electron track, and hence these 'double' events are the most difficult ones to interpret.

The discussion of the cascade evidence is confined to those cases in which at least one of the electrons is 'certain'. There are seven or eight examples in the cascades of the occurrence of electron tracks having 14 to 18 grains, or an energy of about 35 keV. That a conversion line of this energy is present in the AcX spectrum is suggested by slight bulges in the smoothed curves of Figures 11 and 12 ; however the work of §III.3 shows that such bulges may be spurious. Some confirmation of its existence is also found in Surugue's (1937) spectrum, for there he has a line at 33.92 keV (not shown in Table VI) which appears too strong to be entirely accounted for as L_{III}

conversion of the 50 keV transition following the RdAc decay (Frilley et al., 1954). This line may be assigned either to L-conversion of a 52 keV transition, for which there is γ-ray evidence[+], or to K-conversion of a 132 keV transition, in which case the γ-ray would be obscured by the second order spectrum of the 268 keV line. It is significant that this 35 keV conversion line should be much more prominent in the cascade events than in the total conversion spectrum.

The detailed information provided by the electron-electron coincidences includes the following:

(a) Conversion of 268 keV with an electron of about 35 keV: 2 cases.

(b) Conversion of 144 or 147 or 62 keV with an electron of about 35 keV: 4 cases.

(c) Conversion of 144 or 147 or 62 keV with conversion of 122 keV: 5 cases.

(d) Conversion of 144 or 147 or 154 keV with conversion of 179 or 182 keV: 5 to 7 cases.

(e) There are 5 or 6 events which could be K-conversions followed by K-Auger electrons.

If the 144, 154, and 268 keV transitions occurred in cascade, as discussed at the end of §IV.6.3, one would have expected about 20 144-154 keV coincidences, 5 144-268 keV coincidences, and 5 154-268 keV

+ Frilley (1940) has attributed to the RdAc spectrum a strong γ-ray of this energy.

coincidences. The fact that these were not observed constitutes convincing evidence against this scheme. Other than this, the 'double' events provide little confirmation of the scheme illustrated in Figure 16. A high-resolution coincidence experiment would be of great value in this connection, but the difficulties mentioned above prevent the nuclear emulsion technique from furnishing any decisive information.

IV.8. Intensity of K-Fluorescence.

It is of interest to assess the total intensity of K-X-radiation excited by the decay of AcX. The absolute conversion intensities observed in the present work, coupled with the relative intensities listed in Table VI, make it appear that the total intensity of K-shell ionization lies between 30 and 55 ionizations per 100 disintegrations. Since the decay scheme of Figure 16 requires almost all the doubtful electrons to be included in order to obtain sufficient intensity in the transitions, it is probable that the ionization intensity is nearer to the higher figure. The number of K-Auger electrons seen in the electron-electron coincidence events is 5 or 6, considering only those coincidences in which at least one of the two electrons is 'certain'. The total number of K-Auger electrons may be nearer to 10 out of the 809 events studied. This indicates a fluorescence

yield of about 98 ± 1% and a K-fluorescence between 30 and 55 quanta per 100 disintegrations. This is certainly an abnormally high intensity and is entirely consistent with Frilley's (1940) statement that the K-fluorescence of element 86 is ten times that of any other element in the actinium series.

IV.9. Implications of the Proposed Level Scheme of Actinon.

IV.9.1. The total disintegration energy of AcX.

The existence of the true ground level of An 122 keV below the level excited by the swiftest AcX α-particles helps to explain an anomaly pointed out by Feather (1953) in his study of last neutron binding energies. Feather considers the following two sequences of disintegrations:

$$\left(^{232}_{90}\right) \overset{\alpha}{\Longrightarrow} \left(^{228}_{88}\right) \overset{\beta}{\longrightarrow} \left(^{228}_{89}\right) \overset{\beta}{\longrightarrow} \left(^{228}_{90}\right) \overset{\alpha}{\Longrightarrow} \left(^{224}_{88}\right) \overset{\alpha}{\Longrightarrow} \left(^{220}_{86}\right) \overset{\alpha}{\Longrightarrow} \left(^{216}_{84}\right) \overset{\alpha}{\Longrightarrow} \left(^{212}_{82}\right) \overset{\beta}{\longleftarrow} \left(^{212}_{83}\right) \overset{\alpha}{\Longleftarrow} \left(^{208}_{81}\right) \overset{\beta}{\longleftarrow} \left(^{208}_{82}\right)$$

$$\left(^{231}_{90}\right) \overset{\beta}{\longrightarrow} \left(^{231}_{91}\right) \overset{\alpha}{\Longrightarrow} \left(^{227}_{89}\right) \overset{\beta}{\longrightarrow} \left(^{227}_{90}\right) \overset{\alpha}{\Longrightarrow} \left(^{223}_{88}\right) \overset{\alpha}{\Longrightarrow} \left(^{219}_{86}\right) \overset{\alpha}{\Longrightarrow} \left(^{215}_{84}\right) \overset{\alpha}{\Longrightarrow} \left(^{211}_{82}\right) \overset{\beta}{\longleftarrow} \left(^{211}_{83}\right) \overset{\alpha}{\Longleftarrow} \left(^{207}_{81}\right) \overset{\beta}{\longleftarrow} \left(^{207}_{82}\right)$$

The principle of the conservation of energy requires that the sum of the disintegration energies of the

first sequence minus the corresponding sum for the second should equal the difference between the last neutron binding energies of elements $\binom{208}{82}$ and $\binom{232}{90}$. In fact, by performing this calculation and using a value of 5.82 MeV for the disintegration energy of AcX $\binom{223}{88}$, Feather found that the difference between the observed binding energies was 230 ± 80 keV too small. But the AcX disintegration energy proposed in the present work (Figure 16) is 5.962 MeV. Using this value in Feather's calculation brings the discrepancy down to 88 ± 80 keV, which can hardly be considered significant in view of the large number of disintegration energies involved in the calculation. Although this does not constitute a proof of the proposed An level scheme, it is satisfactory that this scheme, deduced from completely different considerations, is able to restore the balance between disintegration and neutron binding energies.

A somewhat similar situation arises in the study of the systematics of α-decay in the heavy radioactive nuclei. By plotting total α-disintegration energy vs. mass number, Perlman, Giorso and Seaborg (1950) have shown that the points representing the isotopes of each element may be joined by a moderately straight line. This plot reveals that a 5.82 MeV disintegration energy for AcX violates the general trend,

whereas the present value of 5.962 MeV is consistent with a smooth variation of energy with mass number. Feather (1952) has plotted α-disintegration energy against proton number and has been able to draw fairly smooth curves connecting the points corresponding to constant values of the isotopic number, A - 2Z. Here again, the higher disintegration energy proposed in the present work reduces an observed discrepancy at AcX.

It has therefore been shown that the decay of AcX does not provide an exception to the general trends exhibited by heavy α-active nuclei. The discrepancies reported up to the present are due instead to a peculiar type of forbiddenness that causes the direct excitation of the ground state of An to be so weak that it has not hitherto been detected.+

Recent results of α- and γ-spectroscopy have revealed other even-odd α-emitters governed by this forbiddenness. Asaro (1953) has found three α-groups in the decay $Cm_{94}^{243} \xrightarrow{\alpha} Pu_{92}^{239}$ having energies of 5.985 MeV (6%), 5.777 MeV (81%) and 5.732 MeV (13%). From a study of the associated γ-radiation he infers the existence of two states of Pu_{94}^{239} below, by 18 and 67 keV respectively, the state excited by the most energetic α-particles. Moreover, internal conversion data lead to the conclusion that the transitions of 277 and 228 keV connecting the level of 81% primary

+ Except for the unpublished result of Rosenblum (1952) quoted by Seaborg.

excitation to these two levels, are both magnetic dipole. This is in very striking analogy with the scheme of Figure 16b, where the transitions of 154 and 144 keV, which also connect the level of highest primary excitation to levels having little or none at all, are both predominantly magnetic dipole. Further examples of this behaviour are afforded by the α-decay of Pu_{94}^{239} and, among the odd-even nuclei, by the α-decay of Am_{95}^{241}. There is at present no adequate theory capable of explaining why the ground-state-to-ground-state α-transitions are so strongly hindered for this class of nuclei.

IV.9.2. Comparison with the predictions of nuclear models.

The nucleus of an atom, like its system of extranuclear electrons, is composed of particles governed by the exclusion principle. In analogy with the atomic case, one can consider each nucleon to be moving independently in an average nuclear binding field. In this way it becomes possible to speak of quantum states of individual nucleons. Then by studying the ordering of the levels for a single nucleon and by applying the restriction that no two identical particles can occupy the same state, one can hope to understand some of the periodicities exhibited by

known nuclear species. In the absence of a comprehensive theory of nuclear forces, it is necessary to make some assumptions about the average binding field. The most successful have been those proposed independently by Mayer (1949) and Haxel, Jensen and Suess (1949). Beginning with an harmonic oscillator potential and then postulating a spin-orbit coupling which reduces the energies of those terms in which $j = \ell + \frac{1}{2}$, these authors are able to account for the observed 'magic numbers' in a very striking way. This is the 'independent-particle' model. From it one gets the 'single-particle' model by assuming that an even number of nucleons of the same type in a level of given j always produce a resultant spin and magnetic moment of zero. Thus for an odd-mass nucleus, the observed spin and magnetic moment will be that of the single odd particle. Here again, the theory has had much greater success than the validity of its assumptions would appear to justify.

Yet in the absence of more precise calculations, empirical evidence has made it necessary to introduce further rules that can only be considered arbitrary at the present time. For example, it has been found that for neutron numbers above 60, the odd neutron has a tendency to occupy states of low angular momentum. This sometimes results in premature occupation of an s state, as in Cd^{111}_{48}. Also, the so-called pairing

energy is required to explain the fact that high spins are not realized in the ground states of nuclei. This refers to a tendency for double occupation of a level of high spin, leaving the odd nucleon in a lower level (e.g. As_{33}^{75}). Furthermore, in order to explain the observed spin of Ag_{47}^{107} (Goldhaber and Sunyar, 1951) one must assume that three nucleons in the $g_{9/2}$ level give rise to a total angular momentum of $^7/_2$.

In the case of An_{86}^{219}, these special rules allow so much freedom that a critical test of the schemes of Figure 16 is impossible. An_{86}^{219} has seven neutrons outside the closed shell of 126 neutrons, and according to the single-particle model its levels will be those of the odd neutron. The first three levels outside this closed shell (in order of increasing energy) should be (Klinkenberg, 1952): $6g_{9/2}$ (10 neutrons), $7i_{11/2}$ (12 neutrons), $5d_{5/2}$ (6 neutrons). Then application of each of the special rules mentioned at the end of the last paragraph would give:

1. Since the odd nucleon has a tendency to occupy a level of low angular momentum, it will go into the $5d_{5/2}$ level. Hence the ground state spin is $^5/_2$.

2. Since the pairing energy favours the double occupation of levels of high angular momentum, one or more pairs out of the seven available neutrons will go into the $7i_{11/2}$ level, leaving the odd neutron in the

$6g_{9/2}$ level. Hence the ground state spin is $^9/_2$.

3. Three of the neutrons in the $6g_{9/2}$ level will combine to yield a total spin of $^7/_2$. Hence the ground state spin is $^7/_2$.

Proceeding similarly, it is possible to provide a number of shell model explanations for the level schemes of Figure 16 which can account for the predominance of magnetic dipole transitions and, in a crude way, the relative intensities of these transitions. But a critical test of the applicability of this model must await further developments in the theory that will enable its predictions to be more specific.

The shell model theory of the nucleus, as outlined above, is based on the analogy between atomic and nuclear systems. There is, however, the characteristic difference that the atomic electrons move in what is essentially an external, fixed Coulomb field, whereas the nuclear field is produced by the particles themselves. Hence the field will not be constant. Its variations are found (A. Bohr, 1951, 1953) to be associated with collective oscillations of the system as a whole. The motion of the individual particle is affected by the collective oscillations, and the behaviour of the entire system is governed by the interaction between these two types of motion. Bohr has shown that a consistent treatment of such a

dynamical system reveals a type of stationary state which is implied by the degree of freedom associated with the collective oscillations. They are called rotational states because of the similarity of their spectrum to that of a rotating rigid body.

The assumptions made in Bohr's theory are realized only when large nuclear deformations can occur, i.e. in regions far removed from closed shells. For the heaviest nuclei, the well-developed rotational spectra can only be expected for mass numbers greater than 225. Nevertheless it is interesting to see the extent to which An_{86}^{219} can be described in these terms.

Whenever a certain level is populated by α-decay, so are its rotational excitations, although with smaller probability (Bohr, 1954). Moreover, for odd mass number nuclei the energies of these states will be given by,

$$E_{rot} = \frac{\hbar^2}{2J} \{I(I+1) - I_0(I_0+1)\} + W$$

where W and I_0 are the energy and spin, respectively, of the lowest state of the rotational band, I is the spin of the rotational excitation ($I = I_0, I_0+1, I_0+2, \ldots$) and J may be termed the effective moment of inertia of the system. For the 154 keV level (see Figure 16) the first rotational excitation might be the 268 or the 335 keV level; the level spacings are such as to eliminate the possibility of their being

first and second excitations, respectively. Whichever level is the first rotational excitation should be connected with the 154 keV level by a rather strong transition. According to the proposed level schemes, however, the principal de-excitations of the 268 and 335 keV levels are provided by transitions direct to the ground state. Nor is it easy to discern the rotational excitations of the 122 keV level, although these may be too weak to be observed. The 444 keV level may be a rotational excitation of the 268 keV level, but it is certainly impossible to reach a decision on the basis of the available material.

It seems, therefore, that the main features of the level schemes proposed in Figure 16 cannot readily be understood in terms of rotational excitations.

IV.10. CONCLUSIONS.

It has been established that strong transitions having energies of 144, 154, and 268 keV, and probably a fourth of 122 keV, are associated with the re-organization of the actinon nucleus following the α-decay of actinium X. These transitions have a predominantly magnetic dipole character. Their existence guarantees that the ground level of actinon lies at least 122 keV below the level excited by the swiftest α-particles whose attribution to the actinium X decay is certain. This explains the anomalous position of actinium X with respect to α-decay systematics, and a discrepancy in neutron binding energies observed by Feather (1953). Two alternative nuclear level schemes are proposed for actinon. Either can be reconciled with the somewhat vague predictions that are possible on the basis of shell model theory. However, the main features of these schemes are not readily understood in terms of the collective model of the nucleus.

The absolute intensity of K X-ray fluorescence emitted by the actinon atom is at least 0.3 and probably 0.5 quanta per disintegration. The fluorescence yield is 98 ± 1%.

Appendix I.

The Effect of Observational Errors on the Range Distribution of Particle Tracks.

In §2.2 it is pointed out that the population of measured track lengths will differ from that of true track lengths because of the nature of the nuclear emulsion method. An approximate expression is derived there for the observed standard deviation in terms of the true one and the errors of measurement. An attempt will now be made to derive the entire observed distribution.

It is assumed that:

1. The track lengths l have a distribution $f(l)$ which vanishes strongly at $l=0$.
2. The directions of the tracks are distributed isotropically in space and independently of l.
3. The measurements ξ of the horizontal projections of tracks having true horizontal projections x are distributed according to a function $\alpha_x(\xi)$.
4. The measurements η of the vertical projections of tracks having true vertical projections y are distributed according to a function $\beta_y(\eta)$.
5. The distributions of $(\xi - x)$, $(\eta - y)$ and l are independent of each other.

From Figure 3, page 30, it can be seen that assumption 2 requires that the angles θ between the

tracks and the horizontal plane are distributed according to the function cos θ. Then the joint distribution of ℓ and θ is given by $P(\ell, \theta) = f(\ell) \cos\theta$.

Now consider a large number of tracks all having the same values of ℓ and θ. Since ξ and η are distributed independently according to the functions $\alpha_{\ell\cos\theta}(\xi)$ and $\beta_{\ell\sin\theta}(\eta)$ respectively, their joint distribution is $\alpha_{\ell\cos\theta}(\xi)\ \beta_{\ell\sin\theta}(\eta)$ and the probability, $F_{\ell,\theta}(\lambda)\,d\lambda$, that $\lambda - \frac{d\lambda}{2} < \sqrt{\xi^2+\eta^2} < \lambda + \frac{d\lambda}{2}$ may be written

$$F_{\ell,\theta}(\lambda)\,d\lambda = \int_{\xi=0}^{\infty}\int_{\eta=0}^{\infty} \alpha_{\ell\cos\theta}(\xi)\ \beta_{\ell\sin\theta}(\eta)\ \bigcup_{\lambda,d\lambda}\left(\sqrt{\xi^2+\eta^2}\right)\,d\xi\,d\eta \qquad (A.1)$$

where

$$\bigcup_{\lambda,d\lambda}(a) = 1 \quad \text{whenever} \quad \lambda - \frac{d\lambda}{2} < a < \lambda + \frac{d\lambda}{2}$$
$$= 0 \quad \text{for all other } a. \qquad (A.2)$$

To get the complete distribution of λ all that is required is an integration over ℓ and θ:

$$F(\lambda) = \int_{\ell=0}^{\infty}\int_{\theta=0}^{\frac{\pi}{2}} F_{\ell,\theta}(\lambda)\,P(\ell,\theta)\,d\ell\,d\theta = \int_{\ell=0}^{\infty}\int_{\theta=0}^{\frac{\pi}{2}} F_{\ell,\theta}(\lambda)\,f(\ell)\cos\theta\,d\ell\,d\theta \qquad (A.3)$$

or substituting (1) into (3),

$$F(\lambda)\,d\lambda = \int_{\ell=0}^{\infty} f(\ell)\,M_{\lambda,d\lambda}(\ell)\,d\ell \qquad (A.4)$$

where

$$M_{\lambda,d\lambda}(\ell) = \int_{\theta=0}^{\frac{\pi}{2}}\int_{\xi=0}^{\infty}\int_{\eta=0}^{\infty} \alpha_{\ell\cos\theta}(\xi)\ \beta_{\ell\sin\theta}(\eta)\ \bigcup_{\lambda,d\lambda}\left(\sqrt{\xi^2+\eta^2}\right)\cos\theta\,d\theta\,d\xi\,d\eta\ . \qquad (A.5)$$

Equations (4) and (5) are the formal solution to the problem. The distribution $F(\lambda)d\lambda$ of measured lengths λ is related by an integral transform to the distribution $f(\ell)d\ell$ of true lengths ℓ, the kernel of this transform being $M_{\lambda,d\lambda}(\ell)$.

To evaluate $M_{\lambda,d\lambda}(\ell)$ it is necessary to find an analytical expression for the discontinuous function $U_{\lambda,d\lambda}(a)$. The Fourier integral theorem makes it possible to write it as,

$$U_{\lambda,d\lambda}(a) \equiv \frac{1}{2\pi} \int_{\omega=-\infty}^{\infty} \int_{\kappa=-\infty}^{\infty} U_{\lambda,d\lambda}(\kappa)\, e^{i\omega(a-\kappa)}\, d\kappa\, d\omega . \tag{A.6}$$

Because of the properties of $U_{\lambda,d\lambda}(\kappa)$ listed in (2), the integral of (6) becomes

$$U_{\lambda,d\lambda}(a) = \frac{1}{2\pi} \int_{\omega=-\infty}^{\infty} \int_{\kappa=\lambda-\frac{d\lambda}{2}}^{\lambda+\frac{d\lambda}{2}} e^{i\omega(a-\kappa)}\, d\kappa\, d\omega , \tag{A.7}$$

and performing the integration with respect to κ,

$$U_{\lambda,d\lambda}(a) = \frac{1}{2\pi} \int_{\omega=-\infty}^{\infty} e^{i\omega a} \left\{ \frac{1}{-i\omega} e^{-i\omega\kappa} \right\}_{\kappa=\lambda-\frac{d\lambda}{2}}^{\lambda+\frac{d\lambda}{2}} d\omega = \frac{1}{2\pi} \int_{\omega=-\infty}^{\infty} e^{i\omega a}\, \frac{2}{\omega}\, e^{-i\omega\lambda} \left\{ \frac{e^{i\omega\frac{d\lambda}{2}} - e^{-i\omega\frac{d\lambda}{2}}}{2i} \right\} d\omega$$

$$U_{\lambda,d\lambda}(a) = \frac{1}{2\pi} \int_{\omega=-\infty}^{\infty} e^{i\omega(a-\lambda)}\, \frac{2}{\omega} \sin\left(\omega \frac{d\lambda}{2}\right) d\omega \longrightarrow \frac{d\lambda}{2\pi} \int_{\omega=-\infty}^{\infty} e^{i\omega(a-\lambda)}\, d\omega \tag{A.8}$$

for infinitesimal $d\lambda$.

Then from (5) and (8)

$$M_{\lambda,d\lambda}(\ell) = \frac{d\lambda}{2\pi} \int_{\omega=-\infty}^{\infty} \int_{\theta=0}^{\frac{\pi}{2}} \int_{\xi=0}^{\infty} \int_{\eta=0}^{\infty} e^{i\omega\left(\sqrt{\xi^2+\eta^2} - \lambda\right)} \underset{\ell\cos\theta}{\alpha(\xi)}\, \underset{\ell\sin\theta}{\beta(\eta)} \cos\theta\, d\eta\, d\xi\, d\theta\, d\omega . \tag{A.9}$$

To proceed, one must make some specific assumptions about α and β, the functions that describe the distribution of the measured values of the projections about their true values. It would not be unreasonable+ to regard them as Gaussian functions,

$$\underset{\ell\cos\theta}{\alpha}(\xi) = \frac{1}{\sqrt{2\pi}\,h}\, e^{-\frac{1}{2h^2}(\xi - \ell\cos\theta)^2}, \tag{A.10}$$

$$\underset{\ell\sin\theta}{\beta}(\eta) = \frac{1}{\sqrt{2\pi}\,v}\, e^{-\frac{1}{2v^2}(\eta - \ell\sin\theta)^2}.$$

Then equation (9) becomes

$$\underset{\lambda,d\lambda}{M}(\ell) = \frac{d\lambda}{(2\pi)^2 hv} \int_{\omega=-\infty}^{\infty} \int_{\theta=0}^{\frac{\pi}{2}} \int_{\xi=0}^{\infty} \int_{\eta=0}^{\infty} e^{i\omega\left(\sqrt{\xi^2+\eta^2} - \lambda\right) - \frac{1}{2h^2}(\xi - \ell\cos\theta)^2 - \frac{1}{2v^2}(\eta - \ell\sin\theta)^2} \cos\theta \, d\eta \, d\xi \, d\theta \, d\omega. \tag{A.11}$$

This cannot easily be integrated as it stands. However, expanding $e^{i\omega\sqrt{\xi^2+\eta^2}}$ about $e^{i\omega\sqrt{\ell^2\cos^2\theta + \ell^2\sin^2\theta}}$ in a Taylor series,

$$e^{i\omega\sqrt{\xi^2+\eta^2}} = \sum_{r=0}^{\infty} \sum_{s=0}^{\infty} \frac{(\xi - \ell\cos\theta)^r}{r!} \frac{(\eta - \ell\sin\theta)^s}{s!} \frac{\partial^{r+s}}{\partial\xi^r \partial\eta^s} e^{i\omega\sqrt{\xi^2+\eta^2}} \Big|_{\substack{\xi=\ell\cos\theta \\ \eta=\ell\sin\theta}},$$

integrating with respect to ξ and η term by term,

+ Except that this assumes that ξ and η are continuous variables, which they are not (due to the limited fineness with which the scales can be read).

and making use of the integral+

$$\frac{1}{\sqrt{2\pi}\,h}\int_{\xi=-\infty}^{\infty}(\xi-\ell\cos\theta)^n\, e^{-\frac{1}{2h^2}(\xi-\ell\cos\theta)^2}\,d\xi=\begin{cases}0 \text{ when } n \text{ is odd}\\ (n-1)(n-3)\cdots 1\; h^n \\ \text{when } n \text{ is even}\end{cases}$$

equation (11) becomes

$$M_{\lambda,d\lambda}(\ell)=\frac{d\lambda}{2\pi}\int_{\omega=-\infty}^{\infty}e^{-i\omega\lambda}\int_{\theta=0}^{\frac{\pi}{2}}\left\{\sum_{r=0}^{\infty}\sum_{s=0}^{\infty}\frac{(2r-1)(2r-3)\cdots 1}{(2r)!}\,h^{2r}\right.$$

$$\left.\frac{(2s-1)(2s-3)\cdots 1}{(2s)!}\,v^{2s}\,\frac{\partial^{2(r+s)}}{\partial\xi^{2r}\partial\eta^{2s}}e^{i\omega\sqrt{\xi^2+\eta^2}}\Big|_{\substack{\xi=\ell\cos\theta\\ \eta=\ell\sin\theta}}\right\}\cos\theta\,d\theta\,d\omega \qquad (A.12)$$

$$M_{\lambda,d\lambda}(\ell)=\frac{d\lambda}{2\pi}\int_{\omega=-\infty}^{\infty}e^{-i\omega\lambda}\int_{\theta=0}^{\frac{\pi}{2}}\left\{\sum_{r=0}^{\infty}\sum_{s=0}^{\infty}\frac{h^{2r}v^{2s}}{r!\,s!\,2^{r+s}}\,\frac{\partial^{2(r+s)}}{\partial\xi^{2r}\partial\eta^{2s}}e^{i\omega\sqrt{\xi^2+\eta^2}}\Big|_{\substack{\xi=\ell\cos\theta\\ \eta=\ell\sin\theta}}\right\}$$

$$\cos\theta\,d\theta\,d\omega. \qquad (A.13)$$

Now $\frac{\partial^{2(r+s)}}{\partial\xi^{2r}\partial\eta^{2s}}e^{i\omega\sqrt{\xi^2+\eta^2}}$ will be of the form $(i\omega)^{2(r+s)}e^{i\omega\sqrt{\xi^2+\eta^2}}B_{2r,2s}(\xi,\eta)$ where $B_{2r,2s}(\xi,\eta)$ is a function of the derivatives of $\sqrt{\xi^2+\eta^2}$. Then

$$\frac{\partial^{2(r+s)}}{\partial\xi^{2r}\partial\eta^{2s}}e^{i\omega\sqrt{\xi^2+\eta^2}}\Big|_{\substack{\xi=\ell\cos\theta\\ \eta=\ell\sin\theta}}=(i\omega)^{2(r+s)}e^{i\omega\ell}B_{2r,2s}(\ell\cos\theta,\ell\sin\theta). \qquad (A.14)$$

+ Rigorously, of course, ξ and η should be integrated from 0 to ∞ since negative measurements are not possible. However integrating them from $-\infty$ to $+\infty$ effects an enormous simplification of the formulae. This approximation is good if h and v are small compared to $\ell\cos\theta$ and $\ell\sin\theta$ respectively. The final formula will be applied to a situation in which ℓ is of the order of 25, h is 0.2 and v is 0.5, and so the conditions will be met except for very shallow and very steep tracks.

Substituting (14) in (13),

$$M_{\lambda, d\lambda}(\ell) = \frac{d\lambda}{2\pi} \sum_{r=0}^{\infty} \sum_{s=0}^{\infty} \frac{h^{2r} v^{2s}}{r!\, s!\, 2^{r+s}} \int_{\omega=-\infty}^{\infty} e^{i\omega(\ell-\lambda)} (i\omega)^{2(r+s)} d\omega \int_{\theta=0}^{\frac{\pi}{2}} B_{2r,2s}(\ell\cos\theta, \ell\sin\theta) \cos\theta \, d\theta .$$

(A.15)

Letting

$$\int_{\theta=0}^{\frac{\pi}{2}} B_{2r,2s}(\ell\cos\theta, \ell\sin\theta) \cos\theta \, d\theta = b_{2r,2s}(\ell) , \qquad \text{(A.16)}$$

this becomes

$$M_{\lambda, d\lambda}(\ell) = \frac{d\lambda}{2\pi} \sum_{r=0}^{\infty} \sum_{s=0}^{\infty} \frac{h^{2r} v^{2s}}{r!\, s!\, 2^{r+s}} \int_{\omega=-\infty}^{\infty} (i\omega)^{2(r+s)} e^{i\omega(\ell-\lambda)} b_{2r,2s}(\ell) \, d\omega .$$

(A.17)

To get the observed distribution $F(\lambda)$ it is now necessary to substitute this expression for $M_{\lambda, d\lambda}(\ell)$ into equation (4) :

$$F(\lambda) = \sum_{r=0}^{\infty} \sum_{s=0}^{\infty} \frac{h^{2r} v^{2s}}{r!\, s!\, 2^{r+s}} \frac{1}{2\pi} \int_{\omega=-\infty}^{\infty} \int_{\ell=0}^{\infty} (i\omega)^{2(r+s)} e^{i\omega(\ell-\lambda)} b_{2r,2s}(\ell) f(\ell) \, d\omega \, d\ell .$$

But according to the Fourier Integral Theorem+,

$$\frac{1}{2\pi} \int_{\omega=-\infty}^{\infty} \int_{\ell=0}^{\infty} e^{i\omega(\ell-\lambda)} b_{2r,2s}(\ell) f(\ell) \, d\omega \, d\ell = b_{2r,2s}(\lambda) f(\lambda)$$

(A.18)

+ Since $f(\ell)$ is 0 for negative ℓ it is a matter of indifference whether ℓ is integrated from 0 to ∞ or from $-\infty$ to ∞ .

and by successive differentiation with respect to λ,

$$\frac{1}{2\pi}\int_{\omega=-\infty}^{\infty}\int_{\ell=0}^{\infty}(i\omega)^{2(r+s)}\, e^{i\omega(\ell-\lambda)}\, b_{2r,2s}(\ell)\, f(\ell)\, d\ell\, d\omega = \frac{d^{2(r+s)}}{d\lambda^{2(r+s)}}\left\{b_{2r,2s}(\lambda)\, f(\lambda)\right\}.$$

Hence
$$F(\lambda) = \sum_{r=0}^{\infty}\sum_{s=0}^{\infty}\frac{h^{2r}v^{2s}}{r!\,s!\,2^{r+s}}\,\frac{d^{2(r+s)}}{d\lambda^{2(r+s)}}\left\{b_{2r,2s}(\lambda)\, f(\lambda)\right\} \qquad (A.19)$$

where the $b_{2r,2s}(\lambda)$ are defined in equations (16) and (14).

The first few differentiations and integrations of (14) and (16) may be easily carried out. They give,

$$F(\lambda) = f(\lambda) + h^2\left[\tfrac{1}{3}\frac{d^2f(\lambda)}{d\lambda^2} - \tfrac{1}{6}\frac{d}{d\lambda}\left\{\frac{f(\lambda)}{\lambda}\right\}\right] + v^2\left[\tfrac{1}{6}\frac{d^2f(\lambda)}{d\lambda^2} - \tfrac{1}{3}\frac{d}{d\lambda}\left\{\frac{f(\lambda)}{\lambda}\right\}\right]$$
$$+ h^2v^2\left[\tfrac{1}{30}\frac{d^4f(\lambda)}{d\lambda^4} - \tfrac{1}{20}\frac{d^3}{d\lambda^3}\left\{\frac{f(\lambda)}{\lambda}\right\}\right] \qquad (A.20)$$
$$+ \cdots\cdots\cdots$$

Figure A.1 shows how $F(\lambda)$ and $f(\lambda)$ are related when $f(\lambda)$ is a Gaussian function of mean = 25 and standard deviation = 1, a situation that might be encountered in the study of the tracks of a homogeneous group of α-particles. The values taken for h and v are those chosen on page 19, namely h = 0.2, v = 0.5. The series (20) converges rapidly in this case, only the first three terms being of importance. It is interesting to note that although individual track lengths may be seriously affected by the observational errors, their effect upon the shape of the distribution curve of measured lengths is not very great.

FIGURE A.I. THE EFFECT OF OBSERVATIONAL ERRORS ON AN α-PARTICLE RANGE DISTRIBUTION

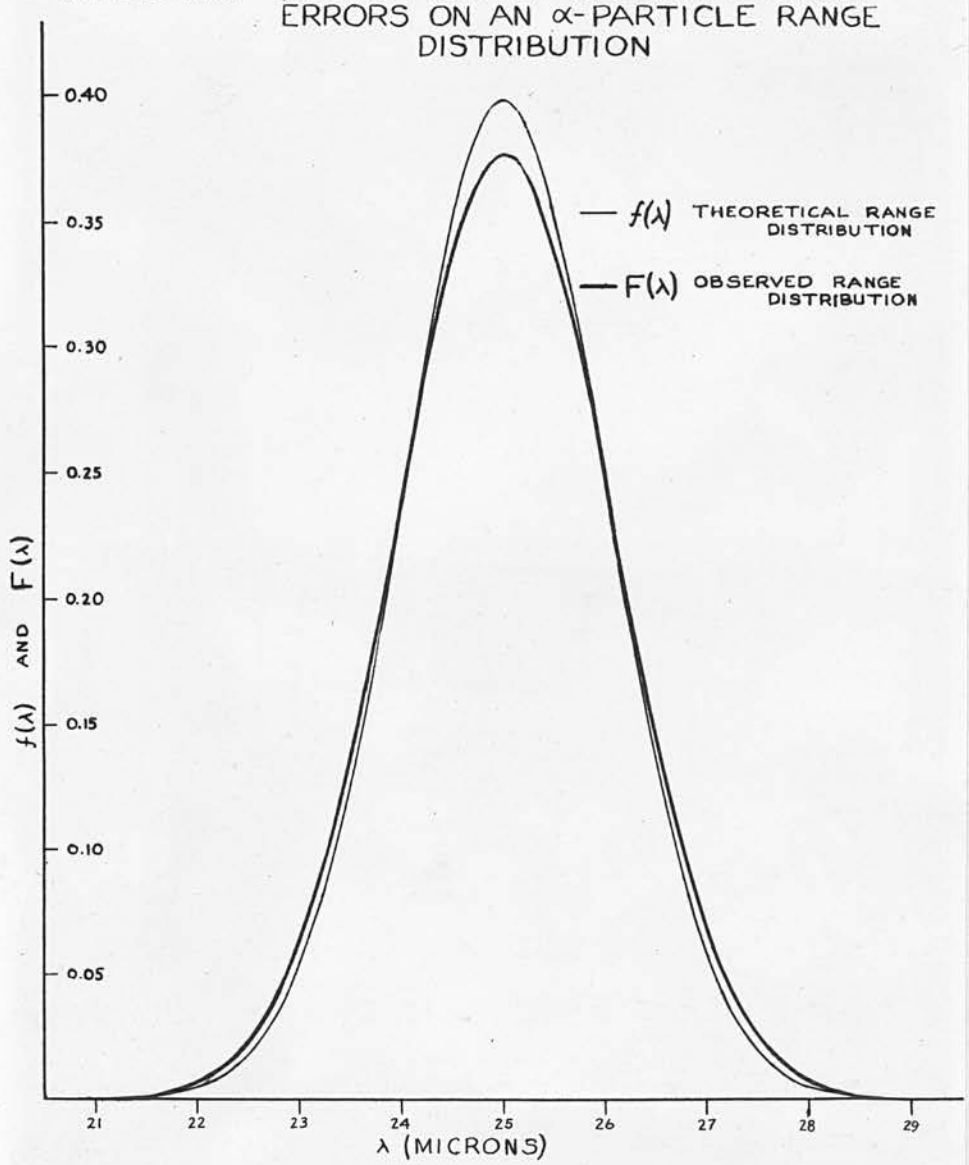

Appendix II.

The Relationship Between $\overline{\frac{dR}{dE}}$ and $\frac{1}{\overline{\frac{dE}{dR}}}$.

Imagine that a large number of particles of energy E all move a distance dR. Because of the statistical nature of the energy loss, all the particles will not lose the same amount of energy. Let the fraction of them whose loss is between δE and $\delta E + d(\delta E)$ be $f(\delta E)d(\delta E)$. Then if $\overline{R}(E)$ is the mean total range of particles of initial energy E,

$$\begin{aligned}\overline{R}(E) &= dR + \int f(\delta E)\,\overline{R}(E-\delta E)\,d(\delta E)\\ &= dR + \int f(\delta E)\left\{\overline{R}(E) - \delta E\,\frac{d\overline{R}(E)}{dE} + \frac{(\delta E)^2}{2!}\,\frac{d^2\overline{R}(E)}{dE^2} - \cdots\right\} d(\delta E)\\ &= dR + \overline{R}(E)\int f(\delta E)\,d(\delta E) - \frac{d\overline{R}(E)}{dE}\int \delta E\, f(\delta E)\,d(\delta E) + \frac{1}{2!}\,\frac{d^2\overline{R}(E)}{dE^2}\int (\delta E)^2 f(\delta E)\,d(\delta E)\end{aligned} \qquad (A.21)$$

But because of the definition of $f(\delta E)d(\delta E)$

$$\int f(\delta E)\,d(\delta E) = 1$$

$$\int \delta E\, f(\delta E)\,d(\delta E) = \overline{\delta E}$$

$$\int (\delta E)^2 f(\delta E)\,d(\delta E) = \overline{(\delta E)^2}\ , \quad \text{etc.} \qquad (A.22)$$

Substituting (2) in (1),

$$\overline{R}(E) = dR + \overline{R}(E) - \overline{\delta E}\,\frac{d\overline{R}(E)}{dE} + \frac{\overline{(\delta E)^2}}{2!}\,\frac{d^2\overline{R}(E)}{dE^2} - \cdots\cdots$$

$$0 = 1 - \frac{\overline{\delta E}}{dR}\,\frac{d\overline{R}(E)}{dE} + \frac{1}{2!}\,\frac{\overline{(\delta E)^2}}{dR}\,\frac{d^2\overline{R}(E)}{dE^2} - \cdots\cdots$$

$$\frac{d\overline{R}}{dE} = \frac{1}{\overline{\frac{\delta E}{dR}}}\left[1 + \frac{1}{2!}\,\frac{\overline{(\delta E)^2}}{dR}\,\frac{d^2\overline{R}(E)}{dE^2} - \cdots\cdots\right] \qquad (A.23)$$

Now $\frac{d\bar{R}(E)}{dE}$ is defined as $\lim_{dE\to 0} \frac{\bar{R}(E+dE) - \bar{R}(E)}{dE}$. But the difference between $\bar{R}(E + dE)$ and $\bar{R}(E)$ is simply the mean distance $\overline{dR}$ moved by the particles in losing an amount of energy dE. Hence $\frac{d\bar{R}(E)}{dE}$ is equal to $\frac{\overline{dR}}{dE}$.

The quantity $\frac{\overline{\delta E}}{dR}$ is essentially the stopping power. Equation (23) shows that the difference between $\frac{\overline{dR}}{dE}$ and the reciprocal of the stopping power depends upon the amount of straggling in the energy losses and upon the non-linearity of $\bar{R}(E)$.

To estimate $\frac{\overline{(\delta E)^2}}{dR}$ one can use a calculation similar to that of equations (21) - (23):

$$\overline{R^2}(E) = (dR)^2 + 2\,dR \int f(\delta E)\,\bar{R}(E-\delta E)\,d(\delta E) + \int f(\delta E)\,\overline{R^2}(E-\delta E)\,d(\delta E)$$

$$0 = 2\bar{R}(E) - \frac{d\overline{R^2}(E)}{dE}\,\frac{\overline{\delta E}}{dR} + \frac{1}{2!}\,\frac{d^2\overline{R^2}(E)}{dE^2}\,\frac{\overline{(\delta E)^2}}{dR} - \cdots\cdots$$

$$\frac{\overline{(\delta E)^2}}{dR} = \frac{2\,\frac{d\overline{R^2}}{dE}\,\frac{\overline{\delta E}}{dR} - 4\bar{R}(E) - \cdots}{\frac{d^2\overline{R^2}}{dE^2}} \qquad \text{(A.24)}$$

The derivatives of $\overline{R^2}$ required in (24) can be calculated from the observed fact that the standard deviation of the ranges of a mono-energetic group of electrons is roughly proportional to the mean range. That is,

$$\sqrt{\overline{(R-\bar{R})^2}} = c\bar{R}$$

$$\left.\begin{aligned} \overline{(R-\bar{R})^2} &= \overline{R^2} - \bar{R}^2 = c^2\bar{R}^2 \\ \overline{R^2} &= (1+c^2)\bar{R}^2 \\ \frac{d\overline{R^2}}{dE} &= 2(1+c^2)\bar{R}\,\frac{d\bar{R}}{dE} \\ \frac{d^2\overline{R^2}}{dE^2} &= 2(1+c^2)\left[\left(\frac{d\bar{R}}{dE}\right)^2 + \bar{R}\,\frac{d^2\bar{R}}{dE^2}\right]. \end{aligned}\right\} \qquad \text{(A.25)}$$

Substituting (25) in (24)

$$\frac{\overline{(\delta E)^2}}{dR} = 2\bar{R}\,\frac{(1+c^2)\,\frac{\overline{\delta E}}{dR}\,\frac{d\bar{R}}{dE} - 1 \cdots\cdots}{(1+c^2)\left\{\left(\frac{d\bar{R}}{dE}\right)^2 + \bar{R}\,\frac{d^2\bar{R}}{dE^2}\right\}} \qquad (A.26)$$

and substituting for $\frac{\overline{\delta E}}{dR}\,\frac{d\bar{R}}{dE}$ in (26) the expression given by (23),

$$\frac{\overline{(\delta E)^2}}{dR} = \frac{2\bar{R}c^2}{(1+c^2)\left(\frac{d\bar{R}}{dE}\right)^2} + \cdots\cdots \qquad (A.27)$$

Then (23) becomes

$$\frac{d\bar{R}}{dE} = \frac{1}{\frac{\overline{\delta E}}{dR}}\left[1 + \frac{c^2}{1+c^2}\,\frac{\bar{R}\,\frac{d^2\bar{R}}{dE^2}}{\left(\frac{d\bar{R}}{dE}\right)^2} + \cdots\right] \qquad (A.28)$$

The correction term in (28) involves $\bar{R}(E)$ and its derivatives. These are as yet unknown. However, as a first approximation they can be calculated by neglecting the difference between $\frac{d\bar{R}}{dE}$ and $1\Big/\frac{\overline{\delta E}}{dR}$. Then the correction term calculated on this basis can be substituted into (28) to give a better estimate of $\frac{d\bar{R}}{dE}$, and so forth. For the experimentally determined value of c, 0.2, this iteration procedure converges so rapidly that only the first correction need be applied. The result of this calculation is shown in Figure 7, page 46.

REFERENCES

1. Arnoult, R., 1939, Ann. Phys., Paris, 12, 282.
2. Asaro, F., 1953, Thesis, University of California, Berkeley, UCRL-2180, 127.
3. Bennett, W.E., 1938, Proc. Camb. Phil. Soc., 34, 282.
4. Bethe, H., 1933, Handbuch der Physik, 24, Pt. 1, 523.
5. Bethe, H., and Heitler, W., 1934, Proc. Roy. Soc. A., 146, 83.
6. Bohr, A., 1951, Phys. Rev., 81, 134.
7. Bohr, A., 1954, Private communication to Dr. M.A.S. Ross.
8. Bohr, A., and Mottelson, B.R., 1953, K. Danske Vidensk. Selsk. Mat.-fys. Medd., 27, No. 16.
9. Briggs, G.H., 1954, Rev. Mod. Phys., 26, 1.
10. Casimir, H.B.G., 1936, Archives du Musée Teyler, 8, 274.
11. Cauchois, Y., and Hulubei, H., 1947, Tables de Constantes et données numériques. I. Longueurs d'onde des émissions X et des discontinuités d'absorption X, Paris.
12. Crookes, W., 1900, Proc. Roy. Soc. A., 66, 409.
13. Curie, Mme. P., and Rosenblum, S., 1932, C.R. Acad. Sci., Paris, 194, 1232; 1933, Ibid., 196, 1598.
14. Demers, P., 1947, Phys. Rev., 72, 536.

REFERENCES (Contd).

15. Dilworth, C.C., Occhialini, G.P.S., and Payne, R.M., 1948, Nature, Lond., 162, 102.

16. DuMond, J.W.M., and Cohen, E.R., 1951, Phys. Rev., 82, 555.

17. Eichholz, G.G., and Flack, F.C., 1951, J. Chem. Phys., 19, 363.

18. Feather, N., 1952, Nuclear Stability Rules, Cambridge University Press, p. 63.

19. Feather, N., 1953, Advances in Phys., 2, 141.

20. Fisher, R., 1950, Statistical Methods for Research Workers, Oliver and Boyd, p. 52.

21. Fisher, R., and Yates, F., 1949, Statistical Tables for Biological, Agricultural and Medical Research, Oliver and Boyd.

22. Frilley, M., 1940, J. Phys. Radium, 1, 34.

23. Frilley, M., Rosenblum, S., Valadarèz, M., and Bouissières, G., 1954, J. Phys. Radium, 15, 45.

24. Giesel, F., 1904, Jahrbuch d. Radioakt. u. Elektronik, 1, 358.

25. Glendenin, L.E., 1951, Radiochemical Studies: The Fission Products, Book 3, McGraw-Hill Book Co., Inc., p. 1460.

26. Godlewski, T., 1905, Phil. Mag., 10, 35.

27. Goldhaber, M., and Sunyar, A.W., 1951, Phys. Rev., 83, 906.

28. Greenberg, L.H., and Haslam, R.N.H., 1953, Canad. J. Phys., 31, 1953.

REFERENCES (Contd.).

29. Hahn, O., and Meitner, L., 1925, Z. Phys., 34, 795.

30. Haxel, O., Jensen, J.H.D., and Suess, H.E., 1949, Phys. Rev., 75, 1766.

31. Hollander, J.M., Perlman, I., and Seaborg, G.T., 1953, Rev. Mod. Phys., 25, 469.

32. Horan, J.R., 1953, Phys. Rev., 90, 717.

33. Jarvis, C.J.D., 1950, Thesis, Edinburgh, p. 32.

34. Jenny, L., and Hürlimann, T., 1951, Helv. Phys. Acta., 24, 235.

35. Kendall, M.G., 1952, The Advanced Theory of Statistics, Vol. 1, Griffen & Co.,Ltd., p. 290.

36. Klinkenberg, P.F.A., 1952, Rev. Mod. Phys., 24, 63.

37. Lieber, C., 1939, Naturwissenschaften, 27, 421.

38. Lindström, G., 1951, Phys. Rev., 83, 465.

39. Martin, S.L., 1949, Aust. J. Sci. Res. A., 53, 389.

40. Marton, L., and Schiff, L.I., 1941, J. App. Phys., 12, 760.

41. Mayer, M.G., 1949, Phys. Rev., 75, 1969.

42. Meitner, L., 1925, Z. Phys., 34, 807.

43. Ouang, T.T., and Surugue, J., 1944, C.R. Acad. Sci., Paris, 218, 591.

44. Perlman, I., Giorso, A., and Seaborg, G.T., 1950, Phys. Rev., 77, 26.

45. Rose, M.E., Goertzel, G., Spinrad, B.I., Harr, J., and Strong, P., 1954, Private communication.

REFERENCES (Contd.).

46. Rosenblum, S., 1952, Private communication to G.T. Seaborg, quoted: 1953, Rev. Mod. Phys., 25, 469.

47. Rosenblum, S., Guillot, M., and Perey, M., 1936, C.R. Acad. Sci., Paris, 202, 1274; 1937, Ibid., 204, 175.

48. Rotblat, J., 1950, Nature, Lond., 165, 387.

49. Rotblat, J., and Tai, C.T., 1949, Nature, Lond., 164, 835.

50. Rutherford, E., and Soddy, F., 1902, Phil. Mag., 4, 370.

51. Surugue, J., 1937, Ann. Phys., Paris, 8, 484.

52. Weyl, P.K., 1953, Phys. Rev., 91, 289.

53. Williams, E.J., 1928, Proc. Camb. Phil. Soc., 24, 315.

54. Williams, E.J., 1930, Proc. Roy. Soc. A., 130, 310.

55. Yagoda, H., 1949, Radioactive Measurements in Nuclear Emulsions, Chapman and Hall, p. 132.

56. Zajac, B., 1949, Thesis, Edinburgh, p. 25.

57. Zajac, B., and Miller N., 1952, Phil. Mag., 43, 264.

58. Zajac, B., and Ross, M.A.S., 1949, Nature, Lond., 164, 311.

ACKNOWLEDGEMENTS.

I wish to thank Professor N. Feather, F.R.S., for extending to me the facilities of his laboratory. I am deeply indebted to Dr. M.A.S. Ross for suggesting the subject of this thesis, and for her advice and encouragement throughout the course of the work. Thanks are due to Dr. N. Miller for his advice concerning the radiochemical separations. The provision and renewal of a Fulbright Award by The United States Educational Commission in the United Kingdom is also gratefully acknowledged.
